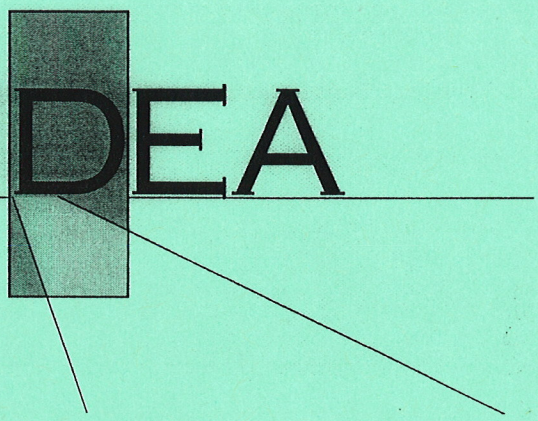

Innovations Deserving
Exploratory Analysis Programs

Highway IDEA Program

Liquefaction Mitigation Using Vertical Composite Drains: Full-Scale Testing for Pile Applications

Final Report for Highway IDEA Project 103

Prepared by:
Kyle M. Rollins and Spencer R. Strand, Brigham Young University, Provo, UT

March 2007

TRANSPORTATION RESEARCH BOARD
OF THE NATIONAL ACADEMIES

INNOVATIONS DESERVING EXPLORATORY ANALYSIS (IDEA) PROGRAMS
MANAGED BY THE TRANSPORTATION RESEARCH BOARD (TRB)

This NCHRP-IDEA investigation was completed as part of the National Cooperative Highway Research Program (NCHRP). The NCHRP-IDEA program is one of the four IDEA programs managed by the Transportation Research Board (TRB) to foster innovations in highway and intermodal surface transportation systems. The other three IDEA program areas are Transit-IDEA, which focuses on products and results for transit practice, in support of the Transit Cooperative Research Program (TCRP), Safety-IDEA, which focuses on motor carrier safety practice, in support of the Federal Motor Carrier Safety Administration and Federal Railroad Administration, and High Speed Rail-IDEA (HSR), which focuses on products and results for high speed rail practice, in support of the Federal Railroad Administration. The four IDEA program areas are integrated to promote the development and testing of nontraditional and innovative concepts, methods, and technologies for surface transportation systems.

For information on the IDEA Program contact IDEA Program, Transportation Research Board, 500 5th Street, N.W., Washington, D.C. 20001 (phone: 202/334-1461, fax: 202/334-3471, http://www.nationalacademies.org/trb/idea)

Liquefaction Mitigation using Vertical Composite Drains: Full-Scale Testing for Pile Applications

Final Report Project 103

Prepared by

Kyle M. Rollins and Spencer R. Strand

Department of Civil & Environmental Engineering
Brigham Young University
368 CB, Provo, UT 84602

Prepared for

IDEAS Program
Transportation Research Board

March 2007

Acknowledgements

Funding for this study was provided by a grant from the National Cooperative Highway Research Program-Ideas Deserving Exploratory Analysis (NCHRP-IDEA) program as project 103. This support is gratefully acknowledged. The conclusions from this study do not necessarily reflect the views of the sponsors.

We express our appreciation to the British Columbia Ministry of Transportation for allowing us to use the Vancouver test site. Nilex, Inc. donated all equipment, personnel and materials necessary to install the drains at the test site which made this project possible. Advanced Drainage Systems, Inc. donated the EQ-Drain pipes installed at the test areas. ConTec, Inc. provided equipment and personnel necessary to perform CPT soundings at no cost to the project. These donations and contributions made this project feasible.

Abstract

Liquefaction has typically been mitigated by in-situ densification; however, this is often time-consuming and expensive. Vertical composite earthquake (EQ) drains offer the possibility of preventing liquefaction and associated settlement while reducing the cost and time required for treatment. To evaluate the behavior of these drains under full-scale conditions, controlled blasting techniques were employed to test loose liquefiable sand in Vancouver, Canada with and without drains. In addition, the influence of the drains on the development of downdrag on piles was measured. Test piles were driven through the liquefiable clean sand layer from 6 to 13 m below the ground surface and into a denser stratum at depth.

A pilot liquefaction test was used to determine an appropriate sequence of explosive charges to produce liquefaction in 12 to 16 seconds. This charge sequence was then used to test an area without drains and an area with drains spaced at 1.22 m on centers. An instrumented test pile was located at each site which was loaded to failure prior to blast testing to determine ultimate skin friction and end-bearing. Each test pile was loaded to about one-half of the failure load prior to blasting and downdrag forces were measured. Installation of the piles did not produce significant settlement but installation of the drains produced about 210 mm of settlement or 2.9% volumetric strain in the loose liquefiable sand zone. Although settlement clearly showed densification, CPT soundings conducted one month after drain installation did not show any significant increase in cone resistance.

The blast sequence produced liquefaction at the site without drains which eventually resulted in 270 mm of settlement or over 3% volumetric strain. Immediately after liquefaction the unit skin friction decreased to zero. Then, as pore pressures dissipated and the sand settled, negative skin friction developed but the magnitude was only about one-half of the positive friction. Apparently the semi-fluid state of the reconsolidating sand did not allow full development of skin friction. The blast sequence also produced liquefaction at the site with drains but the settlement was reduced to 220 mm or 3.7% volumetric strain a decrease of 17% relative to the untreated site. Nevertheless, the dissipation rate at site with drains was dramatically increased and pore pressures dissipated faster than at the site without drains. This indicates that the drains were performing a function but that spacing or drain diameter was inadequate to prevent liquefaction. Because of the rapid rate of dissipation, the skin friction did not decrease to zero in the liquefied sand and negative skin friction increased to a value equal to the positive skin friction in the liquefied layer. Negative skin friction did not develop in the solid overlying the liquefied zone for either test. For both test piles, the increased load due to negative skin friction was resisted by skin friction and end-bearing resistance in the denser underlying sand and settlement of the pile was less than 7 to 10 mm.

With lower bound permeability values, computer analyses performed using FEQDrain were generally successful in matching measured pore pressure and settlement response during the blasting. This clearly points out the need to measure permeability in-situ, if possible, and to evaluate drain spacing using a range of permeability values with FEQDrain during design. The calibrated model was then used to evaluate the response with closer drain spacing and larger drain diameter. For these cases, the maximum pore pressures and settlement were brought to levels which would be acceptable for many applications (shallow foundations, embankment dams, slopes). However, the settlement would not likely be reduced enough to prevent development of downdrag on deep foundations. Nevertheless, these results suggest that the drains could be an effective solution for mitigating liquefaction hazard and that conservative permeability parameters should be used in designing drain spacing and diameter.

Table of Contents

Acknowledgements
Abstract
Table of Contents

1. Introduction

Every year earthquakes cause enormous amounts of damage worldwide. Much of the damage can be directly attributed to liquefaction. For instance, liquefaction caused nearly $1 billion worth of damage in the 1964 Niigata, Japan earthquake (NRC, 1985). Liquefaction was also responsible for $99 million in damage in the 1989 Loma Prieta earthquake (Holzer, 1998) and over $11.8 billion in damage just to port and wharf facilities during the 1995 Kobe, Japan earthquake (EQE, 1995).

Liquefaction occurs naturally during earthquakes in loose, saturated, cohesionless soils. The ground shaking causes the loose soil to compact. However, the water in the interparticle voids cannot escape immediately. As the soil attempts to compress, the pore pressure increases, temporarily decreasing the stress felt by the soil particles. If the pore pressure increases enough, the water will carry the entire weight of the overlying soil and any structures that happen to be built above. At this point the particle-to-particle forces in the soil are reduced to zero and the soil begins to behave as a liquid and is said to be "liquefied".

Liquefied soils loose shear strength and are susceptible to large lateral displacements; very gentle and even flat slopes have exhibited the propensity for lateral movement known as "lateral spreading". Liquefied soil is also incapable of supporting concentrated vertical loads, without excessive settlement. Other common signs of liquefaction include sand boils, ground distortion, and ground fissures (see Figure 1 through Figure 4).

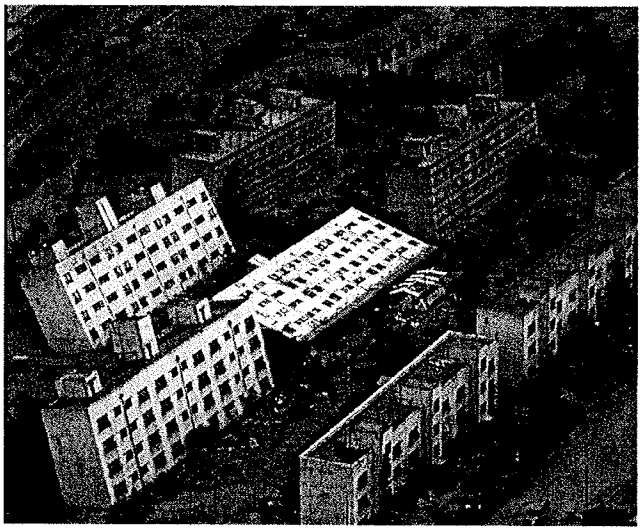

Figure 1 1964 Niigata Japan: Liquefaction caused major settlement. The building at center rotated 70 degrees from vertical. Surprisingly, little structural damage occurred to the apartment buildings. Some buildings were later righted and re-inhabited.

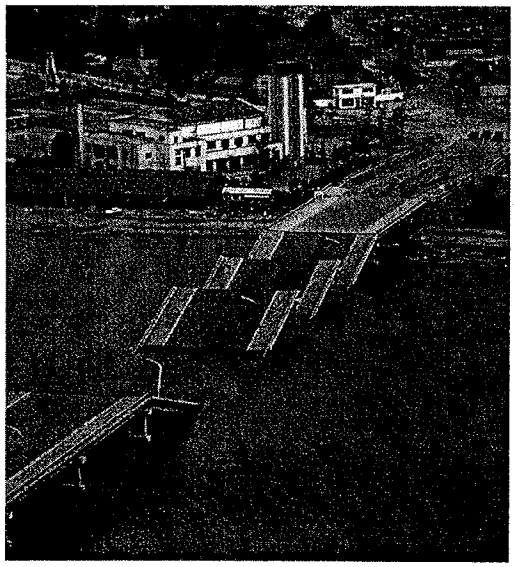

Figure 2 1964 Niigata Japan: Showa bridge collapse due to pier collapse caused by liquefaction.

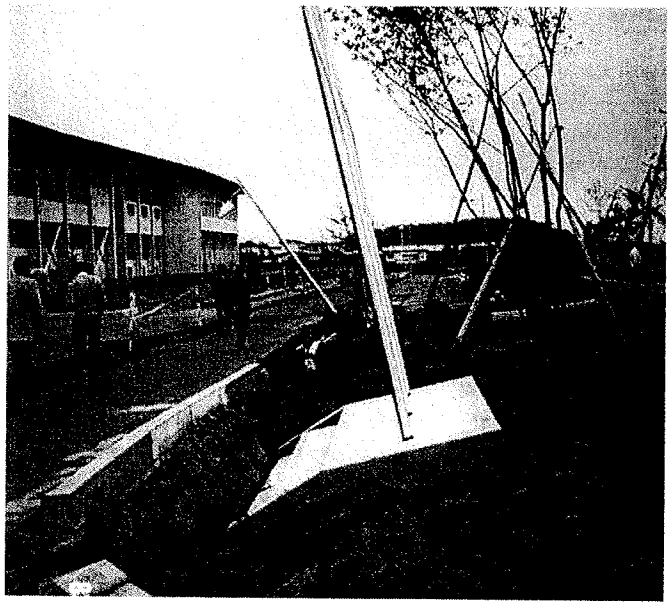

Figure 3 1983 Nihonkai-Chubu: Liquefaction caused unstable soils to fail. Flagpole foundation in foreground was placed shallowly. School building to the left was founded on a pile foundation and suffered no damage.

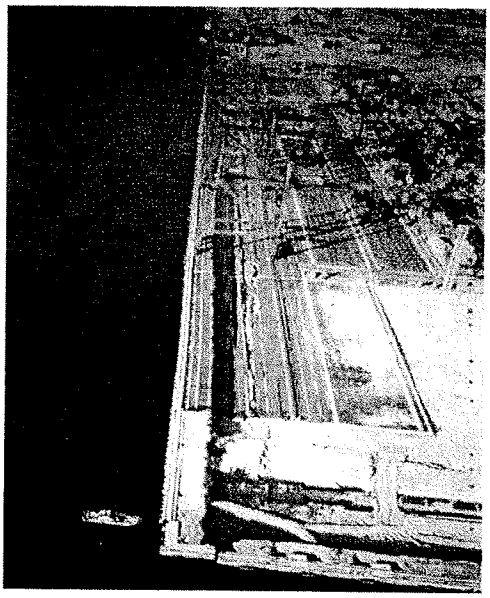

Figure 4 Lateral spread damage to port facilities due to Great Hanshin Earthquake of 1995 in Kobe Japan

1.1. Liquefaction Mitigation

Liquefaction hazards have typically been mitigated using two types of techniques: in situ soil improvement and foundation design (Lew and Hudson, 2004). Soil improvement techniques typically involve some type of soil densification process, such as vibro-compaction, stone columns, dynamic compaction, or compaction grouting as illustrated in Figure 5. These techniques tend to compact the soil, reducing the tendency for contraction during an earthquake, thus preventing liquefaction. Although these techniques are generally effective, they are also expensive and time-consuming.

1.1.1. Liquefaction mitigation through pore pressure dissipation

An alternative to soil densification is to provide for rapid pore pressure dissipation to prevent liquefaction. Seed and Booker (1977) pioneered the development of vertical gravel drains for just that purpose. Vertical drains allow for pore pressure dissipation through horizontal flow, as shown in Figure 6, which significantly decreases the drainage path length. When drainage is impeded by a horizontal silt or clay layer, vertical drains can be particularly relative effective. The effectiveness of the drains increases as drain diameter increases and drain spacing decreases.

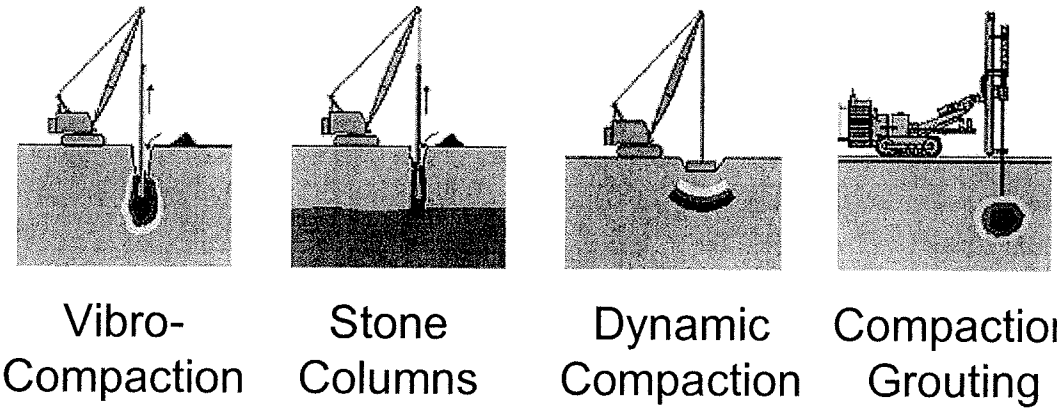

Figure 5 Typical soil improvement techniques for densifying loose saturated sands to prevent earthquake induced liquefaction.

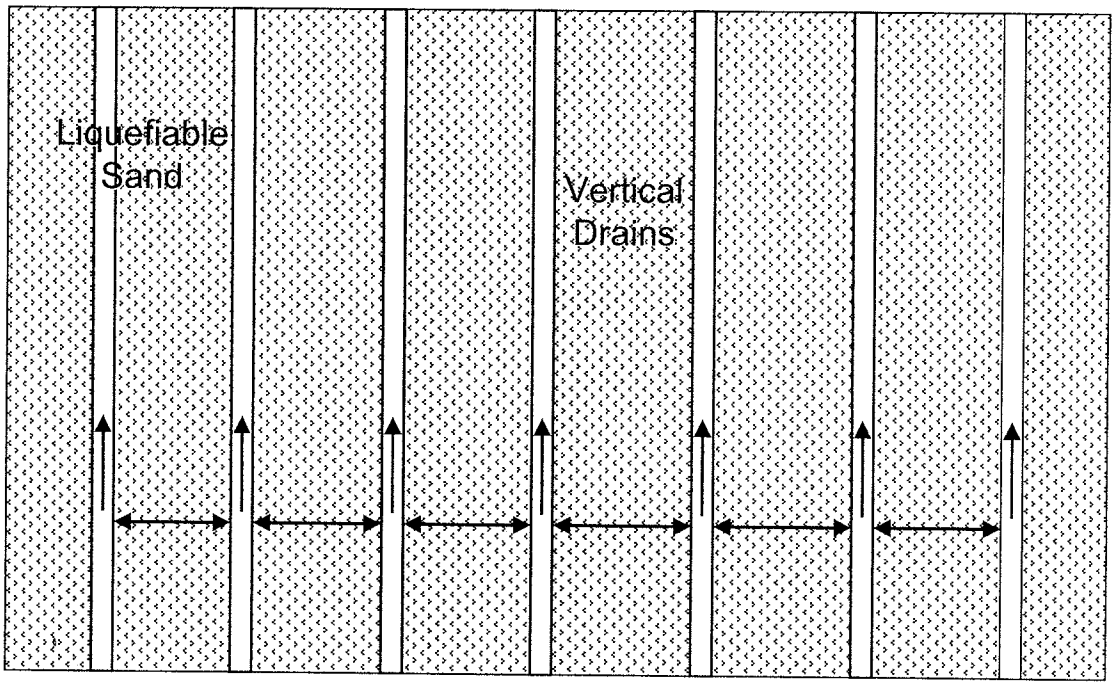

Figure 6 Vertical drains for mitigating the liquefaction hazard posed by loose saturated sand.

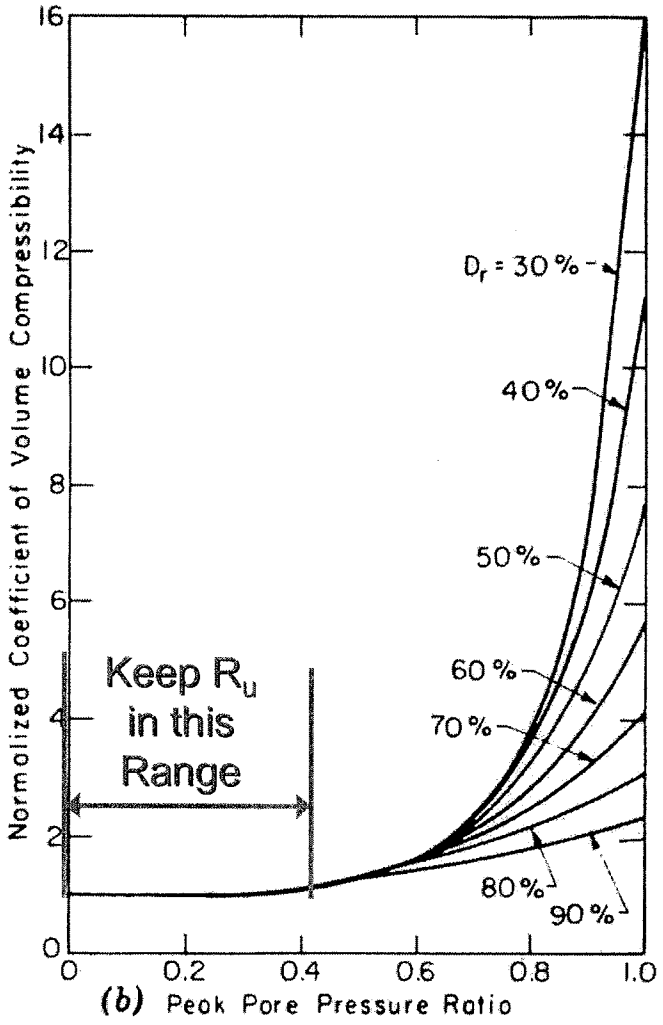

Figure 7 Normalized coefficient of volume compressibility versus pore pressure rato for sands at various relative densities.

Although gravel drains have been utilized at many sites for liquefaction mitigation, most designers have relied on the densification caused by drain installation rather than the drainage which they provide (Rollins and Anderson, 2004). Some designers have worried that the use of drainage alone would still allow unacceptable settlement to develop. The key appears to be in keeping excess pore water pressures less than about 40% of the pressure causing liquefaction ($R_u \approx 0.40$). As pressure levels increase above this value as shown in Figure 7, the compressibility of the sand increases markedly and excessive settlement could result.

Composite vertical earthquake drains (EQ drains) have the potential to provide the rapid pore pressure dissipation needed to prevent liquefaction without the need to first densify the soil and could prevent large settlements from occurring. EQ drains are perforated plastic drain pipes 75 mm to 150 mm in diameter. The drains are installed vertically with a vibrating mandrel in

much the same way that pre-fabricated vertical drains (PVD's) are installed for consolidation of clays.

EQ drains are typically installed in a triangular pattern with center-to-center spacings of about 1 to 2 meters, depending upon the permeability of the soil to be treated. In contrast to PVDs which have a limited flow rate ($2.83x10^{-5}$ m^3/s at a gradient of 0.25), a 100 mm EQ drain can carry a very large flow volume (0.093 m3/s at the same gradient) sufficient to relieve pore pressure in sands. This flow volume is more than 10 times that provided by a 1 m diameter gravel column (6.51x10-3 m3/s). Filter fabric sleeves are placed around the drains to prevent infiltration of soil.

EQ drains can be installed in a fraction of the time and for a fraction of the cost of typical mitigation techniques. For example, for treatment of a 12 m thick layer, stone columns would typically cost $\$107/m^2$ of surface area and vibro-compaction would cost $\$75/m^2$, while EQ drains would cost only $\$48/m^2$. Also, the EQ drains can be installed in about one-third to one-half the time needed for conventional means (Nilex, 2002).

1.1.2. Liquefaction mitigation through foundation design

Due to the geologic setting in which earthquakes commonly occur, areas prone to earthquakes typically have an overabundance of surficial deposits of soft soils (silts, clays, etc.) underlain or interbedded with liquefiable sand layers. Hence special foundations must be designed to accommodate the soft and liquefiable soils. Commonly mat foundations are used to "raft" the structure above the unstable soils, distributing the load across a large area and decreasing the stress applied to the ground. These foundations must be capable of withstanding the total and differential settlements caused by liquefaction. It may be possible to re-level this type of foundation after a liquefaction event (Lew and Hudson, 2004).

Another common method is to use pile foundations to transfer loads through the weak, near-surface deposits to deeper, stiffer soils. Because liquefied soils are prone to lateral spreading, the piles must be designed to withstand lateral forces. In addition, they must be designed to accommodate any downdrag forces that may develop due to negative skin friction when the liquefied soils settle relative to the piles.

1.2. Previous Research

While EQ drains have been utilized at 12 sites around the United States, no site has experienced an earthquake. As a result, the efficacy of EQ drains in preventing liquefaction is uncertain. Nor is it clear the extent to which EQ drains may reduce or prevent the loss of skin friction of a pile foundation or improve bearing capacity under a mat foundation during liquefaction. While much research has studied lateral spreading as it relates to pile foundations, little research has focused on the development of downdrag and other vertical aspects of the soil/pile interaction related to liquefaction. This lack of field performance and research data has been a major impediment to further the use of EQ drains for liquefaction mitigation.

In the absence of earthquake performance data, field tests have been performed using small explosive charges (Rollins and Anderson, 2004; Rollins et al. 2004) or oil prospecting trucks to simulate the shaking produced by an earthquake (Rathje et al, 2004). Tests with explosive charges were performed at a site on Treasure Island in San Francisco Bay and in Vancouver, Canada with and without drains in place (Rollins et al, 2004). These tests

investigated the pore pressure dissipation properties of EQ drains and the densification produced during drain installation. At Treasure Island, drain installation in the $D_r \approx 50\%$ sand produced about 2.8% volumetric strain within the 9 m length of the drains. The drains did not prevent initial liquefaction due to the rapid loading rate (less than 2 seconds); however, the rate of dissipation was substantially increased. Post-treatment liquefaction settlements were reduced from about 100 mm in the untreated control zone to less than 25 mm in the site with drains.

At Vancouver, two test sites had drains installed with and without vibration to produce different degrees of soil densification during installation. An untreated area (without drains) was used as a control site and compared against the two test sites (Rollins and Anderson, 2002). Drain installation in the $D_r \approx 40\%$ sand produced volumetric strains of about 5% with vibration and about 1.4% without vibration along the lower 7 m length of the drains. The drains did not prevent liquefaction due to the large charge weights and the rapid load rate (less than 2 seconds); however, the rate of dissipation was significantly higher in the zone with drains. Settlement was only reduced about 20% relative to the untreated sand, but back-analyses indicated that the drains could prevent liquefaction for less intense earthquake motions.

Rathje et al (2004) conducted field tests on a 1.2 m x 1.2 m x 1.2 m volume of reconstituted saturated sand surrounded by an impervious membrane. Tests were conducted with and without a vertical drain in the center of the test volume and identical sand density ($D_r \approx 35\%$). Stress cycles were applied using a large Vibroseis oil prospecting truck and pore pressure and acceleration were measured at several points within the test volume. Plots of the measured excess pore pressure ratio with and without a drain from this test are presented in Figure 8. Without a drain, liquefaction was produced during the application of 60 stress cycles (3 second duration), while the excess pore pressure ratio did not exceed 25% for the test volume with a drain subjected to the same vibrations. Volumetric strain decreased from 2.1% without a drain to less than 0.5% with a drain in place.

The current testing, which is the subject of this report, continues the examination of the pore pressure dissipation capabilities of EQ drains and the densification caused by their installation under full-scale conditions. To better simulate an earthquake motion, the explosive charges were detonated sequentially over a 16 second period In addition, the development of downdrag and other associated aspects of the soil/pile interaction during a liquefaction event were investigated.

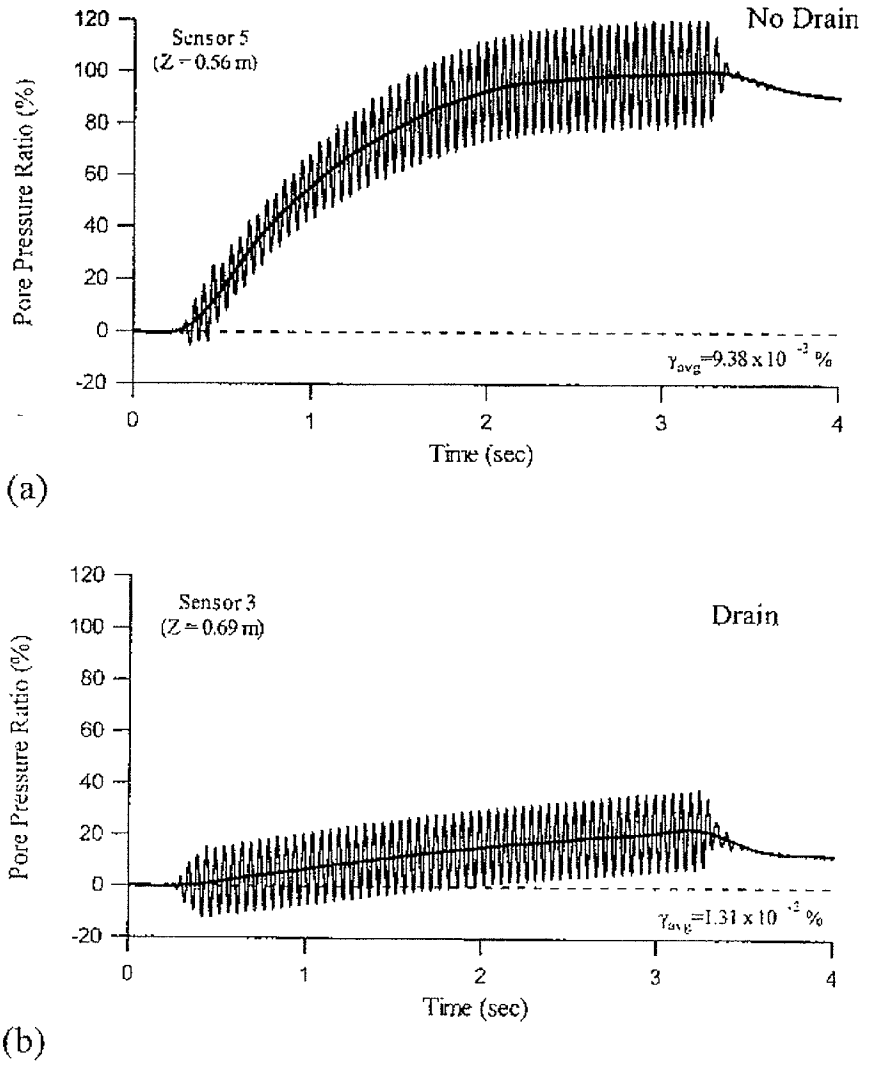

Figure 8 Excess pore pressure rato time histories induced by vibroseis seimic truck for sand volume (a) with a drain and (b) with a single drain.

1.3. Investigative Approach

As stated above, the testing has two main objectives: (1) Test the capability of the EQ drains to prevent liquefaction and associated negative consequences, and (2) Examine the soil/pile interaction, particularly the development of downdrag, during a liquefaction event. Other secondary objectives included: (i) determine the surface settlement caused by blasting and drain installation; (ii) examine the variation of settlement with depth below the ground surface; and (iii) examine the increase in soil density and strength with time associated with blasting and drain installation.

The study was organized into three major phases utilizing three test sites. Phase I consisted of preliminary blast testing and installation of EQ drains. The preliminary blast testing was designed to determine the size of explosive to be used in later tests and took place at Site 1. EQ drains were also installed at Site 3 during this phase. During Phase II steel piles were installed at Sites 2 and 3. Phase III consisted of the final blast testing at both Sites 2 and 3.

1.3.1. Earthquake Drain Testing

Sites 2 and 3 were the locations of actual blast testing. Site 2 was maintained as the control area where explosive charges would be set off to liquefy the soil. Pore pressure was monitored before, during, and after blasting to determine the rate of pore pressure dissipation without the benefit of EQ drains. After blasting was completed at Site 2, the same size explosive charges were set off at Site 3 to test the capability of the drains to dissipate pore pressures rapidly enough to prevent liquefaction. Again, pore pressures were monitored before, during, and after blasting. The pore pressures developed in Site 3 were then compared to those of Site 2 to determine the effectiveness of the drains.

1.3.2. Pile Testing

Pile foundations necessary for a load test were installed at the centers of both Sites 2 and 3. One test pile, instrumented with vertical strain gauges, was installed at the center of each site and was surrounded by four reaction piles. A reaction frame was connected to the reaction piles so that hydraulic jacks could apply axial loads to the test pile. A complete description of the construction of the test foundations is provided in Chapter 4. During blasting, a constant vertical load on the pile was maintained by the jack. Data collected from the strain gauges was then analyzed to examine the soil/pile interaction before, during, and after liquefaction.

1.3.3. Concurrent studies

Several other studies were performed concurrently with this one. These studies include: a comparison of results from static and statnamic pile load tests in collaboration with Prof. Gray Mullins at the University of South Florida; field verification of a method to perform an *in situ* vane shear test of a liquefied soil in collaboration with Prof. Travis Gerber at Brigham Young University; and field evaluation of colloidal silica grouting techniques for preventing liquefaction with Prof. Patricia Gallagher of Drexel University. Since these studies reach beyond the scope of this paper, they will not be discussed here; however, each of these studies yielded significant new findings which will appear in the technical literature in the future.

2. Site Characterization

The test sites are located on Deas Island next to the south portal of the George Massey tunnel on Route 99 near Vancouver, British Columbia, Canada as shown in Figure 9. Situated in the delta region of the Fraser River, Deas Island is formed of naturally emplaced channel and alluvial sands. The soil deposits are only about 200 years old according to studies by Monahan et al. (1995). Previous site characterization consisting of cone penetration tests, standard penetration tests, shear wave logging, and undisturbed sampling was performed during studies associated with the CANLEX project (Robertson, *et al.*, 2000, Monahan, *at al.*, 1995) along with previous research performed for the British Columbia Ministry of Transportation (Gohl, 2002)

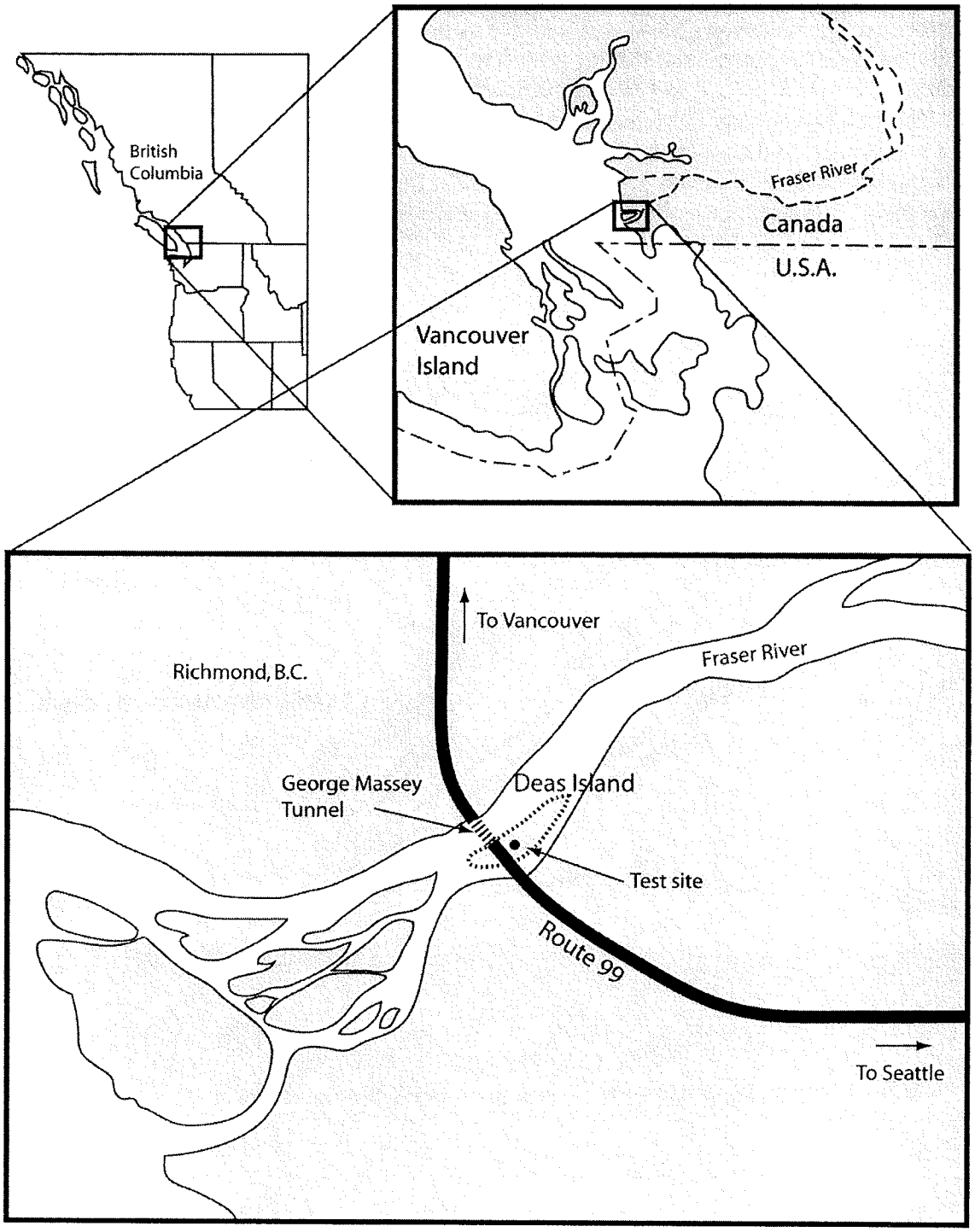

Figure 9 Location of test site

and by Rollins and Anderson (2004) with support from the IDEAS program. Similar site characterization efforts were used for this project to provide site specific data at each test location.

The area is relatively flat lying and grass covered. The centers of the three test sites lie along a line parallel to the access road approximately 18.3 m east of the road. The test sites are located approximately 150 meters south of a CANLEX Phase II test site (the Massey site) and approximately 30 meters north of the previous EQ drain test sites (see Figure 10). Figure 11 shows a detailed view of the test site layout.

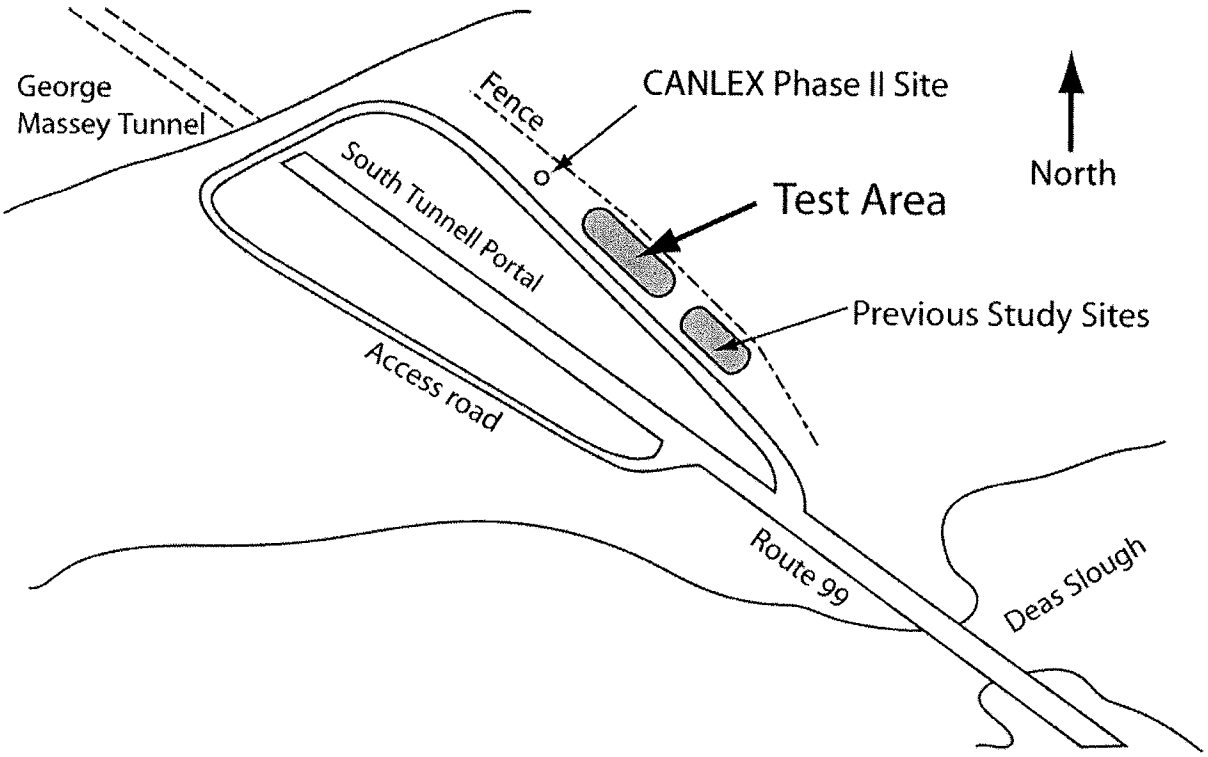

Figure 10 Relative location of the test area to previous study sites and the CANLEX Phase II site.

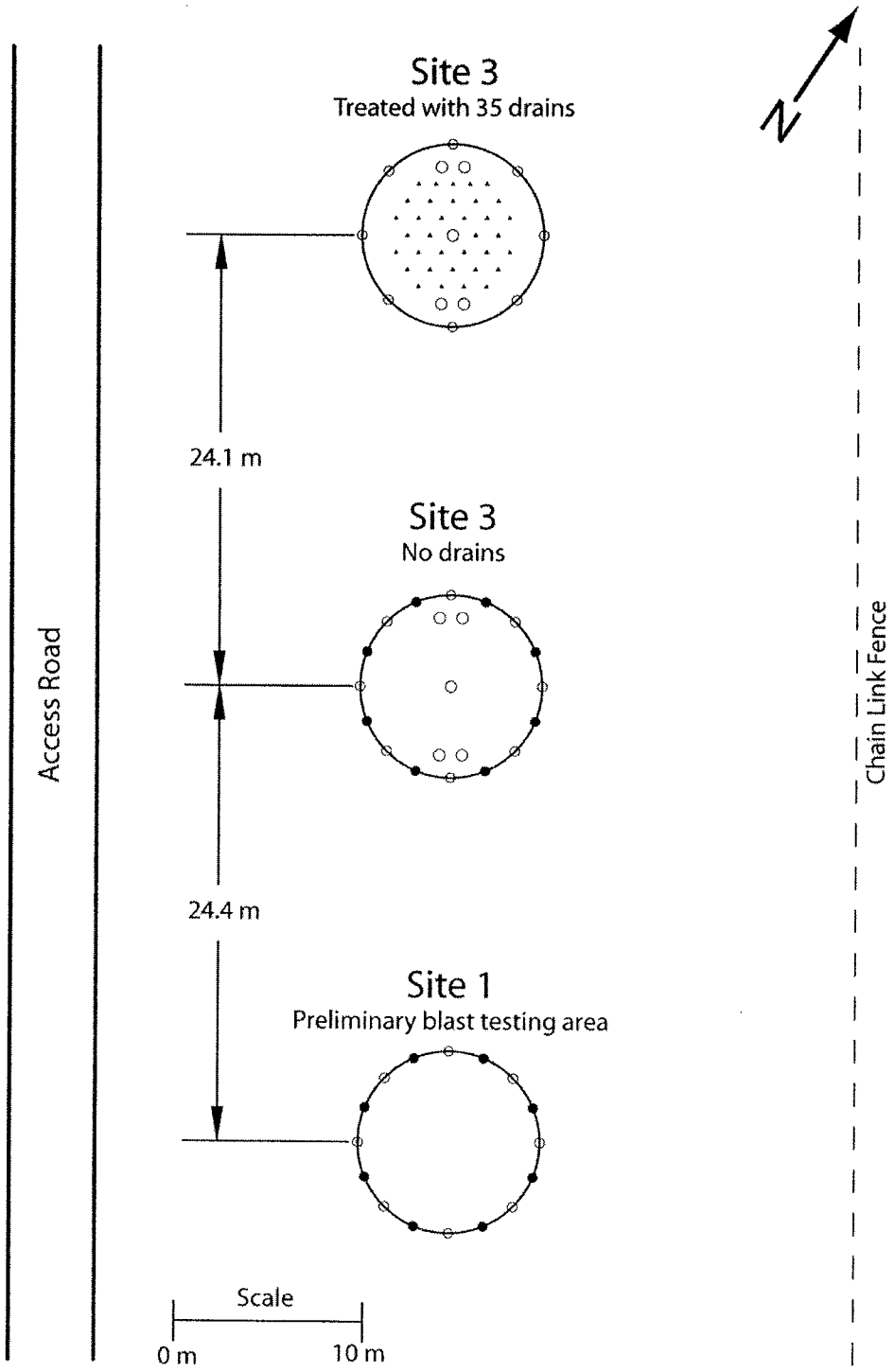

Figure 11 Detail of test site layout.

2.1. *CPT Data*

Prior to installation of any sensors, drains, or piles, cone penetration tests (CPTs) were performed by ConeTec Investigations Ltd. at the center of each of the three sites to confirm the assumed soil properties and profile. All tests used an integrated electronic piezocone and were carried out in general accordance with ASTM D-5778-95. Each test recorded tip resistance, sleeve friction, and dynamic penetration pore pressure at 0.025 m depth intervals. Relative density was estimated from CPT cone tip resistance measurements using the equation

$$D_r = \left[\frac{\left(\frac{q_c C_n}{p_a} \right)}{305} \right]^{0.5} \quad (1)$$

developed by Kulhawy and Mayne (1990), where:
D_r = relative density,
q_c = cone tip resistance
$C_n = (1/\sigma'_o)^{0.5}$
P_a = atmospheric pressure.
σ'_o = initial effective stress in tons/ft^2 or kg/cm^2

Figure 12, Figure 13 and Figure 14 show the results of the initial CPTs for Site 1, Site 2 and Site 3, respectively. The soil profile at each site was interpreted according to Robertson *et al* (1986). In general the soil profile consists of four major units (see Figure 15). The top unit, approximately 2.7 meters thick, consists of interlayered sand and silty sand. The second unit, approximately 2.8 meters thick (from 2.7 m to 5.5 m depth), consists of sandy silts, silts, and clayey silts. The third unit, approximately 9.1 meters thick (5.5 m to 14.6 m depth) consists of silty sands and sand. The target zone from 6 m to 13 m depth is contained within this unit. The fourth unit, comprising everything below 14.6 m depth, primarily consists of clean sands with some thin beds of silty sand. At Site 1 a fifth unit, consisting of silts and clayey silts was found at 20.7 m depth. Subsequent CPTs failed to reveal this unit and therefore it is unclear whether the unit actually exists or is just a very localized zone. Nevertheless, the existence of this unit is irrelevant as no drains, sensors, or piles were installed at this depth and thus this layer does not affect the study.

As will be shown, the third unit, which contains the target layer, is relatively uniform throughout the test area on Deas Island and should be susceptible to liquefaction. Figure 16 shows a comparison of cone tip resistance and relative density versus depth curves for all three sites. From the plots in this figure it can be seen that all three test sites are comparable and should behave similarly. Between 2 and 3 m below the ground surface, all three CPT soundings penetrated a relatively dense sand layer at somewhat different depths; however, apart from this layer, the average relative density is approximately 40% with a standard deviation of about 7%. In contrast, the relative density of unit 1 ranges from 50 to 70%.

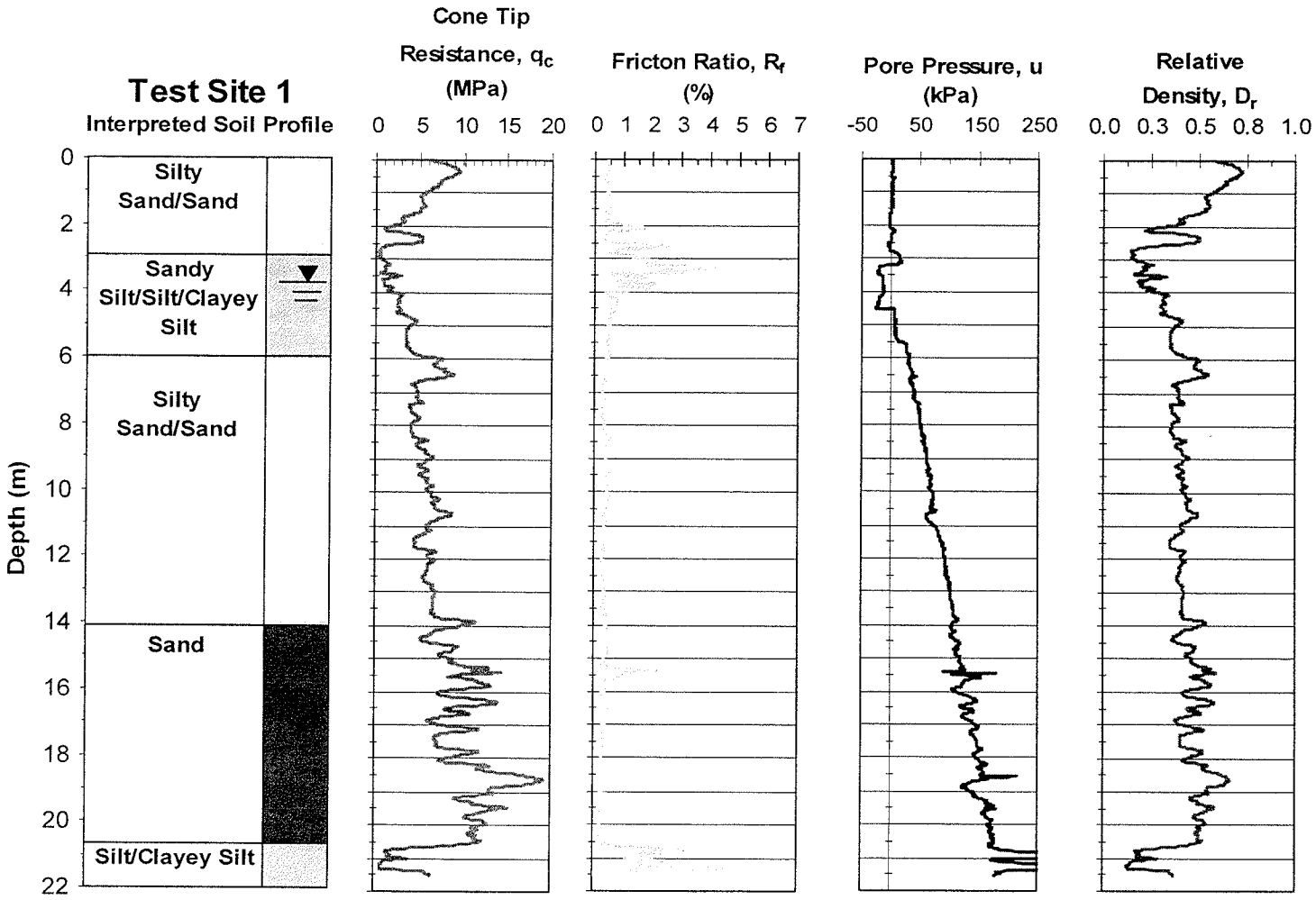

Figure 12 Initial CPT results and interpreted soil profile at Site 1.

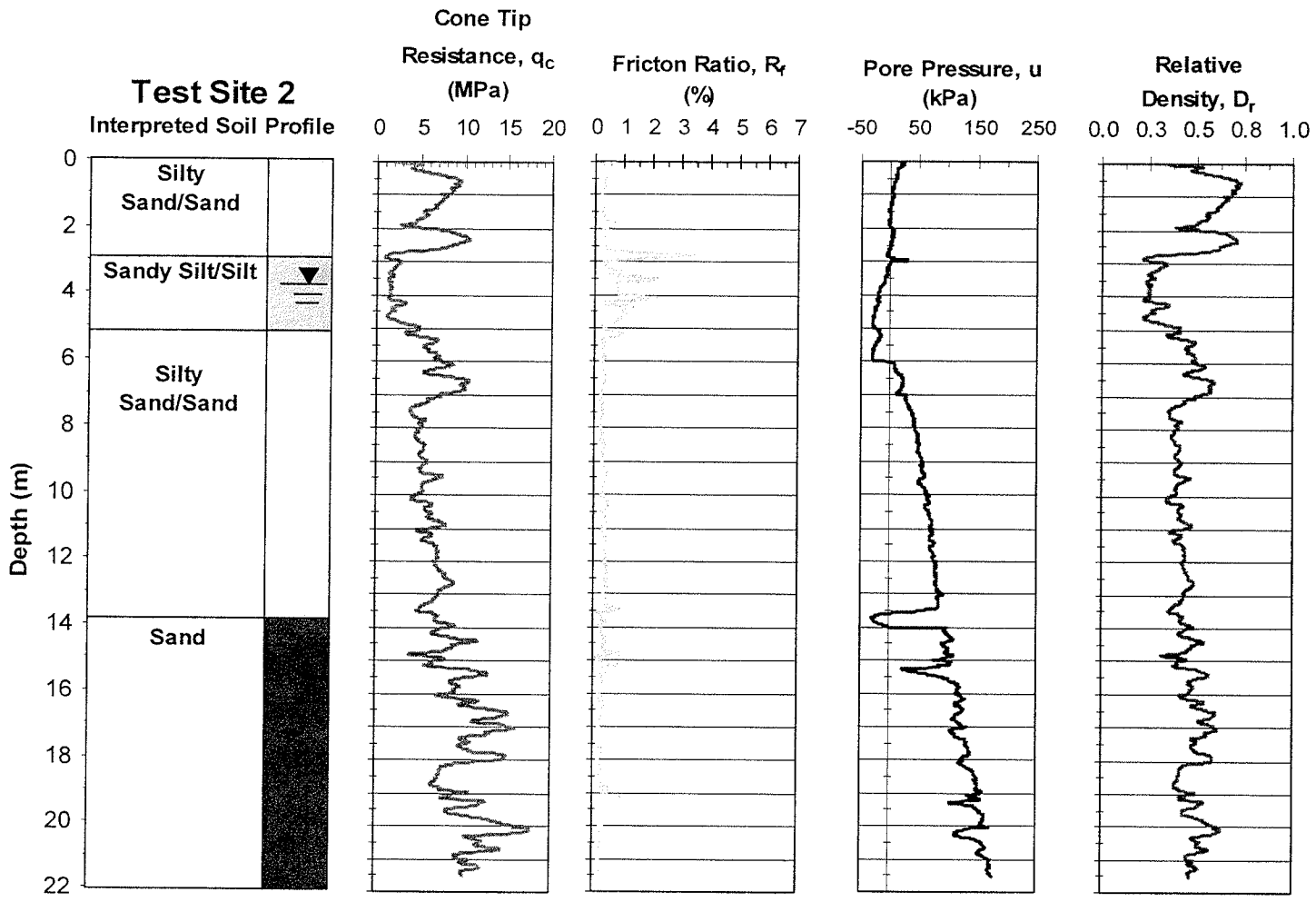

Figure 13 Initial CPT results and interpreted soil profile atSite 2.

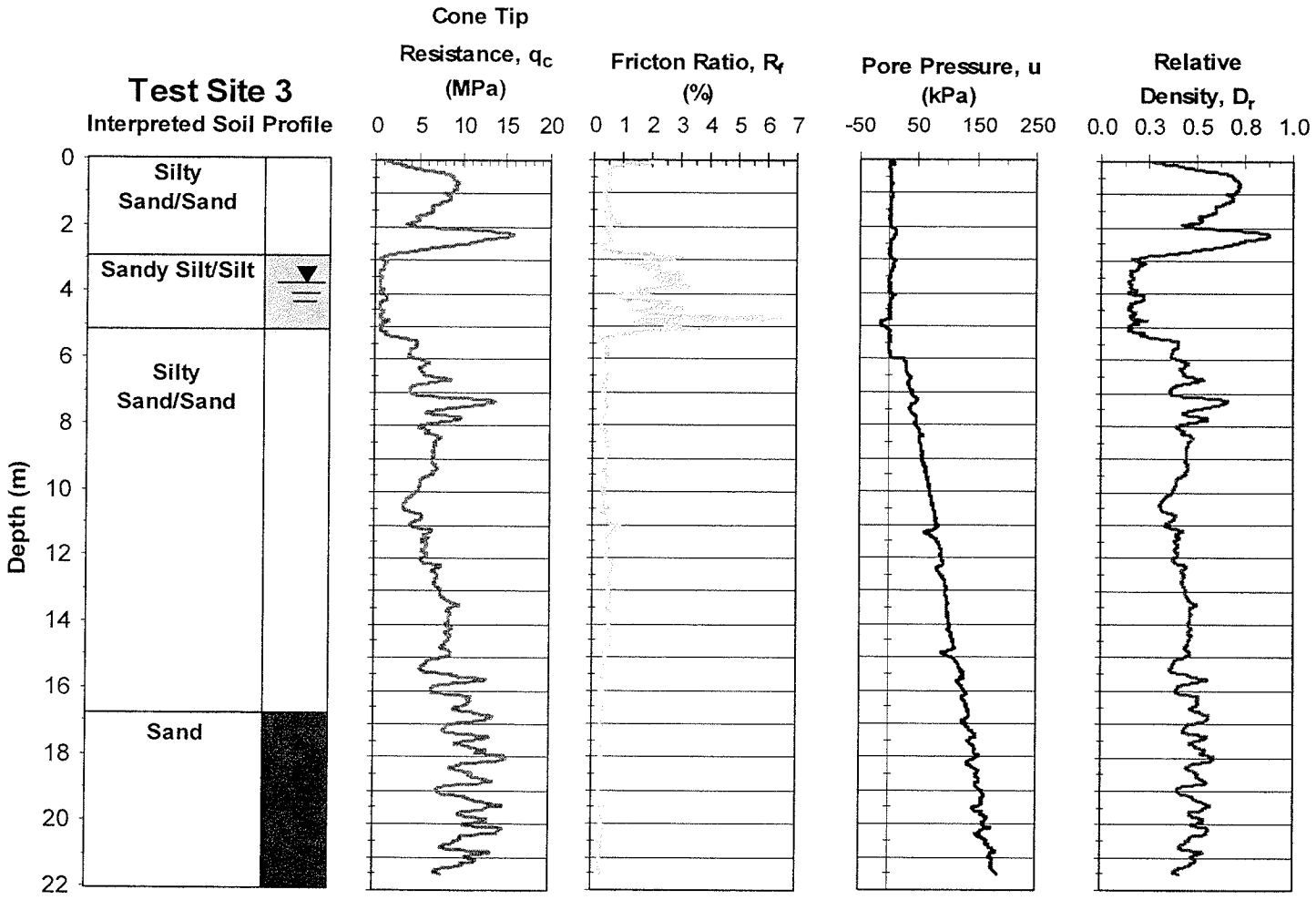

Figure 14 Initial CPT results and interpreted soil profile at Site 3.

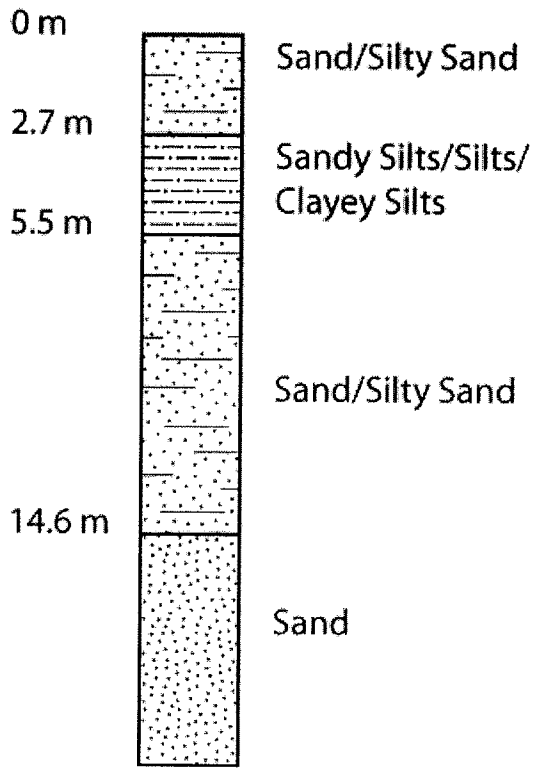

Figure 15 Generalized soil profile based on CPT tests.

2.2. Shear Wave Velocity

Shear wave velocity measurements were taken at 1 m intervals during cone penetration testing at Site 1. A shear wave was created by striking a steel I-beam coupled to the ground by the weight of the test rig with an instrumented hammer. Shear wave velocity (V_s) measurements were made in accordance with procedures described by Robertson *et al.* (1986). Figure 17 shows the results of the test at Site 1 along with V_s measurements made previously at the CANLEX project test site (Wride et al, 2000) and at a nearby test site by Rollins and Anderson (2002). The shear wave velocity profile at Site 1 for this study was quite similar to that for the CANLEX project but was somewhat higher than that measured at adjacent sites. According to Andrus and Stokoe (2000), sands with V_s values less than about 190 m/s are susceptible to liquefaction. Figure 17 shows that the target zone of Site 1 is clearly susceptible to liquefaction based on the Andrus and Stokoe criterion.

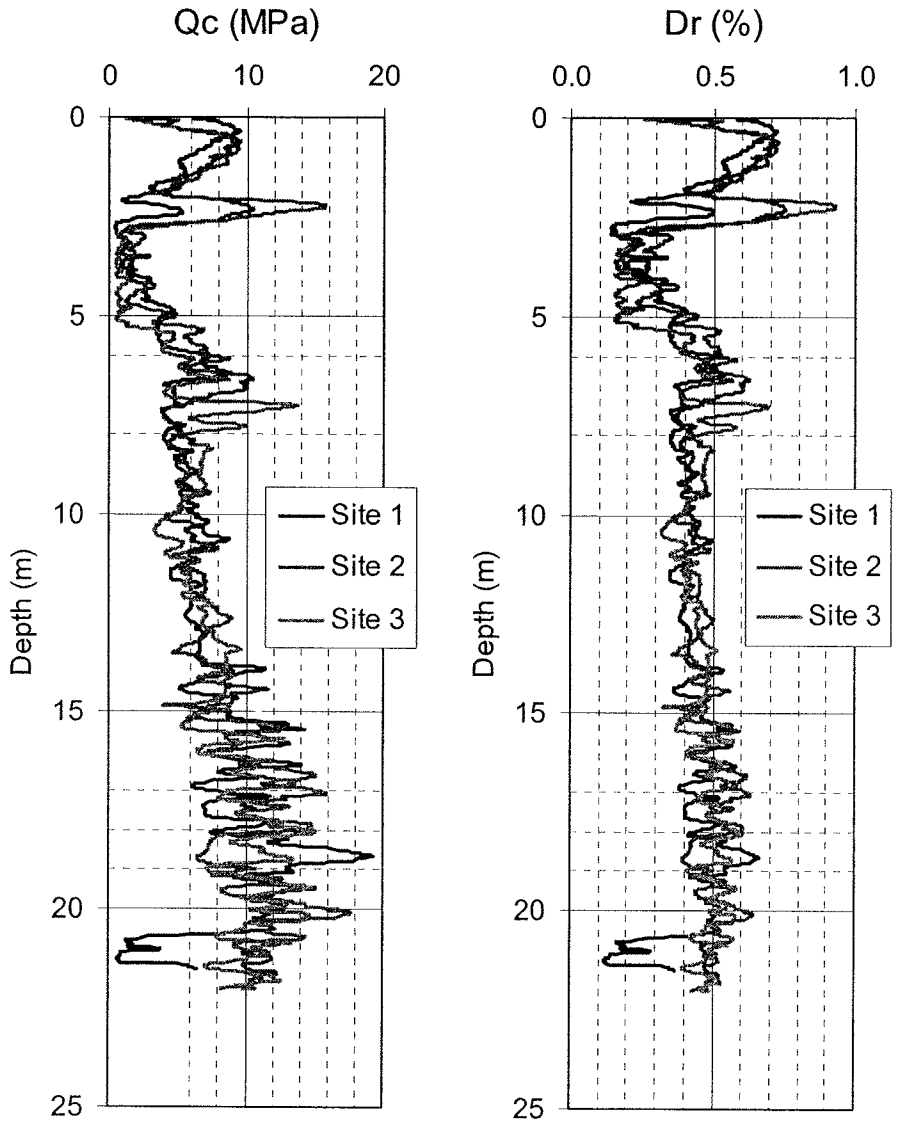

Figure 16 Comparison of cone tip resistance, Q_c, and relative density, D_r, for all three test sites from the preliminary CPT's.

During the course of sensor installation at Site 1 in preparation for preliminary blast testing, a standard penetration test was performed and a soil sample retrieved from a depth interval of 7.93 meters to 8.38 meters. Another sample was retrieved during the course of blast-hole installation from a depth estimated to be between 7.5 meters to 10 meters. Sieve analyses were performed on these two samples and the grain size distribution curves are plotted in

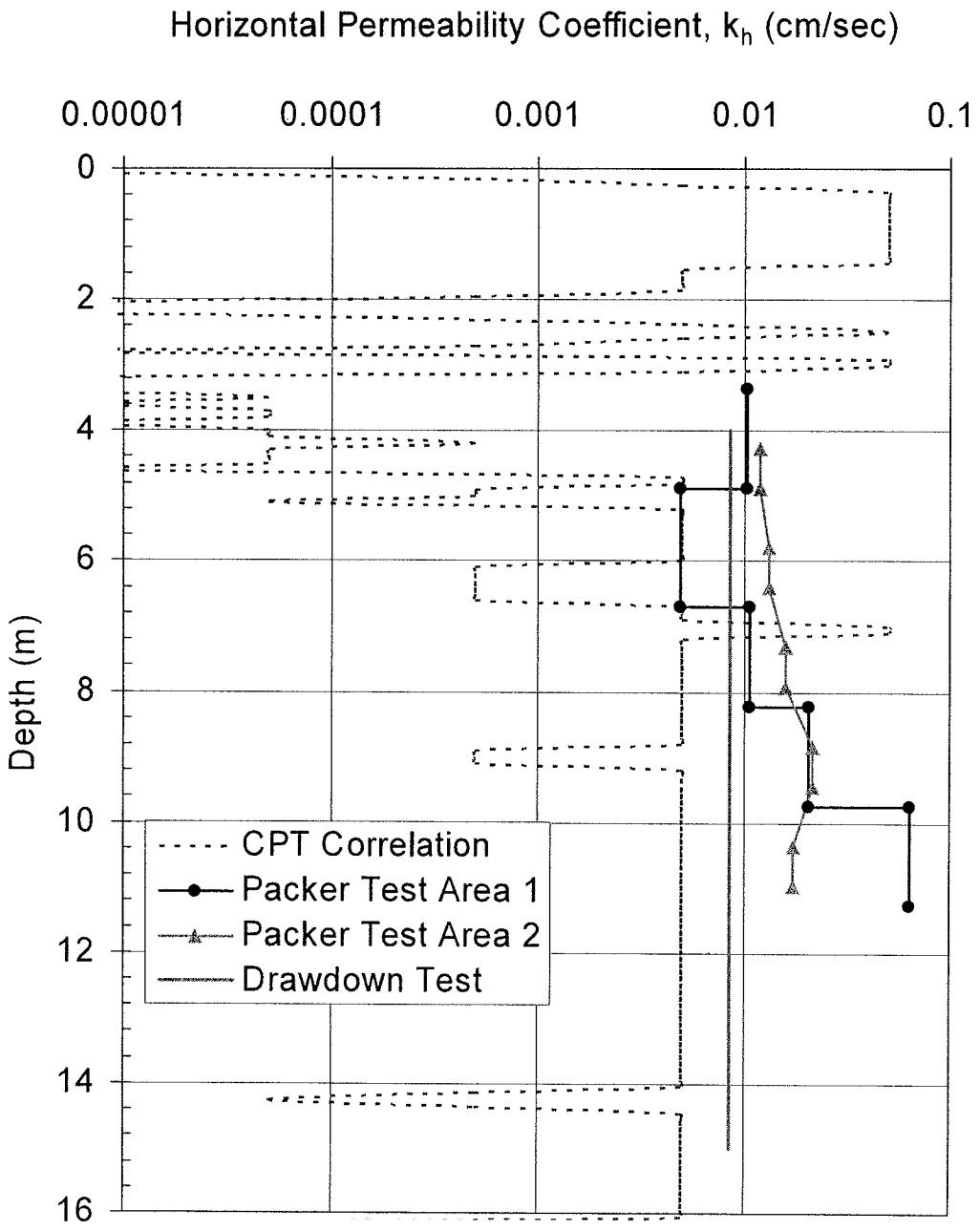

Figure 18 Horizontal permeability versus depth curve obtained from several test near the test site.

Figure 20. The boundaries plotted in Figure 19 are re-plotted in Figure 20 for reference. Both samples were quite similar, consisting almost entirely of fine grained sand with a fines content of 10% or less. Both of these samples classify as SP-SM and plot near the upper boundary as reported by Gohl (2002). Samples of the sand from the upper 0 to 1.33 m of the profile were obtained from a hand excavated test pit adjacent to Site 2. Grain size distribution curves for these samples obtained from laboratory testing are plotted in Figure 21. Grain size boundary curves are re-plotted again for reference. These samples classified as SP type soils and were very similar to the sands from 5.5 to 11.5 m. A sample of the silty- and clayey-sands found in Unit 2 was recovered in a Shelby tube. Grain size distribution analyses were performed on the sample and the results are also plotted in Figure 21.

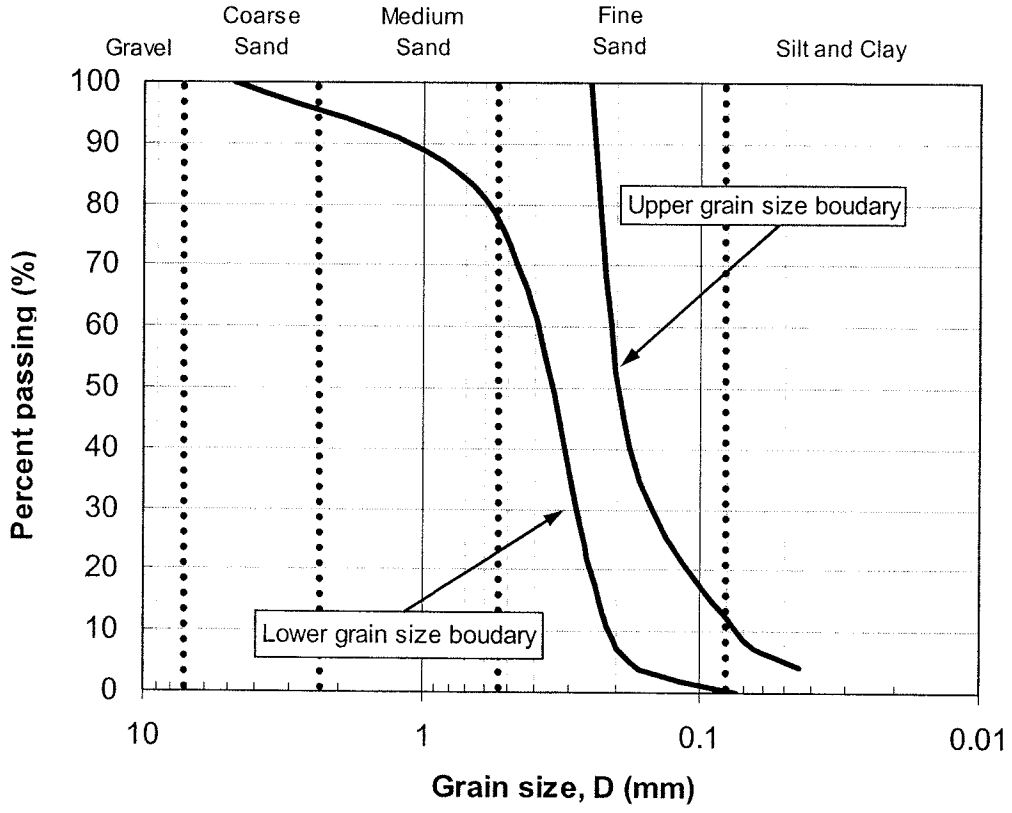

Figure 19 Range of grain size distributions for Fraser River sand in the target zone according to Gohl (2002).

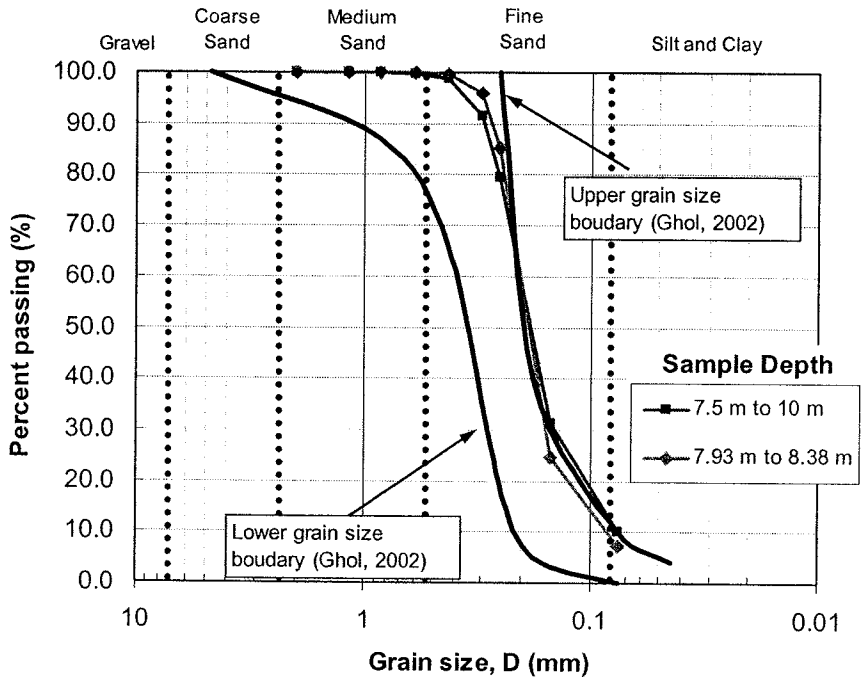

Figure 20 Grain size distribution curves for samples recovered during sensor and drain installation at Site 1 relative to boundaries provided by Gohl (2002)..

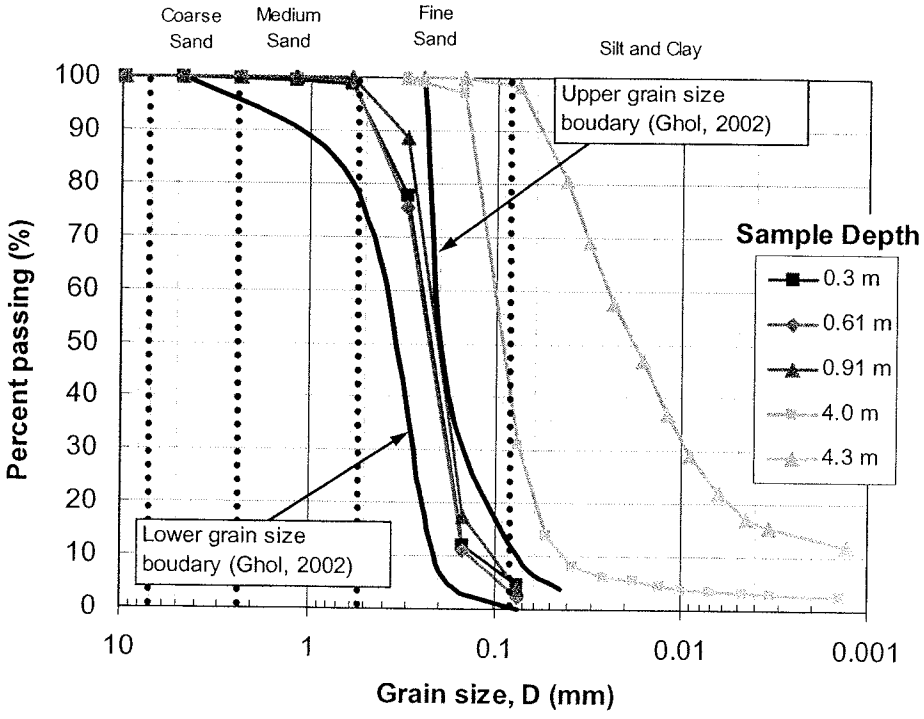

Figure 21 Grain size distribution curves for soil samples recovered from hand-excavated pit and shelby tube.

2.5. *In-situ Density and Moisture Content*

A variety of tests were performed to better define the unit weights of the soil layers in the profile. The dry unit weight and natural moisture content of the sands in the upper 1.4 m of the profile were determined by nuclear density gauge tests performed by Trow Inc. in the same hand-excavated trench from which the samples discussed above were taken. A summary of the test results is presented in Table 1.

Table 1 Summary of in-situ unit weight and moisture content for top 1.40 meters of soil at test site.

Depth (m)	Dry Unit Weight, γ_d (kN/m^3)	Natural Moisture content, w (%)	Moist Unit Weight, γ (kN/m^3)
0.100	12.24	12.7	13.79
0.200	12.69	11.4	11.14
0.400	13.56	7.3	14.55
0.500	14.63	6.1	15.52
0.700	14.00	8.1	15.13
0.800	13.78	7.7	14.84
1.000	14.15	10.9	15.69
1.100	14.07	10.5	15.55
1.300	11.95	20.7	14.43
1.400	12.92	16.3	15.07
Average	13.40	11.17	14.57

The unit weight and natural moisture content of the more fine-grained materials within unit 2 were obtained from thin-walled "Shelby" tube samples obtained from a depth between 4.0 and 4.4 m at the test site. Test results are listed in Table 2.

Table 2 Summary of in-place weight and moisture content for unit 2 at Vancouver test site.

Depth (m)	Dry Unit Weight γ_d (kN/m^3)	Moisture content w (%)	Moist Unit weight, γ (kN/m^3)	USCS Symbol
4.0-4.2	13.78	33.1	18.34	SM
4.2-4.4	13.09	41.3	17.98	ML
Average	13.44	37.2	18.16	

Finally, unit weights for the poorly graded sands (unit 3) in the target zone from 6 to 13 m were evaluated based on previous CANLEX testing. In this unit, the in-place void ratio was computed from two geophysical soundings along with a number of undisturbed frozen samples. A plot of the void ratio versus depth in this layer is provided in Figure 22. The void ratio in the depth range from 6 to 13 m typically ranges from about 0.9 to 1.1 with an average value of approximately 0.95. With a measured specific gravity of 2.68, this average void ratio translates into a dry unit weight of 13.5 kN/m^3, a moisture content of 35.4% and a saturated unit weight of 18.5 kN/m^3.

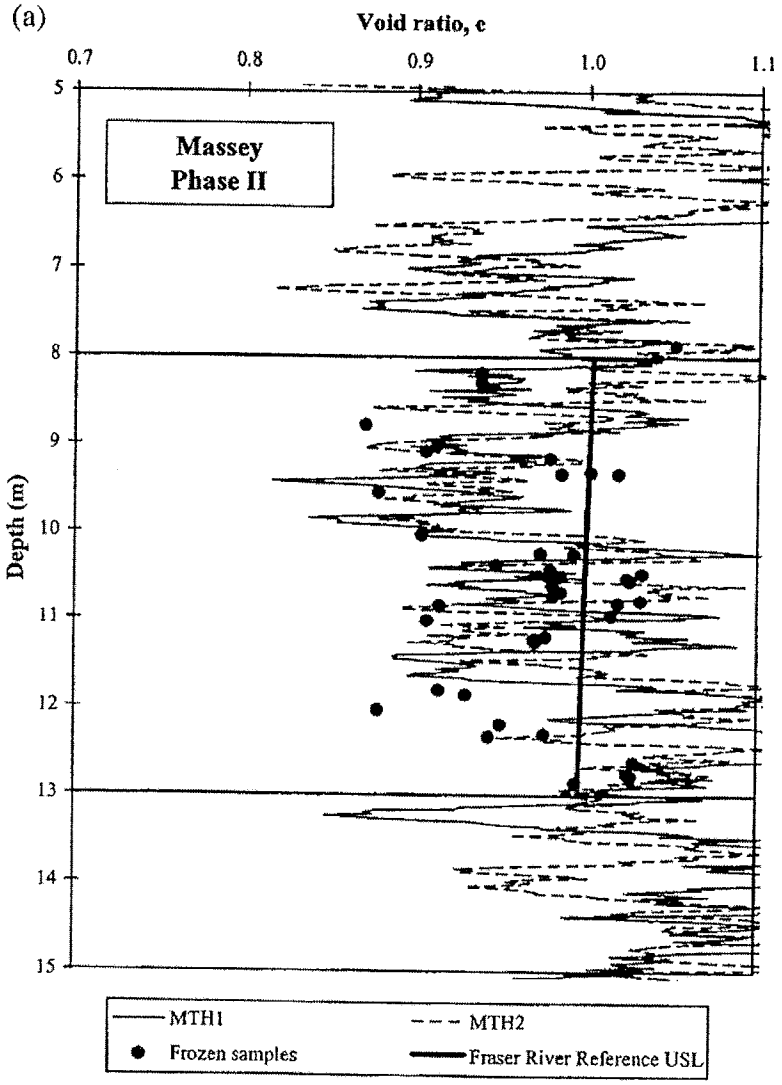

Figure 22 Void ratio versus depth curves developed as part of the CANLEX study.

2.6. SPT Blow Count Correlations

As part of the CANLEX project, site specific correlations between CPT q_c and $(N_1)_{60}$ values were developed. For the Massey site (the CANLEX site approximately 300 m north of the test site), the average value of $q_c/(N_1)_{60}$ was 0.58 with a standard deviation of 0.17 (Wride et al, 2000). At Site 1, an average value of q_c equal to 5.6 MPa in the target layer results in an estimated $(N_1)_{60}$ value of approximately 10. For Sites 2 and 3, average q_c values in the target zone were 5.5 MPa and 6 MPa respectively and also have estimated $(N_1)_{60}$ values of about 10. According to Youd et al (2001), soils with $(N_1)_{60}$ values less than about 25 to 30 are susceptible to liquefaction during earthquakes. Accordingly, all three test sites should be liquefiable.

3. Pilot liquefaction Testing at Test Site 1

As indicated in section 1.2, previous testing used explosive charges large enough to overwhelm the ability of the EQ Drains to dissipate the pore pressures. Rather than inducing liquefaction in a couple seconds with one or two large charge detonations, a better simulation of an earthquake event would be produced with sequential detonation of smaller charges with a duration of 10 to 16 seconds. Ideally, the explosive charges would be sized such that they would induce liquefaction in the untreated area without overwhelming the drains in the treated area. Accordingly, Site 1 was chosen as the location to carry out preliminary blast tests in order to determine the appropriate size of charges. These tests were monitored for changes in pore pressure, ground movement, and settlement.

3.1. Test blasting design

Three separate blast tests were used in the pilot testing. In the first test, a total of 24, 0.227 kg (1/2 lb) explosive charges were placed in eight blast holes, three charges in each hole. The eight blast holes were equally spaced around a circle 10 meters in diameter (see Figure 23). The blast holes were created by vibrating the earthquake drain pipes into the ground. The explosive charges in each hole were placed into three levels or "decks". The lowest deck was placed at 10.1 m depth; the middle deck at 8.5 m depth; and the top deck of charges at 6.4 m depth. Each charge consisted of Pentex explosive, which is a commercial form of Pentolite 50/50. Pentolite 50/50 is an organic explosive compound consisting of 50% pentaerythritol tetranitrate (PETN) and 50% trinitrotoluene (TNT), with excellent water resistance characteristics. In addition, Pentex is resistant to sympathetic detonation from other charges. Gravel stemming was packed in between the charges to prevent premature detonation and direct the energy of each charge radially, rather than just vertically. All handling, installation, wiring, and detonation of the explosives were handled by professional, licensed blasters. The explosives were detonated sequentially, with a one-second delay between charges using two electrical blasting boards. Blasting began in the bottom deck and proceeded upwards, with all charges in a deck being detonated before continuing to the deck above.

The first blast series generated pore pressures much less than expected. This appears to be a result of the blast hole installation as discussed subsequently. When the first blast test generated less than expected pore pressures, a second blast test was performed to determine the increase in pore pressure produced by an individual charge. Thus, the second blast test consisted of a single, 1.135 kg (2.5 lb) explosive charge placed at 8.5 m depth in the blast hole indicated in Figure 23.

With the results of the first two blast tests, the third blast test was performed using 1.36 kg (3 lb) charges. A total of 21 charges were placed in three decks in the seven blast holes as indicated in Figure 23. Detonation of the charges followed the same procedure used in the first test. The third blast test indicated that the 1.36 kg charges would provide the desired results.

3.2. *Blast Hole Installation*

Blast holes were installed using the same procedure as that used to install the EQ drains, as described subsequently in Section 6.2. The drain hose, geosynthetic fabric and anchors used for the blast holes were identical to those used for the drains. The only difference in installation procedure was the use of a smooth mandrel (without fins). A smooth mandrel was used to avoid excessive vibration of the surrounding soil during insertion. Another concern was the potential for collapsing a nearby blast hole. Any collapse of the blast hole would render it useless. The smooth mandrel was of the same outside diameter as the finned mandrel but the wall thickness was only 9.5 mm rather than 25 mm. During drain insertion with hanging leads, it was difficult to maintain verticality and rotation of the mandrel occurred which fractured the connection between the mandrel and the vibratory hammer. Fortunately another smooth mandrel was on hand and blast hole installation was only temporarily delayed.

The use of the drains kept the blast hole open, allowing the explosive charges and gravel stemming to be positioned as desired. For the first blast test eight holes were installed in a circular patter with a 5 meter radius, 45 degrees between each hole (see Figure 23). After the first blast another eight blast holes were installed in a similar manner. This second set of holes was rotated 22.5 degrees from the first set. Unfortunately, rotation of the mandrel during the

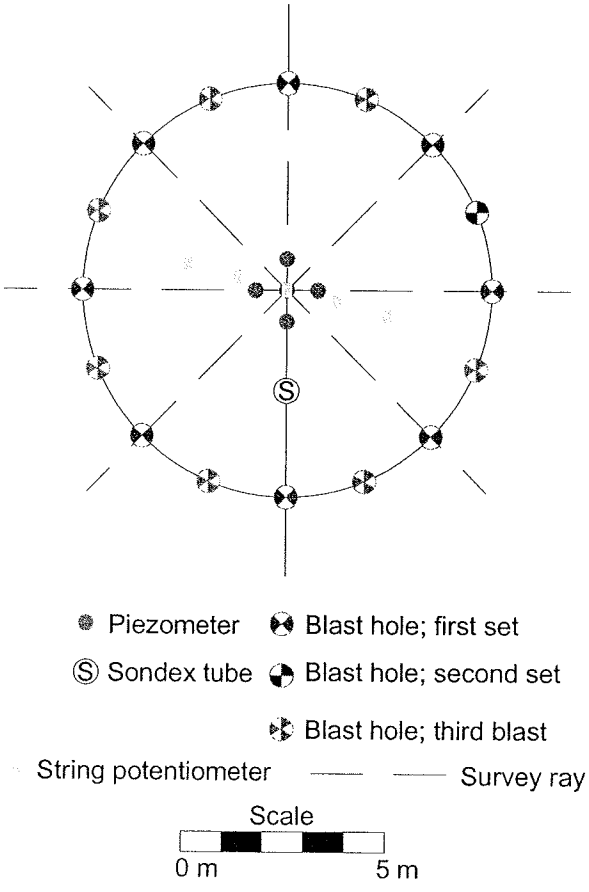

Figure 23 Layout of blast holes and instrumentations

drain installation procedure also appears to have created small gaps around the periphery of the drain pipe which appear to have reduced the energy transmitted by the explosive charge to the surrounding sand. In addition, the perforations in the drain pipes may have allowed more gas to be injected into the surrounding sand during the detonation process than with a solid casing.

3.2.1. Blast hole installation induced settlement

A level survey was conducted immediately after installation of the first set of eight blast holes. At two individual points around the blast holes settlement was measured to be 15 mm. In general, however, settlement was generally less than 9 mm which is about twice the measurement error of the survey.

3.3. Pore Pressure Monitoring

Figure 23 shows the locations of the various types of sensors and instruments used to monitor the preliminary blast testing. Pore pressures were monitored using six piezometers located at depths of 5.5 m, 7.6 m, 9.5 m, 11.6 m, and 13.7 m (two piezometers were installed at 7.6 m). One piezometer was located at the center of Site 1; four more were located 0.76 m from the center, spaced 90 degrees apart. The sixth piezometer was 6.22 m from the center. This sixth piezometer was used mainly in conjunction with the *in situ* vane shear test mentioned in the introduction. For clarity, the location of the vane shear apparatus and the sixth piezometer are not included in Figure 23 and results from this piezometer will not be discussed in this report.

The piezometers consisted of a pore pressure transducer encapsulated in a hard nylon protective body as shown in Figure 24. The transducers were designed to withstand a transient blast pressure of up to 41.4 MPa and then record the residual pore pressure with an accuracy of ± 0.7 kPa. The transducer was screwed into a hard nylon cone tip with ports open to the surrounding ground water. These ports were packed with cotton and boiled to remove any free air prior to assembly with the transducer. The transducer/cone tip assembly was then screwed into the hard nylon protective body and the complete assembly installed to the desired depth. A steel cable attached to the protective body provided a means to withdraw the piezometer once the testing was complete.

To determine the degree of pore water pressure generation and whether liquefaction occurred, the excess pore pressure ratio was calculated from the data for each piezometer. The excess pore pressure ratio (R_u) is simply the increase in pore pressure above the static pressure caused by the blasting as measured by the piezometer divided by the initial effective stress at the level of the piezometer. In mathematical terms, $R_u = \Delta u/\sigma'_o$. An excess pore pressure ratio of one ($R_u = 1.0$) indicates full liquefaction. Accurate evaluation of R_u depends upon an accurate estimate of the effective stress which in turn depends upon accurate measurements of soil unit weights and depth to the water table.

Values of R_u for the preliminary blast testing were calculated using a moist unit weight of 14.72 kN/m^3 for Unit 1, and saturated unit weights of 18.16 and 18.2 kN/m^3 for Units 2 and 3, respectively based on field and laboratory testing as described in Section 2.5.

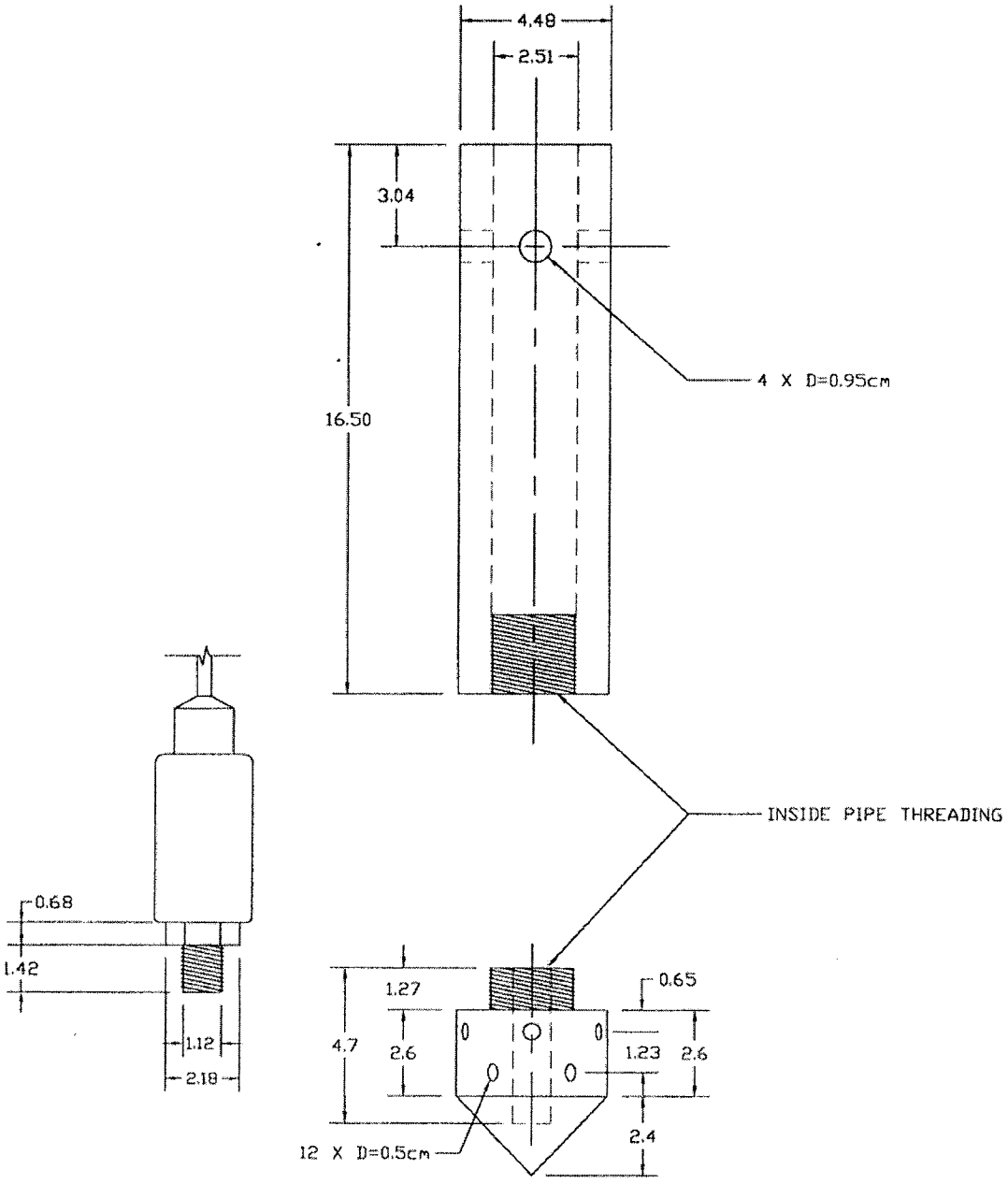

Figure 24 Schematic drawing of pore pressure transducer and hard nylon protective body (after Rollins and Anderson, 2004).

The piezometers were installed using a rotary drill rig to first drill to 0.3 m above the desired depth. Drilling mud consisting of bentonite slurry prevented the hole from collapsing. The sensor was then pushed the remaining 0.3 m to the desired depth using the drill rod. A special adapter was used to connect the piezometers to the drill rod. All piezometers were successfully extracted once testing was completed.

3.4. Settlement

Settlement was monitored using three methods. Total ground surface settlement was measured using a level survey. In addition, five string potentiometers measured the real-time settlement. Finally, settlement as a function of depth was measured using a "Sondex tube" as described later in section 3.4.3.

3.4.1. Total ground surface settlement

Total ground surface settlement was measured using conventional survey equipment to conduct a level survey. Elevation measurements were made before and after each event that may have produced settlement (such as instrument installation, blast tests, etc.) and the resulting ground surface settlement calculated. Measurements were made at regular intervals along eight rays emanating from the center and spaced 45 degrees from each other. Survey points were spaced at 0.91 m intervals for the first 4.57 meters and then at 1.54 m intervals out to 18.3 meters (see Figure 23). Occasionally obstructions prevented measurements at each point along the array.

3.4.2. Real-time settlement

Ground surface settlements caused by the blast tests were monitored using five string potentiometers attached to a tensioned, steel cable strung above the test site. The cable was anchored beyond the edges of the test site in an effort to prevent the blast testing from causing the cable to sag. The string potentiometers were spaced 1.2 meters apart along a line through the center of the test site (see Figure 23). The middle potentiometer was located over the center of the test site. Real-time settlement was measured during the first and third blasting events.

3.4.3. Depth-related settlement

In addition to the surface settlement measurements, settlement as a function of depth was also investigated with a Sondex tube. The Sondex tube consisted of a 7.6 cm diameter non-perforated corrugated hose inside a sleeve of geosynthetic material and an anchor. The geosynthetic fabric and anchor were of the same type used for the EQ drains. Before covering with the geosynthetic material, thin steel bands that fit in between the corrugations were secured tightly around the outside of the hose at approximately 0.76 m intervals and wrapped with electrical tape. After tying the anchor on to the bottom of the hose with the geosynthetic, the assembly was then installed with the vibratory hammer and a smooth mandrel to a depth of 11 meters. The use of the smooth mandrel will be discussed more fully in section 4.3.

The depth to the steel bands was determined using a Sondex probe which indicated the location of each steel band magnetically. A length of 6.35 cm diameter schedule 40 PVC pipe was slipped down the center of the corrugated hose and seated firmly at the bottom of the hole. The PVC pipe provided a consistent pathway for the Sondex probe and prevented the collapse of

the corrugated tubing. The top of the PVC pipe also served as a reference point for making depth measurements. The flexibility of the plastic drain pipe was such that it could shorten as the surrounding soil settled. The change in depth of the steel bands then revealed how settlement developed with depth. Sondex tubes were also installed at Sites 2 and 3 with this same procedure; however, both tubes collapsed within 6 meters of the surface, preventing any measurements. Later, during the installation of the test pile foundations, Sondex tubes were installed at Sites 2 and 3 using conventional rotary drilling equipment.

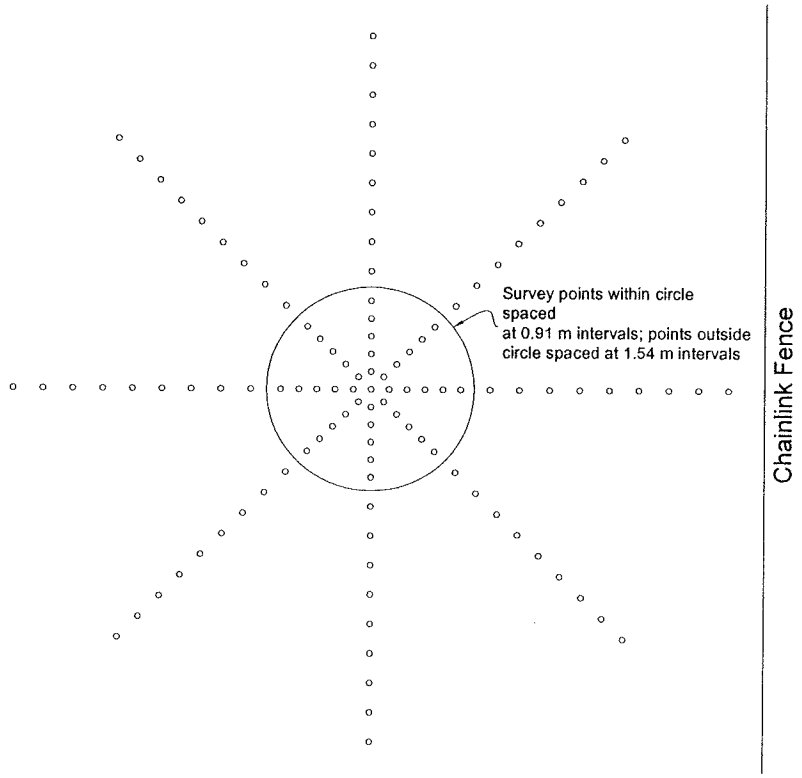

Figure 25 Schematic sketch of survey measurement points layout used at each of the three test sites to monitor total ground surface settlement.

3.5. Results of preliminary blast testing at Site 1

3.5.1. Blast induced excess pore pressure

Figure 27 shows plots of excess pore pressure ratio time histories measured by each of the transducers during the first blast. The plots in Figure 27 are limited to the first 30 seconds so that pore pressure generation due to each individual blast can be clearly identified. For each blast a large transient pressure pulse was produced followed by an increased residual excess pore pressure which remained relatively constant until the next charge was detonated. While the sequential blasting did produce a significant progressive increase in the pore pressure ratio, the peak residual values did not exceed about 0.70. Therefore, liquefaction was not achieved in this blast sequence. The R_u time histories for most of the piezometers were relatively similar; however, R_u values for the deepest piezometers were somewhat lower because they were further

away from the blast charges in general and the sand at this depth was also denser. Complete time histories showing both the generation and dissipation of R_u are plotted in Figure 28. R_u values decreased to about 0.1 within 3 minutes for the lowest piezometer and 10 minutes for the uppermost piezometer. Dissipation progressed more slowly near the top of the soil profile, likely due to the presence of the overlying silty clay layer (Unit 2) which would provide an impervious boundary or at least impeded drainage.

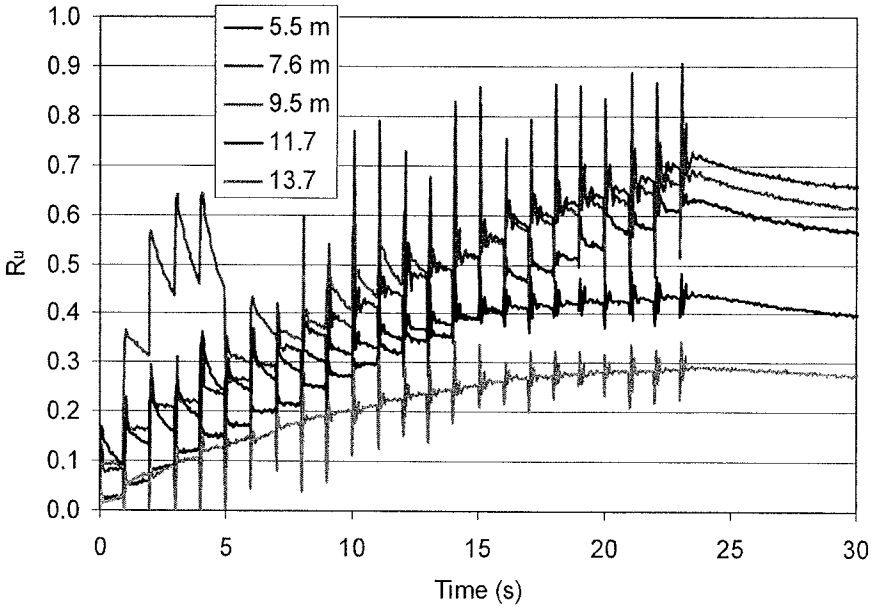

Figure 26 Generation of pore pressure during the first blast test at Site 1.

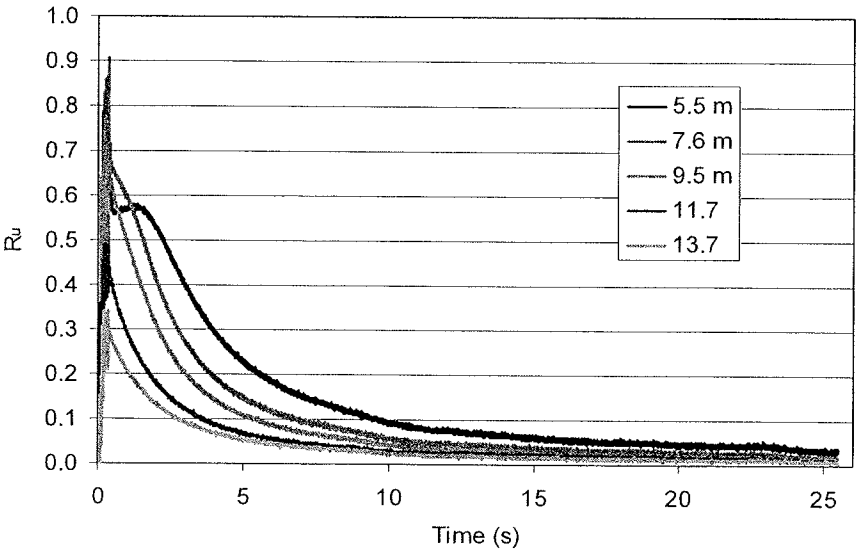

Figure 27 Dissipation of pore pressure after the first blast test at Site 1.

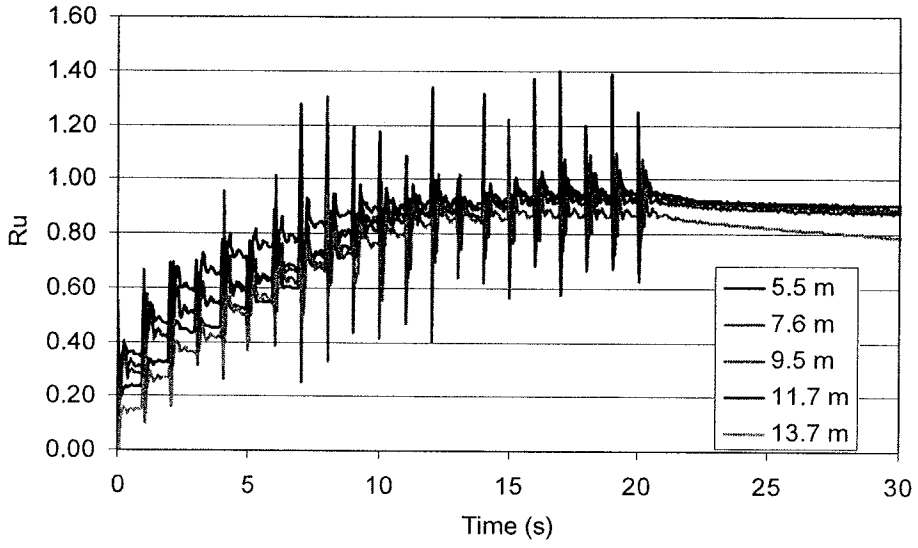

Figure 28 Generation of pore pressure during the third blast test at Site 1.

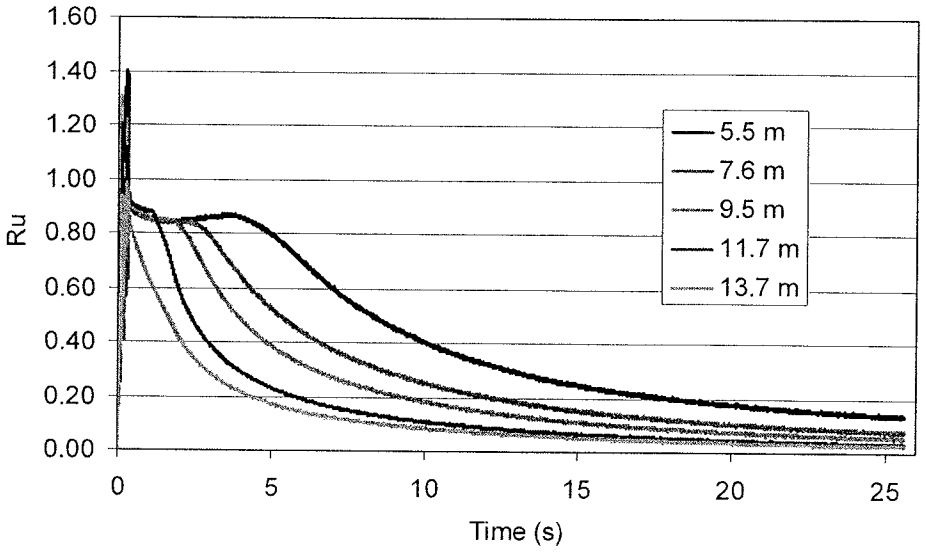

Figure 29 Dissipation of pore pressure after the third blast test at Site 1.

Figure 28 and Figure 29 depict the generation and dissipation of pore pressures during and after the third blast test at Site 1, respectively. As can be seen in these figures, both the generation and dissipation curves have the same general shapes as the corresponding curves for the first blast test. For the third blast test, the maximum excess pore pressure ratios generally exceeded 0.9 indicating that the soil had essentially liquefied. The effectiveness of each charge detonation in generating excess pore pressure appears to decrease with the number of detonations and relatively little extra pore pressure increase was observed after about 16 charges had been detonated.

R_u values decreased to about 0.1 for the bottom-most piezometer within approximately 10 minutes. Pore pressures were not recorded long enough after the third blast test for the R_u values measured by the top-most piezometer to decrease to the same level. Interpolating beyond the end of recording, R_u would likely have decreased to 0.1 by about 35 minutes after blasting.

It is obvious that the larger explosive charges generated larger pore pressures which took longer to dissipate than those associated with the first blast test. Again, pore pressures dissipated most rapidly in the lower layers and most slowly near the surface, indicating that the clayey-silt layer acted to decrease the rate of pore pressure dissipation.

3.5.2. Blast induced settlement

Settlement was measured during blasting using five string potentiometers as described above to monitor real-time settlement caused by the blasting. Figure 30 shows time histories of the ground surface settlement measured in real-time by the string potentiometers. All the potentiometers indicate that settlement started very soon after the blasts began and terminated at about 7.5 minutes after blasting, when the excess pore pressure ratio for the bottom four piezometers had decreased below 0.4 and R_u for the top piezometer was about 0.6. The plots indicate that maximum settlement was approximately 110 mm. Maximum settlement was somewhat greater on one side than the other but generally decreased with distance from the center. The shapes of the settlement curve are all consistent. Close examination of the curves shows that some of the surface settlement occurred in a step-wise fashion. Two major events are apparent; the first at about 6.5 minutes and the second at about 7.5 minutes. The vertical part of the steps is possibly caused by the collapse of soil bridges which could temporarily arch over the settling sand at depth.

Figure 31 shows the real-time settlement due to the third test blast at Site 1. Again the settlement occurred very soon after blasting and essentially ended within 10 minutes after blasting. Maximum settlement was approximately 400 mm and occurred at the center potentiometer settlement typically decreased with distance from the center point.

Figure 32 shows a contour map of the total blast induced settlement. As expected, the maximum settlement (approximately 110 mm) occurred near the center and the contours are generally concentric about the center. Plots of average settlement versus radial distance from the center of the site are shown in Figure 33 and Figure 34 for the first and third test blasts, respectively. In both cases, beyond a distance of approximately 10 m from the center the surface experienced little to no settlement.

A discrepancy was observed between total settlement measurements made by the string potentiometers and the level survey as shown in Figure 35 for the first blast. In general, the string potentiometers measured about 20 mm less settlement than the level survey for the first blast test and 80 mm less settlement for the third blast test (see Figure 35 and Figure 36). In both cases, the difference is about 20%. The level survey was made as soon as possible after the blasting. The possibility that the missing 20 mm of settlement occurred after the survey is refuted by the flat-line trend shown by the string potentiometer data that occurs after about 550 seconds. The smaller total settlement measured by the string potentiometer was likely due to a reduction in tension in the cable resulting from minor movement in the support anchors. A relaxation of the cable tension results in greater sag and less measured settlement.

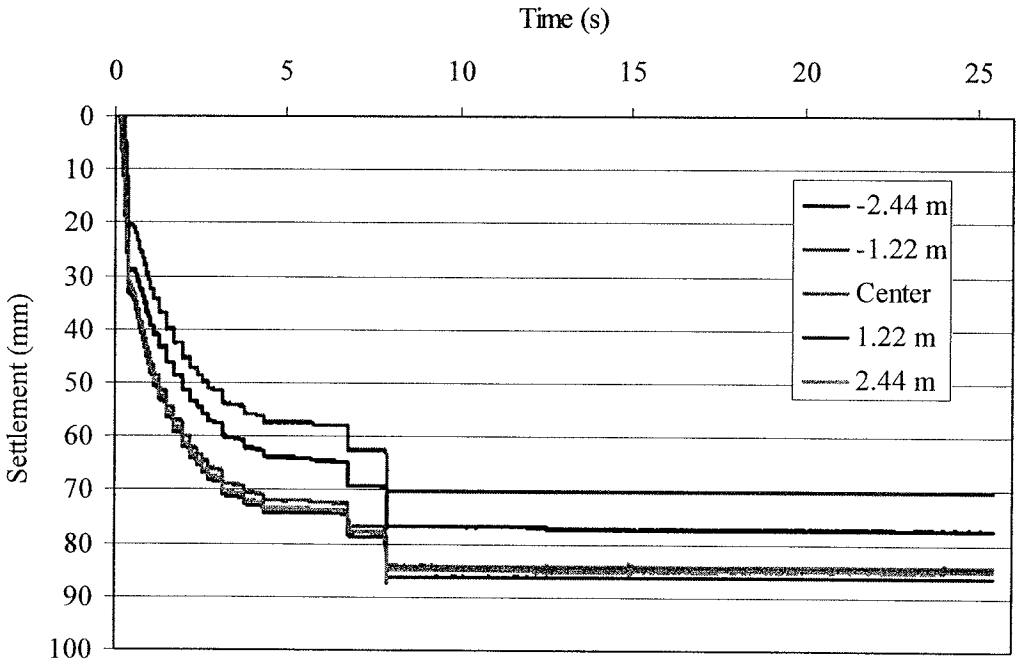

Figure 30 Time history of real-time ground surface settlement measured by the string potentiometers for the first blast test at Site 1.

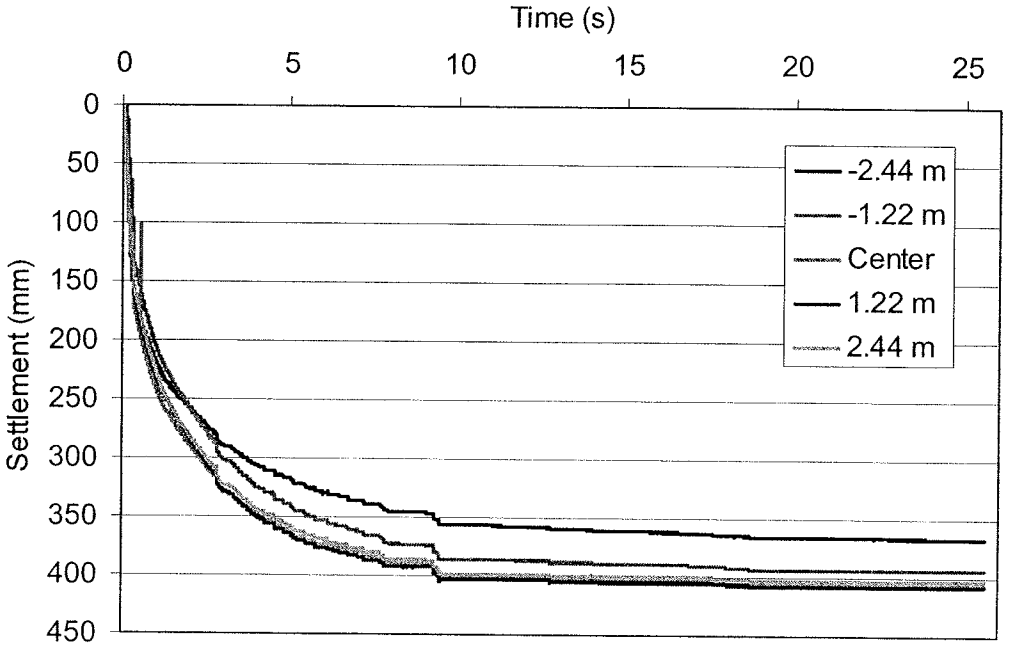

Figure 31 Real-time ground surface settlement time history recorded during the third blast test at Site 1.

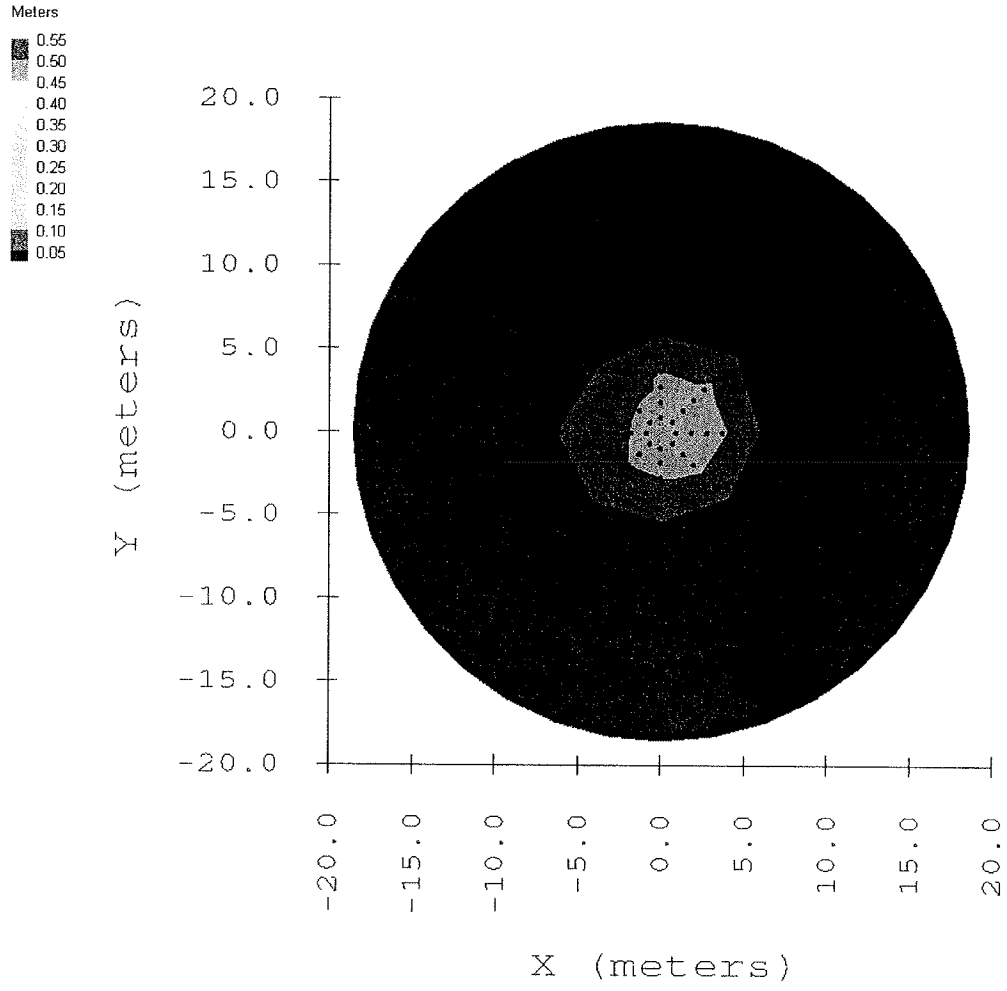

Figure 32 Contour plot of ground surface settlement resulting from the first test blast at Site 1.

The settlement profiles obtained from the Sondex probe for both the first and third test blasts are plotted in Figure 37. The settlement increases relatively linearly within the target zone where excess pore pressures were developed by the blasting, but remains nearly constant in the upper portion of the profile. For the first blast test, the settlement was nearly constant for the upper 2 m; for the third blast test the settlement was nearly constant in the upper 4 m. This profile indicates that the top layer is essentially settling as a unit due to settlement of the underlying sand layer. The top layer (0 to 5.5 m) consists of an unsaturated sand layer and a clayey silt layer, both of which would be relatively insensitive to blast induced pore pressure generation. Therefore, the settlement profile seems to match the behavior expected for the soil profile. The maximum ground surface settlement obtained from the Sondex probe was about 130 mm for the first blast. Compared to the 100 mm of settlement measured by the level survey, the Sondex measured about 30 percent more settlement. For the third blast test, the maximum ground surface settlement measured by the Sondex tube was 360 mm. The ground surface settlement at the location of the Sondex tube as measured by the level survey was approximately 375 mm which is only about 4 percent higher.

Because the Sondex tube extended only to 11 m, it did not fully penetrate the target zone and the bottom of the tube experienced significant settlement. The depth at which settlement would be expected to end was approximated by extending the lower portion of the settlement profiles linearly to zero settlement (refer to the red dashed lines in Figure 37). As can be seen in Figure 37, the extensions of both profiles indicate that settlement should end at approximately 14 meters depth. Since settlement would be expected to end at the bottom boundary of the liquefied zone, the interpolated lines indicate that the lower boundary of liquefaction should occur at about 14 m depth for this blast sequence.

Since the bottom of the Sondex tube experienced significant settlement, it is difficult to calculate the volumetric strain for the entire layer caused by the blast testing. However, using 14 m depth as a lower bound, the average volumetric strain from 6 m to 14 m depth can be estimated. Accordingly, the volumetric strains are approximately 0.7 percent and 5 percent for the first and third test blasts respectively.

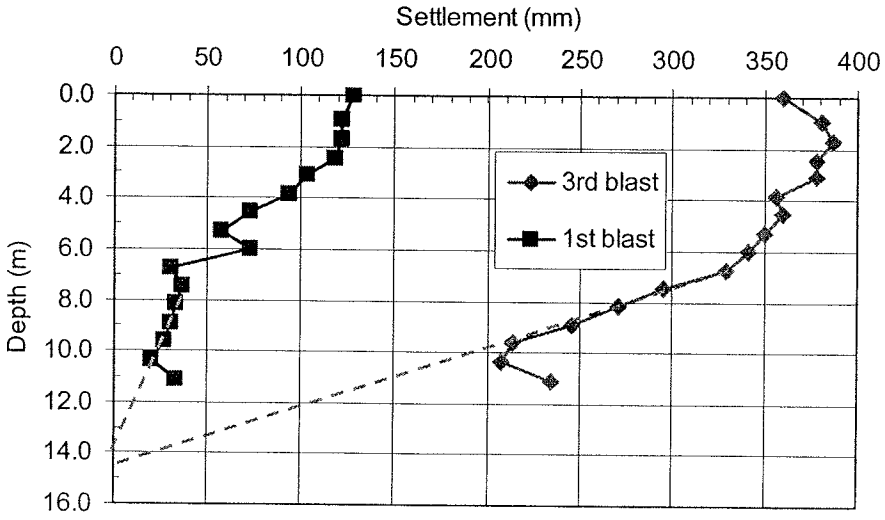

Figure 37 Settlement as a function of depth as measured with the Sondex tube for the first and third blast tests at Site 1.

4. Pile Foundation Design, Instrumentation and Installation

As indicated in Section 1.3, one of the major objectives of this study was to examine the interactions between a pile foundation and the surrounding soil during and after a liquefaction event. Of particular interest was the development of negative skin friction during and immediately following a liquefaction event due to settlement and reconsolidation of the liquefied layer.

In a pile foundation, the external load, i.e., the load from the overlying structure, is supported by the shaft and toe resistance of the pile. Shaft resistance is the shear force developed between the side of the pile and the surrounding soil, commonly called skin friction. Toe resistance is the bearing force developed at the base of the pile. This force is, of course, much larger for closed-toe piles than for open-ended piles.

Under normal conditions, the axial load applied to a pile causes the pile to move downward relative to the surrounding soil. Skin friction that resists downward movement of the pile is termed positive skin friction ("positive" because it acts upward, or in the positive direction). Skin friction becomes fully mobilized after a relative displacement of 2 to 5 mm.

If the ground around a pile settles relative to the pile for some reason, negative skin friction can develop. Settlement relative to the pile can occur due to placement of additional fill load, long term consolidation of a clay layer, a drop in groundwater elevation, or liquefaction induced settlement. As the soil around the pile settles, it tends to "hang" on the pile, transferring a downwardly oriented load to the pile, termed "dragload". Negative skin friction develops in the upper portion of the pile and the resulting dragload plus the applied load is counteracted by pile resistance (positive skin friction and end bearing) in the lower portion of the pile. The location at which negative skin friction turns to positive skin friction is called the neutral plane

Since skin friction is proportional to effective stress (Fellenius, 1998), during a liquefaction event, the skin friction in the liquefied layer should drop to zero causing a redistribution of forces in the pile and surrounding soil. As the excess pore pressure dissipates, the liquefied layer reconsolidates and settles around the pile, imparting a dragload on the pile. Any soil overlying the liquefied layer would also settle, which should cause negative skin friction to develop in this layer as well. As pore pressures return to static levels, the neutral plane continually readjusts, maintaining force equilibrium.

4.1. Pile Foundation Design and Installation

Figure 38 is a plan view of the pile foundations installed at Sites 2 and 3; Figure 39 is a profile view. The foundations consisted of an instrumented test pile in the center of the test site flanked by four reaction piles which supported the reaction frame. The pipe piles conformed to ASTM 252 Grade 3 specifications. The outer diameter was 324 mm (12.75 in) and the wall thickness was 9.5 mm (0.375 in). A 37.5 mm thick plate was welded to the bottom of the test piles to close the end prior to driving. Using the 0.2 percent offset method, the yield strength of the piles was specified to exceed 400 MPa (57,000 psi). The reaction piles were spaced at about 3.65 m on either side of the test pile which is a spacing greater than 11 pile diameters. This spacing exceeds requirements from ASTM and FHWA standards. The two reaction piles were spaced between 1.2 and 1.8 m apart. Hydraulic jacks placed between the center test pile and the

reaction frame exerted an axial force on the pile, simulating the load exerted by an overlying structure.

The foundations were instrumented to provide all the necessary data. The test piles were instrumented to measure strain at 13 depth intervals along the length of the pile. Load cells placed between the reaction frame and the hydraulic jacks monitored total applied load. Finally, string potentiometers measured pile head deflection as load was applied.

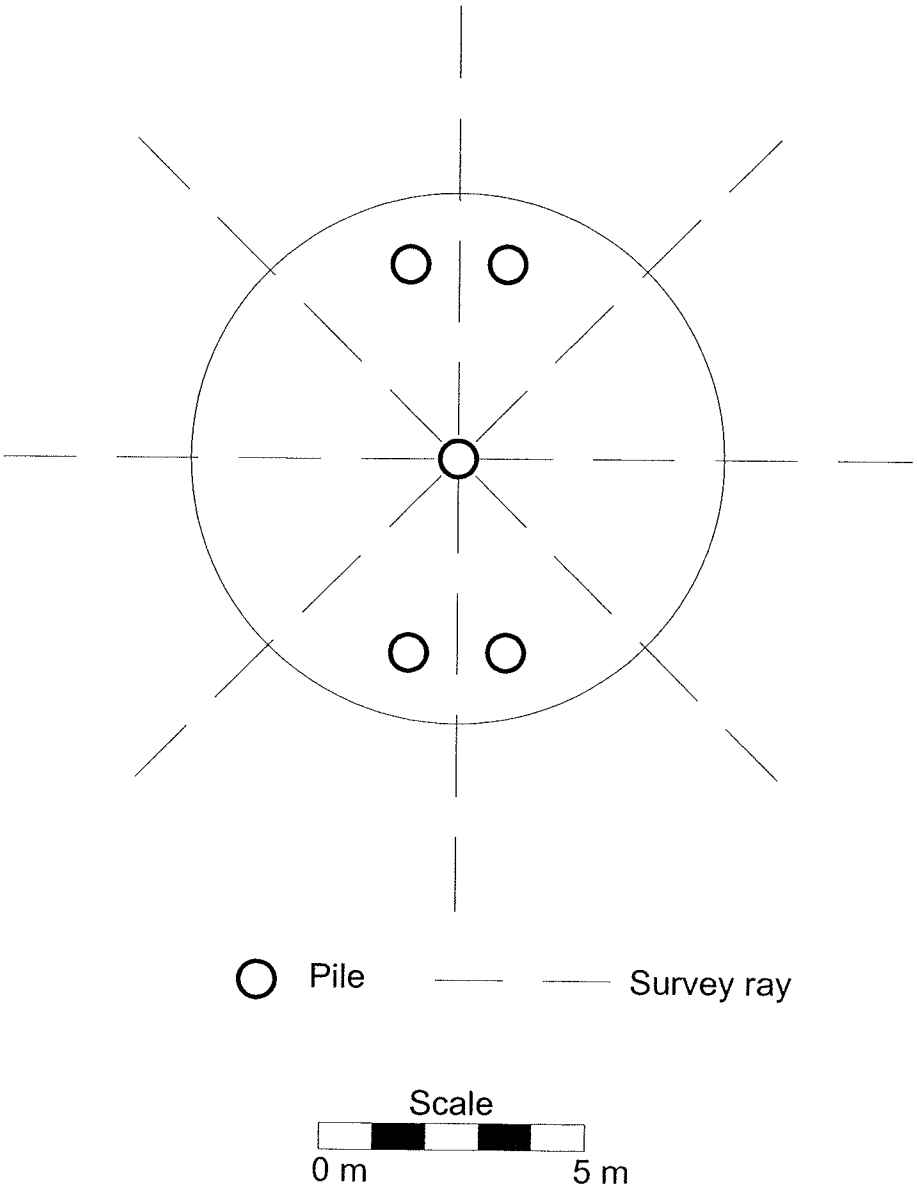

Figure 38 Plan view of pile foundation installed at both Sites 2 and 3.

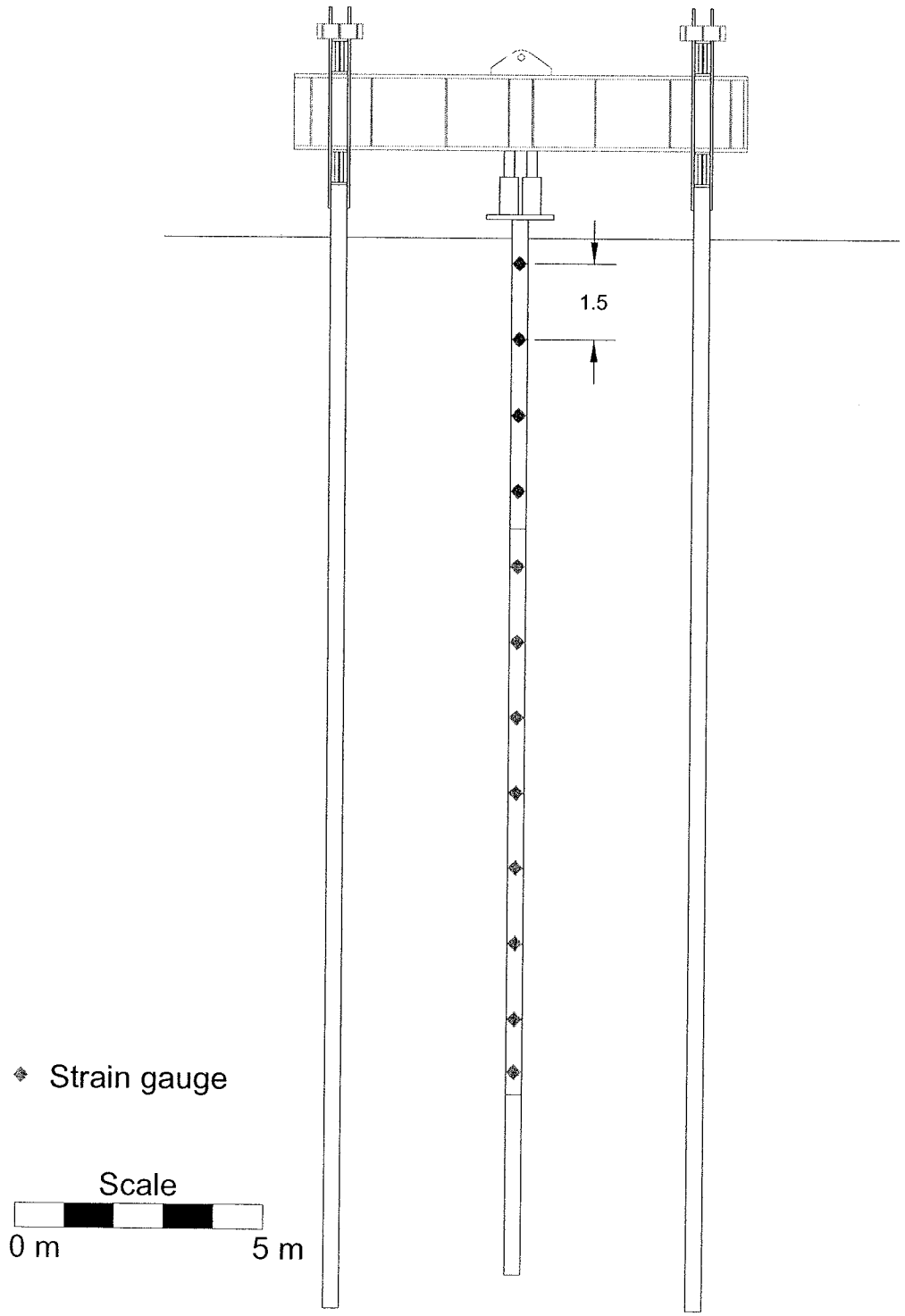

Figure 39 Profile view of pile foundation installed at both Sites 2 and 3.

Table 3 Values of Cs used in the Eslami and Fellenius method to compute unit side friction.

Soil Type	Soil Description	Range of C_s	Avg. C_s
1	Soft sensitive soils	0.0737 – 0.0864	0.080
2	Clay	0.0462 – 0.0556	0.050
3	Stiff clay and mixture of clay and silt	0.0206 – 0.0280	0.025
4	Mixture of silt and sand	0.0087 – 0.0134	0.010
5	Sand	0.0034 – 0.0060	0.004

The unit end-bearing is given by the equation

$$q_p = (q_{c1} q_{c2} q_{c3} \cdots q_{cn})^{1/n} \tag{6}$$

where q_{ci} is each cone tip resistance within the zone from eight pile diameters above the pile tip to four pile diameters below the tip and n is the number of cone resistance values in that zone. This geometric mean value for the end-bearing pressure helps minimize the influence of large peaks and troughs in the cone resistance near the pile tip.

Plots of the side resistance and total resistance versus depth for the test piles at Sites 2 and 3 predicted by the LCPC and the Eslami and Fellenius methods are provided in Figure 42 and Figure 43, respectively. In both figures, the predicted pile resistance is very similar for Sites 2 and 3; however, the resistance predicted by the Eslami and Fellenius method is significantly higher than that predicted by the LCPC method. The average unit skin friction and end-bearing values predicted by these two equations for various layers in the profile are summarized in Table 4. Although the predicted side resistance values are reasonably similar, the end-bearing resistance predicted by the Eslami and Fellenius approach is nearly three times higher than that predicted by the LCPC method. Therefore, the large difference between the predicted ultimate loads is largely due to differences in interpreting end-bearing resistance.

Table 4 Summary of unit side friction and end-bearing resistance predicted by LCPC and Eslami and Felleius methods for layers in the soil profile at test sites.

Soil Layer	Resistance Type	LCPC Unit Resistance (kPa)	Eslami & Fellenius Unit Resistance (kPa)
Fine Sand (0-2.7 m)	Side Friction	24.9	42.0
Silty Clay (2.7-5.5 m)	Side Friction	30.9	33.5
Sand to Silty Sand (5.5-14.6 m)	Side Friction	24.6	31.1
Sand to Silty Sand (14.6-21 m)	Side Friction	27.2	44.1
Sand to Silty Sand (21 m)	End-Bearing	340	860

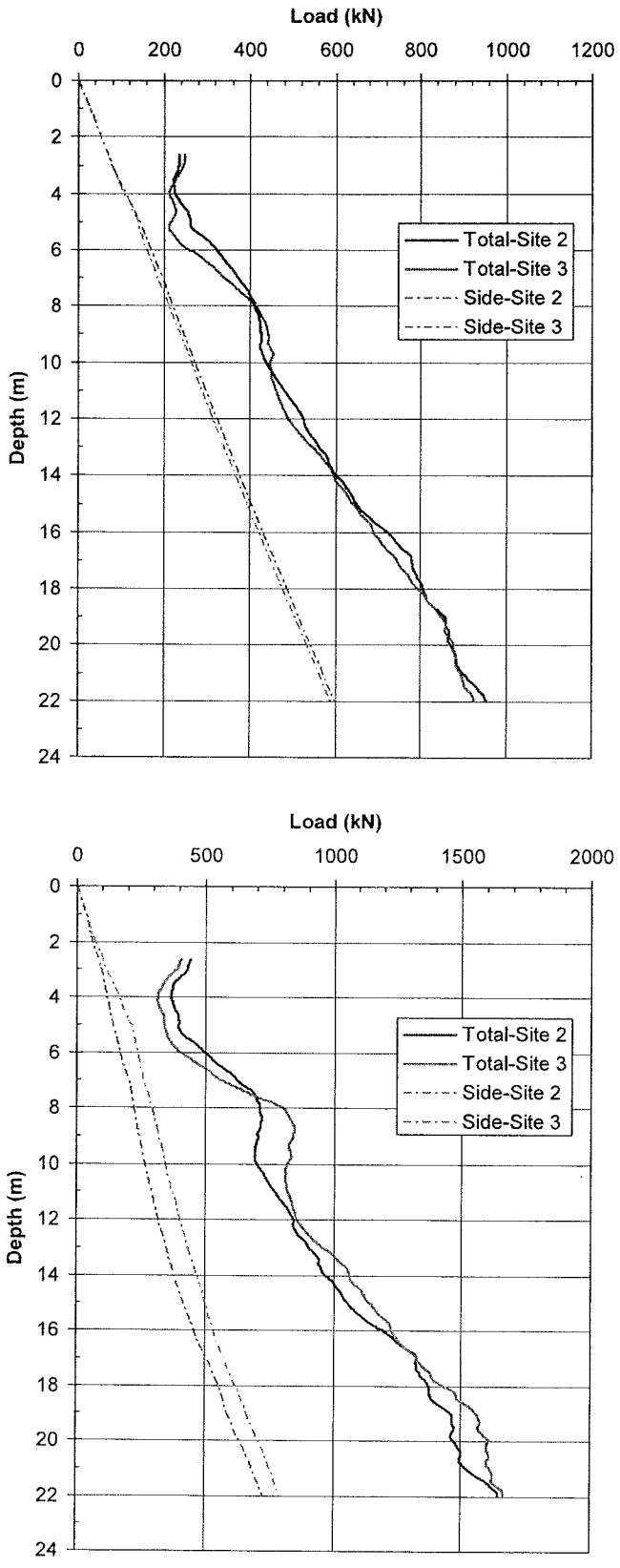

Figure 43 Predicted side resistance and total resistance for test piles and Site 2 and 3 using the Eslami and Fellenius method.

Each test pile consisted of three sections. Preliminary design called for 18.3 meter, closed-end test piles. Subsequent estimations of soil bearing capacity indicated the test piles needed lengthening by 3.7 meters. Because the instrumentation of the top two sections had already been completed it was impossible to instrument the bottom section without much inconvenience and increased cost.

Using the same procedure as was used for the test piles, it was determined that the reaction piles needed to be 21.3 meters long. Subsequent estimations determined that the reaction piles should be 22.9 meters long. Fortunately the reaction piles had not yet been cut, allowing the increase in length to be accommodated without much inconvenience. The reaction piles were made from two sections, one 12.8 meters long and the other 10.1 meters long. Since the reaction piles were designed to resist an upwards vertical load, they were driven open-ended.

4.1.2. Instrumented test pile construction

Prior to pile driving, the test piles were instrumented with strain gauges at approximately 1.5 m depth intervals along the length of the piles. At each depth interval, four strain gauges were applied to the pile at 90 degree spacings around the circumference of the test pile. The gauges consisted of water-proof electrical resistance type strain gauges manufactured by Texas Measurements, Inc. (model WFLA-6-12). In preparation for gauge attachment, the surface of the pile was ground, sanded, and polished smooth where each gauge was to be attached. Once the surface preparation was complete, the gauges were attached directly to the pile using an epoxy-based glue. Once all the gauges on a side of the pile were attached, the leads were wrapped together with electrical tape and extended to the top of the pile. A length of angle iron was then placed over the gauges and welded to the pile at regular intervals to protect the gauges. The interior gap between the pile and the angle iron was then filled with expanding polyurethane foam to seal the gauges from soil and water intrusion. The foam also helped shield the gauges from excess vibrations experienced during pile driving.

4.1.3. Pile Driving

All the piles were driven between June 7 and 10, 2005. After the piles had been delivered to the test site, the two instrumented sections of the test piles were welded together horizontally while still on the ground (see Figure 44). This allowed the instrumented section of pile to be driven in one piece. Care was taken to ensure that no damage occurred to either the strain gauges or the electrical leads from rough handling, excessive heating from welding, etc.

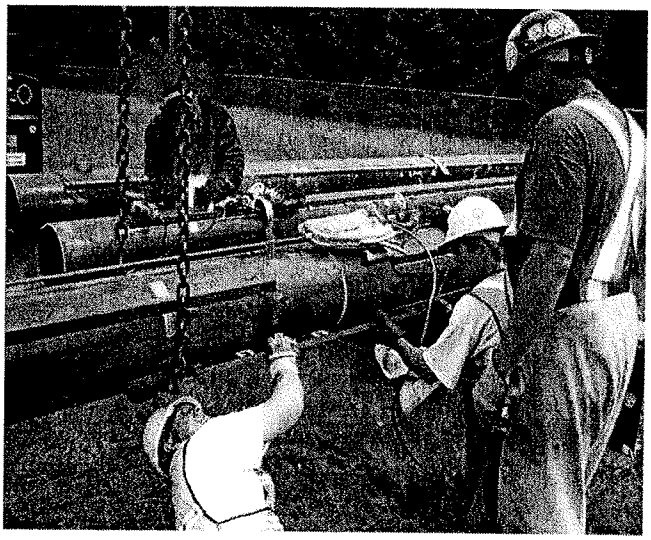

Figure 44 Welding of the instrumented segments of the test piles before driving.

Due to the limited height capacity of the pile driving rig, the lower 3.7 meter section of the test piles could not be attached while all three sections were on the ground. Thus the 3.7 meter "starter" section was first driven to within one meter of the ground surface at which point the upper two sections

(now welded together) were stood up, positioned over the bottom section, and welded together. Because the starter section was driven to only about 2.7 meters, the upper two sections were constantly tethered to the driving rig during welding and until it had been completely driven. The test piles were driven to a final depth of approximately 20.9 meters.

The piles were driven with a 2500 kg drop hammer which was typically dropped from heights ranging from 1.5 to 2.5 m (see Figure 45). The number of hammer drops and the drop heights were recorded at 0.3 m intervals. Summaries of the field data is provided for both test pile foundations in Table 8 and Table 9 (see appendix).

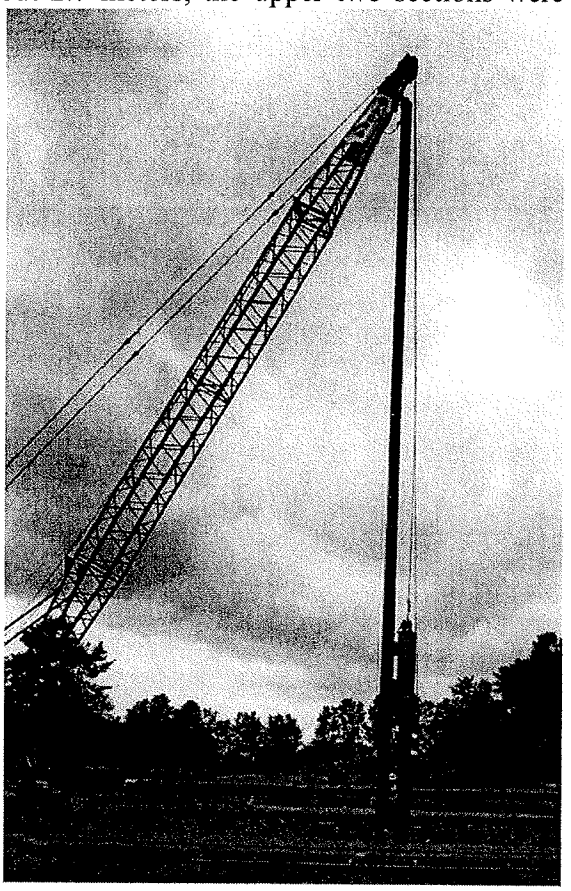

Figure 45 Piles were driving using a 2500 kg drop hammer.

4.1.4. Reaction frame construction

Once all five piles in a given group were driven, the reaction frame was constructed. The tops of the reaction piles were cut off level with each other, approximately 1 meter above the ground surface. The test pile was cut off approximately 0.5 meters above the ground surface. The difference in height provided enough clearance to install the hydraulic jacks once the reaction frame had been set up. Figure 46 shows a photograph of the completed reaction frame. A short I-beam (the blue beam on the bottom) was placed on top of each pair of reaction piles. The main reaction beam (the red beam in the figure) was then placed on top of these cross-beams. The main beam was carefully positioned to rest on the centers of the bottom beams and pass directly above the center test pile. A second short beam (the top blue beam) was then placed on top of the main beam at each end, directly above the bottom beam. Dywidag threadbars secured the reaction beam to the reaction piles. A large plate was placed on top of the test pile to provide a seat for the hydraulic jacks.

Figure 46 Photograph of the completed test frame. The test pile is visible at center, capped with a thick steel plate upon which rest two hydraulic jacks. Two short I-beams at each end (the blue beams) tie the reaction beam (the large red beam) to the reaction piles.

5. Site 2—Untreated Area Pile Testing

As indicated in section **Error! Reference source not found.**, Site 2 was maintained as the control site where no EQ Drains were installed. As such, the results of the testing at Site 2 describe the development of downdrag forces without the contributions of the EQ Drains.

5.1. Test Layout and Instrumentation

Plan and profile views of the layout of the test pile relative to the blast holes and instrumentation are shown in Figure 47 and Figure 48 respectively.

The test pile was located at the center of the ring of blast holes having a radius of 5 m. Two sets of eight blast holes were distributed equally around the circumference of the ring so that two independent series of eight blast sequences could be detonated. The second set of blast holes were offset from the first set of eight by 22.5 degrees as shown in Figure 47. In each blast hole, blast charges were located at depths of 6.4 and 8.5 m below the ground surface as shown in Figure 48. The first series of blast holes used 0.45 kg charges while the second set used 1.35 kg charges. The use of two sets of explosive charges is discussed more fully in section 5.5.

Load was applied to the pile using two 150 ton hydraulic jacks placed between the test pile and the main reaction beam. A 100 mm-thick steel plate attached to the top of the test pile, upon which the two jacks were placed, distributed the load evenly into the test pile. The load applied by each jack was measured by a load cell placed between the ram and the main beam. The vertical displacement of the pile was measured using two string potentiometers attached to a tensioned cable which was stretched across the site, similar to that described in section 3.4.1. The cable was anchored at a distance of 19.7 m from the center of test area so that it would not be affected by settlement produced by the blast liquefaction. String potentiometers were also used to measure the deflection of the main reaction beam relative to the tensioned cable and to the relative displacement between the main beam and the pile head.

Settlement of the ground surface was monitored using an array of survey points similar to that described in Section 3.4.1. The élevation of these survey markers was determined with a level survey prior to any construction at the site. Subsequent level surveys were used to evaluate settlement due to blast hole installation and pile installation, as well as blast testing. The settlement as a function of depth was monitored using a Sondex settlement tube located at 1.83 m from the center of the test area as shown in Figure 47.

The generation and dissipation of excess pore pressure during the blasting process was monitored using five identical to those used in the preliminary blast testing at Site 1 (see section 3.3). Piezometers were installed to depths of 6.7, 8.4, 10.7, 12.8 and 16.8 m below the ground surface as shown in Figure 48. The piezometers were typically located about 0.75 m from the center of the test pile (see Figure 47).

5.1.1. Monitoring of real-time ground surface settlement

In addition to the conventional level surveys, surface settlement was also monitored as a function of time after blasting using an array of vertical string potentiometers attached to the tensioned cable running above the ground surface at the site. The string potentiometers were located at distances of 0.61, 1.2, 2.4m and 3.7 m from the center of the test area (see Figure 47). Although the tensioned cable to which these string potentiometers were attached was anchored at a large distance away from the test site in order to prevent the blast testing from causing it to sag, the ground movements caused by blasting introduced a significant amount of sag in the cable. Settlement data from several different sources allowed the amount of sag in the cable to be calculated as a function of time, permitting the settlement of the ground surface to be corrected as described below.

During the pre-blast load testing the deflection of the test pile head was measured using a string potentiometer attached to a stable reference frame independent from the reaction frame. The relative deflection between the test pile head and the reaction frame was measured using another string potentiometer. Subtracting the first measurement from the second produced the deflection of the reaction frame relative to the stable reference frame. When the deflection of the reaction frame was compared to the total load applied by the hydraulic jacks, a linear relationship was developed to describe the amount of deflection in the reaction as a function of total applied load.

Using the relationship developed above, the deflection of the reaction frame could be calculated according to the load applied by the hydraulic jacks. Subtracting this deflection from the total displacement measured between the reaction frame and the test pile head produced the actual deflection of the test pile head measured relative to a hypothetical stable reference frame. Since the displacement between the tensioned cable and the test pile head was known, the

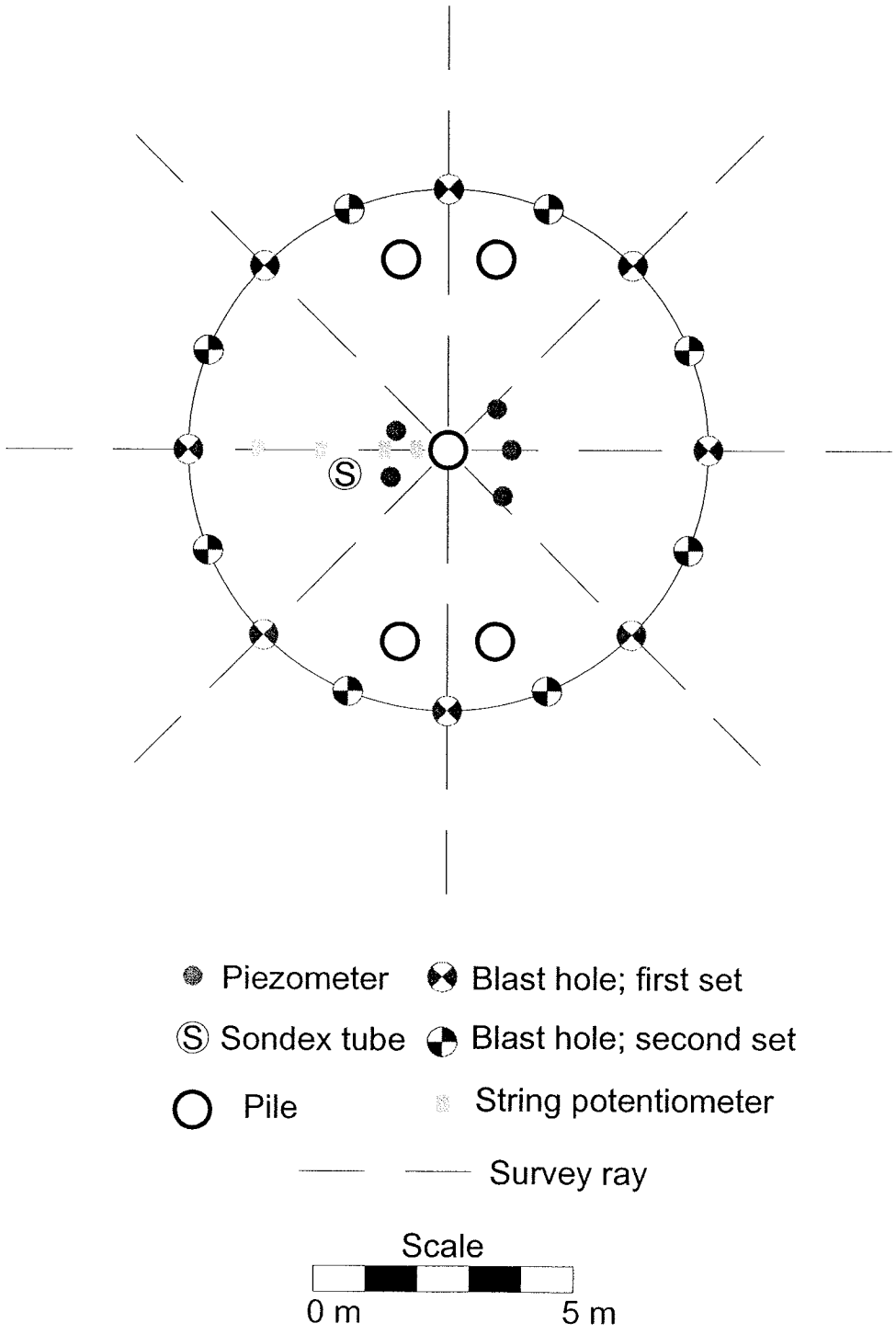

Figure 47 Plan view of pile foundation and instrument layout at Site 1.

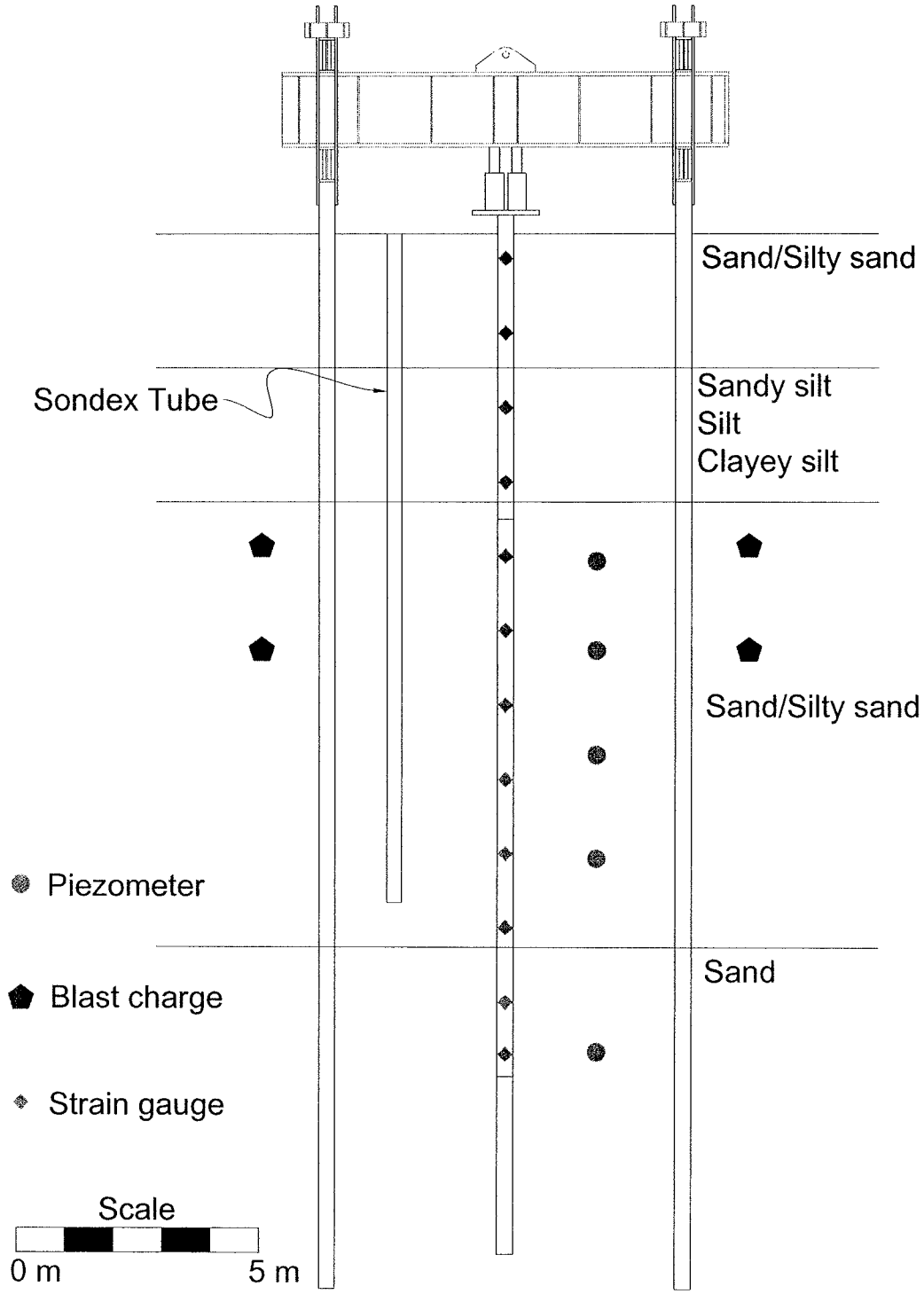

Figure 48 Profile view of pile foundation and instrumentation layout at Site 2.

sag of the cable could then be determined. Once the sag of the cable was determined, the settlement of the ground surface measured by the four string potentiometers connected to the tensioned cable could be corrected.

As the cable lost tension, the center portion of the cable would sag more than the outer portions of the cable. Accordingly, each string potentiometer should be corrected individually according to their respective distance from the test pile. However, since the tensioned cable was anchored more than 17 meters from the center and all the string potentiometers were within 3.7 meters of the center, it was assumed that one correction would be sufficiently accurate for the purposes of this study.

To evaluate the correction procedure explained above, the calculated maximum settlement for the four string potentiometers was compared to the total settlement measured by the level survey. All four maximum string potentiometer settlements corrected in this manner were within 5% of the total settlement as measured by the level survey.

5.2. *Blast Hole Installation and Influence on Surrounding Soil*

The 16 blast holes were installed between May 9 and 11, 2005 using the same procedure used to install the blast holes for the pilot liquefaction test. Each blast hole was cased with a 10 cm EQ drain pipe enclosed in a filter fabric sock to keep the hole open until the time of blasting.

To evaluate potential changes in the sand density due to blast hole installation, the settlement was measured approximately one month after installation and an additional CPT sounding was performed at that same time. The maximum settlement was approximately 18 mm at the center of the site where the test pile was eventually driven. The average settlement was less than 3 mm, which is within the error of the survey itself. This suggests that very little change in soil density was produced by the installation of the blast holes.

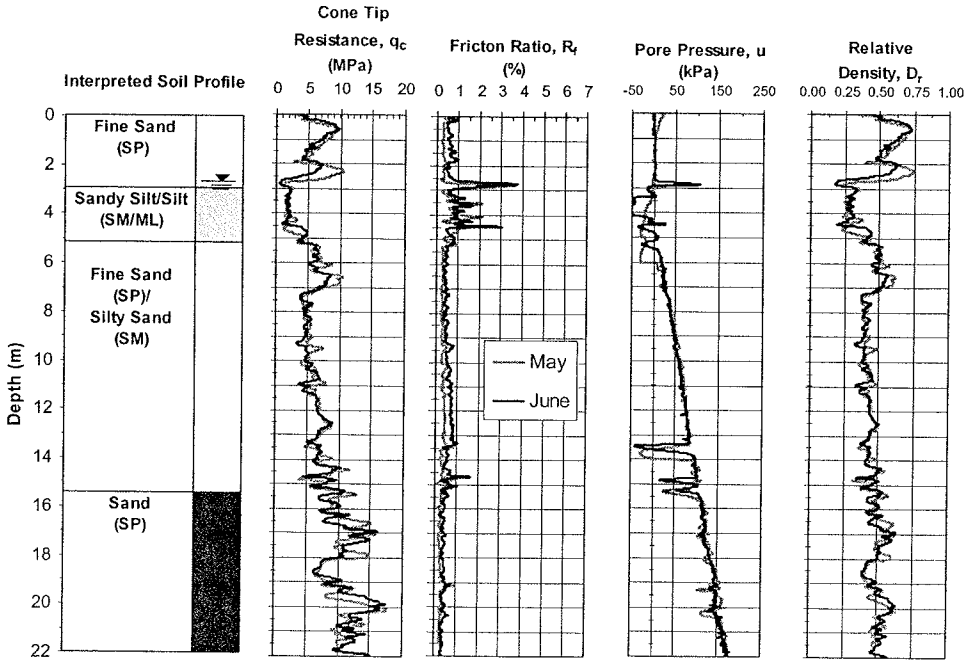

Figure 49 Comparison of CPT soundings performed May 2 and June 6, 2005.

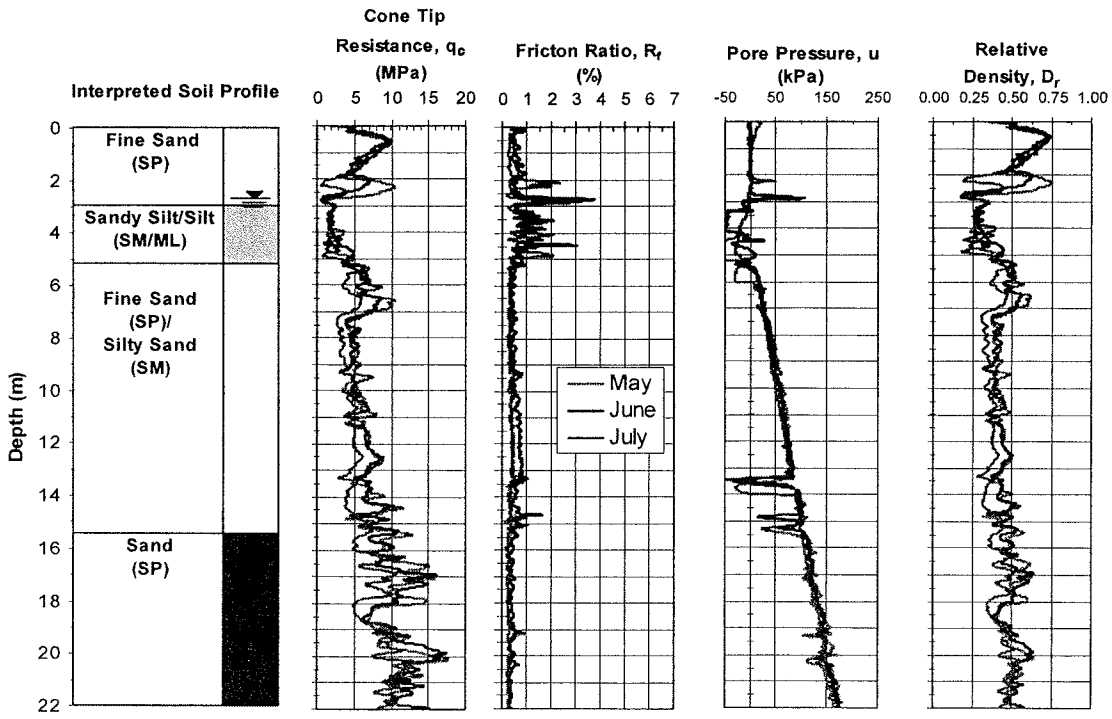

Figure 50 Comparison of CPT's performed May 2, June 6, and July 26.

A CPT sounding was performed on June 6, 2005, approximately one month after installation of the blast holes and was located within a meter of the original CPT sounding. Plots of the measured cone tip resistance, friction ratio, and pore pressure are provided in Figure 49 along with similar curves from the previous CPT sounding at the site along with the interpreted soil profile. A plot of the relative density versus depth was also developed using (1) and is included in Figure 50. Although there are some minor variations, there is no indication that there was any consistent increase or decrease in tip resistance, friction ratio or relative density. The observed variations are likely due to minor natural variations.

5.3. Pile Installation and Influence on Surrounding Soil

The test pile and four reaction piles were driven at this test site between June 7 and 9, 2005. To evaluate potential changes in the sand density due to pile driving, the settlement was measured approximately one month after installation (July 27, 2005) and an additional CPT sounding was performed one day previously. The maximum settlement was approximately 43 mm at a point located between the two northern reaction piles. The majority of the settlement occurred within a circular area 12 m in diameter centered about the test pile at the center of the site. The average settlement within that area was 23 m. Outside the circular area the average settlement was less than 6 mm, which is within the error of the survey itself. This suggests that very little change in soil density was produced by the installation of the piles.

The cone sounding after blast hole installation was performed within a meter of the original CPT sounding. Plots of the measured cone tip resistance, friction ratio, and pore

pressure are provided in Figure 50 along with average curves from the previous two CPT soundings at the site along with the interpreted soil profile. A plot of the relative density versus depth was also developed using (1) and is compared with the average plot from the previous two soundings. Although all indicates are that the soil settled slightly due to pile driving and excess pore pressures should have been dissipated, the cone tip resistance and relative density for this sounding actually show a minor decrease. It is unclear whether this decrease represents a real change in soil conditions or simply a variation in the CPT that was used to conduct this series of tests. Nevertheless, the general profile and soil conditions are still in line with previous tests at the site.

5.4. *Pile Load Testing Prior to Blasting*

An initial pile load test was carried out on June 10, 2005, about one day after the test pile was driven. This pile test was performed to provide reliable data regarding unit side friction and end bearing pressures for use in planning the thickness of the sand layer to be liquefied. As discussed in section 4.1.1, the side friction and end-bearing values computed using the LCPC (Bustamane et al. 1982) and Eslami and Fellenius (1997) methods were significantly different. Therefore, field measurements were necessary to facilitate planning.

The test was performed using the quick maintained load procedure. Load was applied incrementally and held for three minutes at each increment. A plot of the measured pile head load versus pile head deflection curve for the first test is provided in Figure 51. The curve is relatively linear up to a load of about 550 kN after which settlement begins to increase rapidly with load. At a load of approximately 725 kN the pile began to settle very rapidly, or plunge, downward. At the end of the test the load was released and a residual plastic deflection of 67 mm was not recovered as shown in Figure 51.

The failure load was interpreted using the Davisson criteria. According to this method the failure load is located where the elastic compression line for the pile intersects the measured load-deflection curve from the load test. The slope of the elastic compression line is equal to AE/L, where A is the cross-sectional area of the pile, E is the modulus of elasticity of the pile and L is the pile length. The starting point for the elastic compression line is offset by a deflection equal to 3.81 mm plus the pile diameter in mm divided by 120, which is about 6.5 mm for the 324 mm diameter test pile. According to the Davisson criteria, the failure load was 650 kN as shown in Figure 51. This is about 60 percent lower than predicted by the Eslami and Fellenius method and about 32 percent lower than predicted by the LCPC method.

The load in the pile as a function of depth was also determined at each load increment based on the average strain at each level in the pile. The load at each level was computed using the equation

$$P = AE\varepsilon \tag{7}$$

where ε is the average measured strain at a given depth in the pile. Plots of the load versus depth profiles at several load increments are presented in Figure 52. At the top of the pile, the load is equal to the applied load. The decrease in load with depth is a result of load transfer to the

surrounding soil due to side friction, while the load at the base of the pile is provided by end-bearing resistance. As the applied load is increased, the side friction is progressively mobilized to greater depths and eventually end bearing resistance begins to develop. Typically, side friction is fully mobilized at relatively small deflections levels on the order of 2 to 5 mm. In contrast, end-bearing typically requires deflections equal to 4 to 10% of the pile diameter. At the failure load defined by the Davisson criteria, about 55% of the axial resistance is provided by side resistance and 45% is provided by end-bearing.

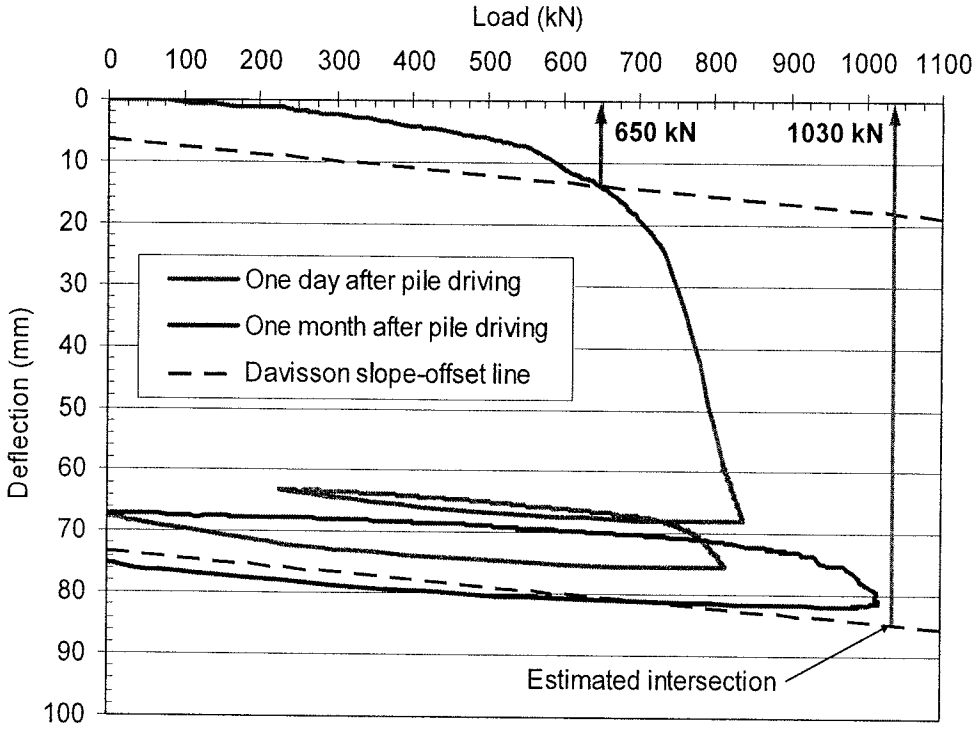

Figure 51 Comparison of the pile-head-load versus pile-head-deflection curves resulting from two vertical load tests.

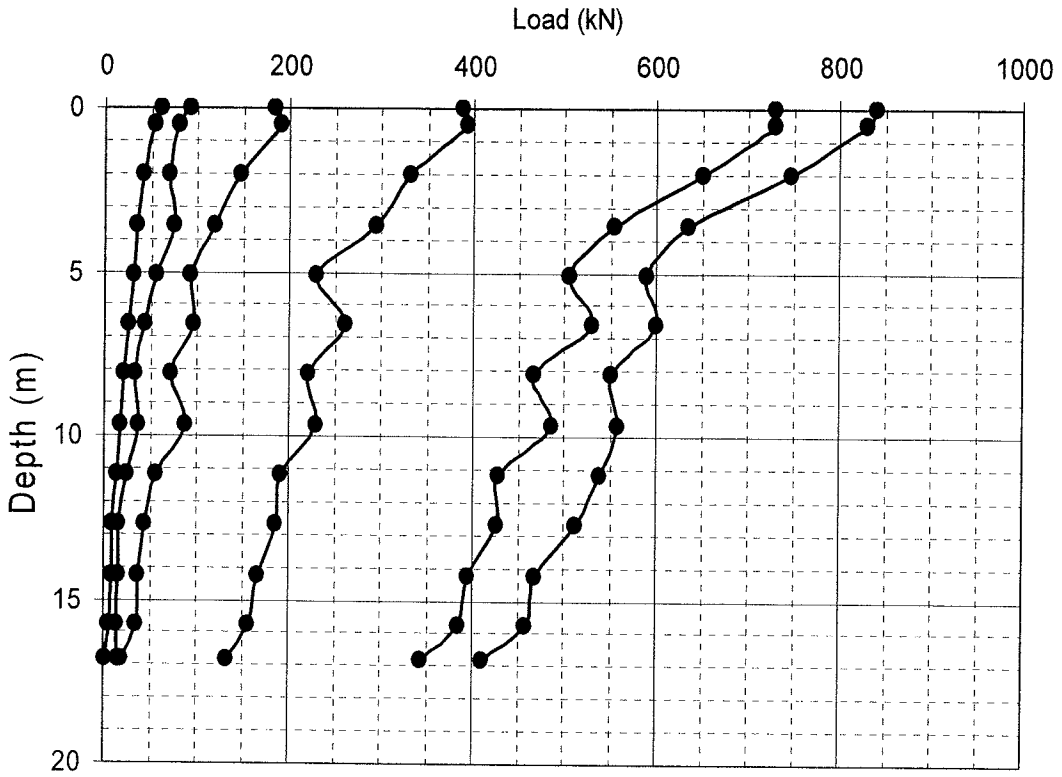

Figure 52 Load-depth curves from the static load test performed one day after pile driving (Jun 10, 2005)

About one month after the initial pile load test, a second load test was performed on the test pile prior to the blast liquefaction test. Because the original test was performed so shortly after the pile driving, the second test was performed to determine if setup might have led to a higher failure load.

The load versus deflection curve for the second pile load test is plotted in Figure 51 along with the curve from the previous load test. Load versus deflection curves at a number of load increments during the second test are provided in Figure 53. Because the load-deflection curve did not intersect the Davisson line, the failure load was estimated by extrapolation to be about 1030 kN which is about 58 percent higher than the load from the first test. The failure load for the second test is slightly higher than predicted by the LCPC method but still about 30% below the failure load predicted by the Eslami and Fellenius (1997) method. For the second test, the load is significantly greater than that which caused the pile to plunge during the original test. Part of this increased resistance is likely due to the fact that the pile had been previously loaded so that deflections were reduced during re-loading. However, this does not explain the fact that the load deflection curves extends beyond the curve from the initial test. This increased resistance would have to be attributed to set-up/re-consolidation effects which developed after the first test. Set-up effects are not often reported for piles in sand; however, most load tests are not performed so soon after driving. Because of the higher permeability in sands, these set-up

effects likely occur quite rapidly and would not be detected unless the first test was performed very soon after driving as was the case in this study.

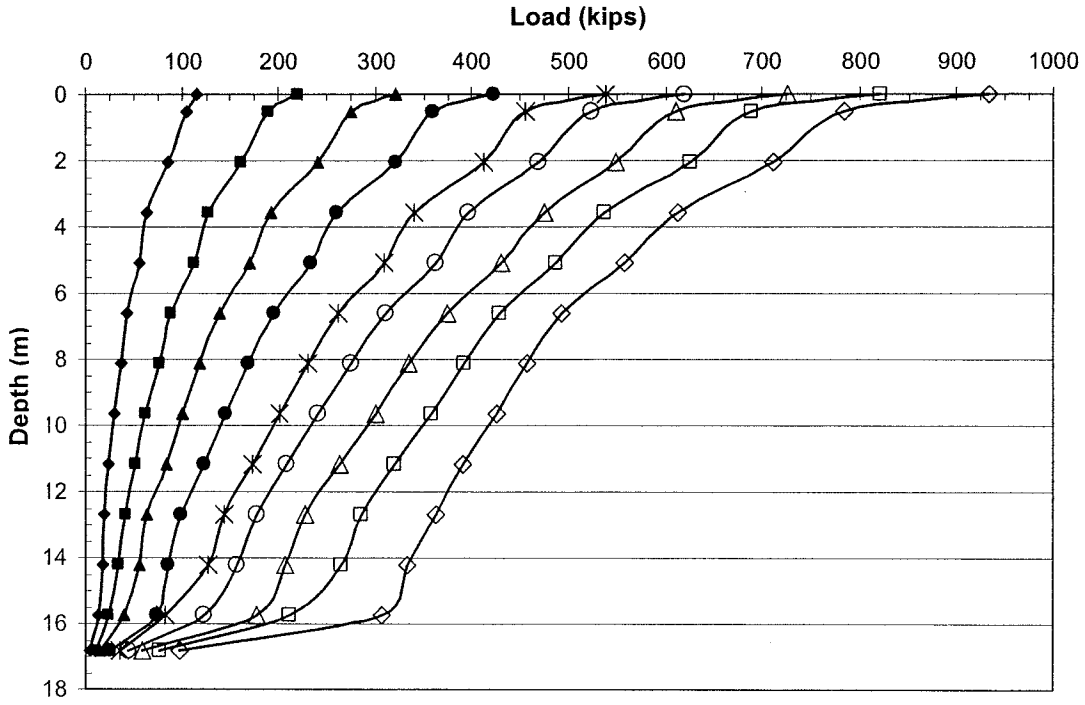

Figure 53 Load vs. depth curves for the static test performed one month after pile driving at Site 2.

5.5. Blast Test 1

The first blast test was performed using smaller charge weights (0.45 kg) than those used for the second blast (1.35 kg). Although the pilot liquefaction testing indicated that the larger charge weights would be necessary to produce liquefaction, these tests had been performed a month earlier when gaps had been observed between the blast hole casing and the surrounding ground. If, during the subsequent month, the ground had tightened in around the casing, then less energy would be required to produce liquefaction. Therefore, the first blast test was performed with lower charge weights to evaluate this possibility as it was desired to induce liquefaction in an incremental fashion more akin to the process observed during an earthquake.

For Blast Test 1, a total of 16, 0.45 kg (1 lb) explosive charges consisting of Pentex were detonated sequentially with a one second delay between detonations. Charges were located at depths of 6.4 and 8.5 m below the ground surface in each of eight drill holes spaced evenly around a 10 m diameter circle centered about the test pile. The eight explosive charges at 8.5 m were detonated first followed by the eight charges at 6.4 m.

5.5.1. Excess Pore Pressure Generation and Dissipation

Time histories of the first 30 seconds of the blast sequence showing the generation of excess pore pressure ratio for each of the five piezometers is presented in Figure 54. Blasting began at about 4 seconds into the time history. The pore pressure increased incrementally with each successive blast as expected and the behavior was relatively consistent at each depth. The piezometer records from depths of 6.7 m, 8.4 m, and 10.7 m indicate an almost identical response. While the excess pore pressure ratios routinely spiked well above 1.0, the residual excess pore pressure ratios reached a maximum of about 0.8 to 0.9. The piezometer located at 12.8 m depth recorded a response similar to that of the top three piezometers for the first three to four blasts. At that point the record diverged, reaching a maximum excess pore pressure ratio of only approximately 0.6. The piezometer located at 16.8 m depth recorded a maximum excess pore pressure ratio of only 0.1, indicating that the soil at that depth never approached the liquefied state. This result confirmed that larger charge weights would be required to produce liquefaction, despite the apparent decrease in the gap width around the blast hole casings.

Full time histories showing the dissipation of excess pore pressure ratios for each of the five piezometers following blasting are presented in Figure 55. The pore pressures dissipated more quickly as the depth increased indicating that the sand reconsolidated from the bottom to the top. Excess pore pressure dissipation was essentially complete after about 30 minutes.

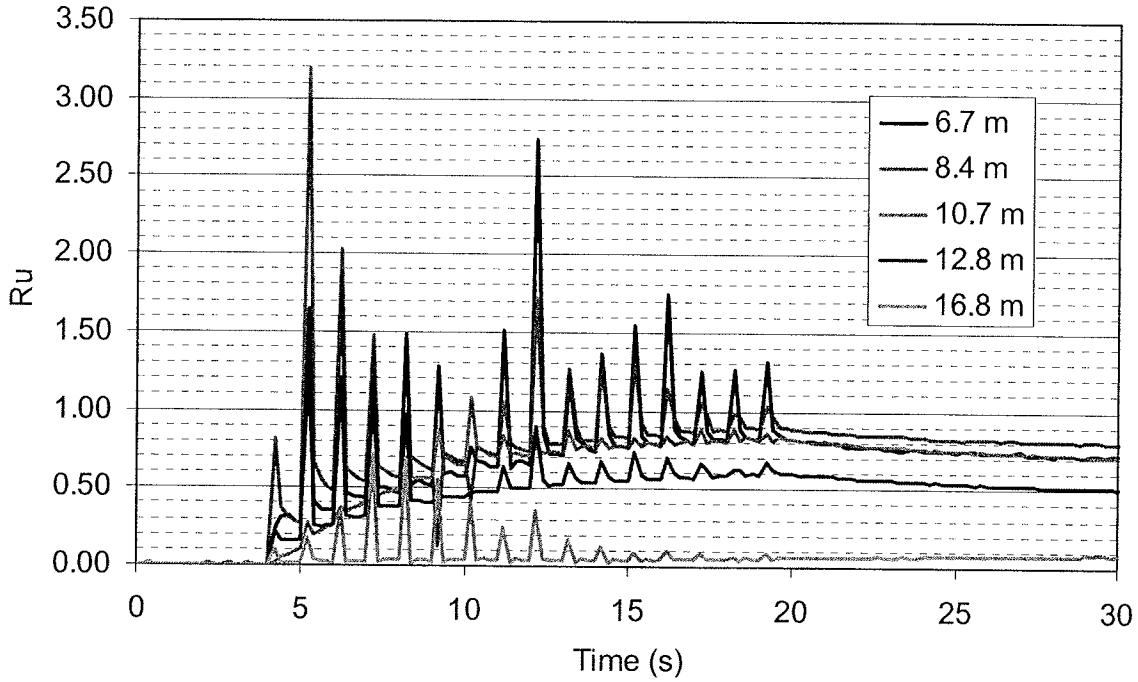

Figure 54 Plot of the generation of pore pressure from the first blast test at Site 2.

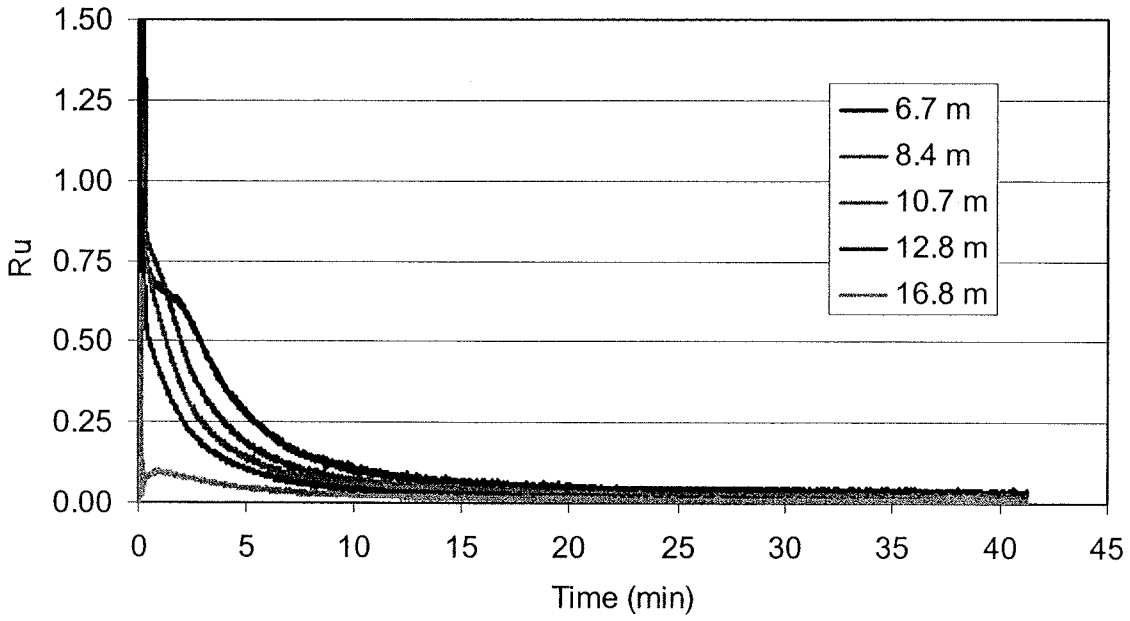

Figure 55 Full time histories of excess pore pressure ratios for the first blast at Site 2.

5.5.2. Blast Induced Settlement

A color contour plot of the ground surface settlement following first blast is provided in Figure 56. The maximum settlement was approximately 155 mm and this value occurred near the center of the test area. Contours of settlement are generally concentric about the center of the test area. A plot of the average ground surface settlement with respect to distance from the center of the test area is provided in Figure 57. On average, settlement decreased to levels below the error of the survey (estimated at approximately 5 mm) at distances greater than about 10 m from the center of the test area.

A plot of the settlement versus depth obtained from the Sondex tube is provided in Figure 58. As can be seen, the settlement decreased in a fairly linear fashion with increasing depth until it reached zero settlement at 13.7 m depth. The fact that the settlement at the surface as measured by the Sondex tube did not equal the settlement measured by the level survey is easily explained. The soil near the surface was extremely dry and loose (see Section 2.5). Ideally, once the soil began to settle as a result of blasting, the plastic corrugated pipe would compress equally with the soil. However, with the soil in its loose, dry state, the corrugated pipe was stiff enough to resist the compression induced in it as the soil around it settled. Based on the Sondex measurements the average volumetric strain in the sand layer from 6 m to 13 m was approximately 1.3 percent.

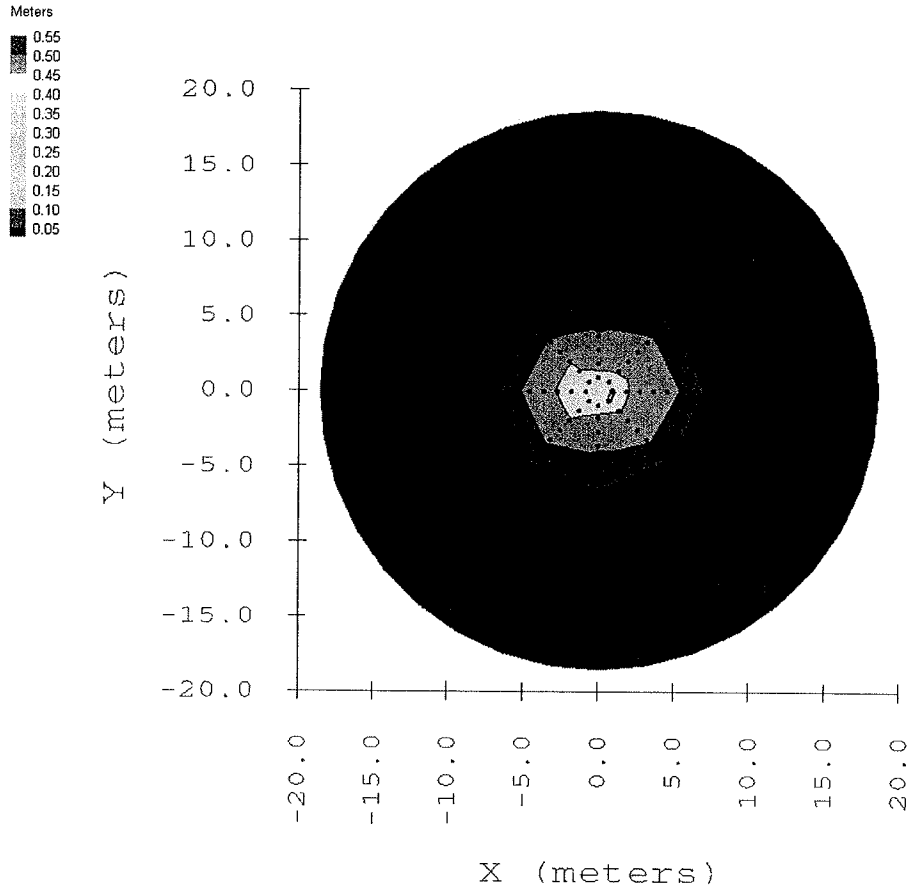

Figure 56 Contour plot of the ground surface settlement caused by the first blast only at Site 2.

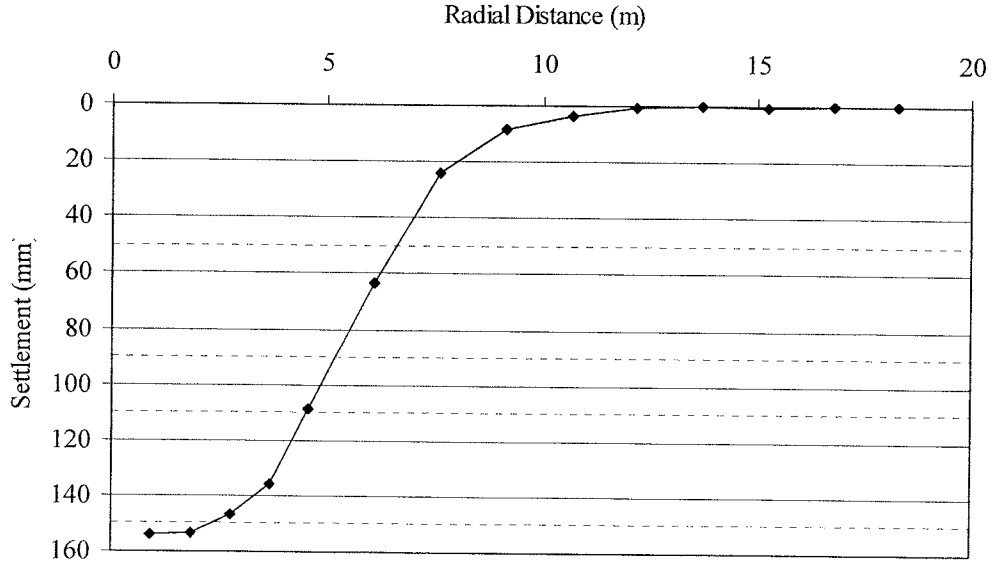

Figure 57 Variation of average settlement caused by the first blast test at Site 2.

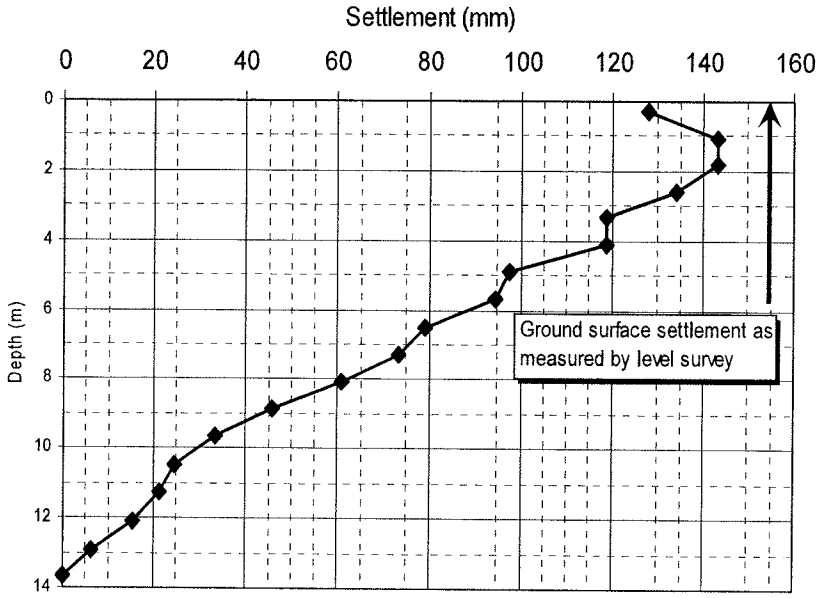

Figure 58 Settlement as a function of depth as measured by the Sondex tube for the first test blast at Site 2.

5.6. Blast Test 2

For blast test 2, a total of 16, 1.36 kg (3 lb) explosive charges (Pentex) were detonated sequentially with a one second delay between detonations. Charges were located at depths of 6.4 and 8.5 m below the ground surface in each of eight drill holes spaced evenly around a 10 m diameter circle centered about the test pile. The eight explosive charges at 8.5 m were detonated first followed by the eight charges at 6.4 m.

5.6.1. Excess Pore Pressure Generation and Dissipation

Time histories showing the generation of excess pore pressure ratio for each of the five piezometers during the blast detonations are plotted in Figure 59. The pattern of pore pressure generation was similar to that which occurred during the first blast test, i.e., a non-linear curve showing the greatest increases during the first several blasts and smaller increases in pressure at subsequent blast. However, the rate of pressure generation is much higher for the second blast than for the first blast. For example, in the first blast an R_u of 0.8 was obtained after 9 to 10 second whereas the same value was obtain in only about six seconds for the second blast. The maximum excess pore pressure ratios were reached by the twelfth blast, with little to no increase with the last four blasts. This pattern was recorded by all piezometers, regardless of the depth.

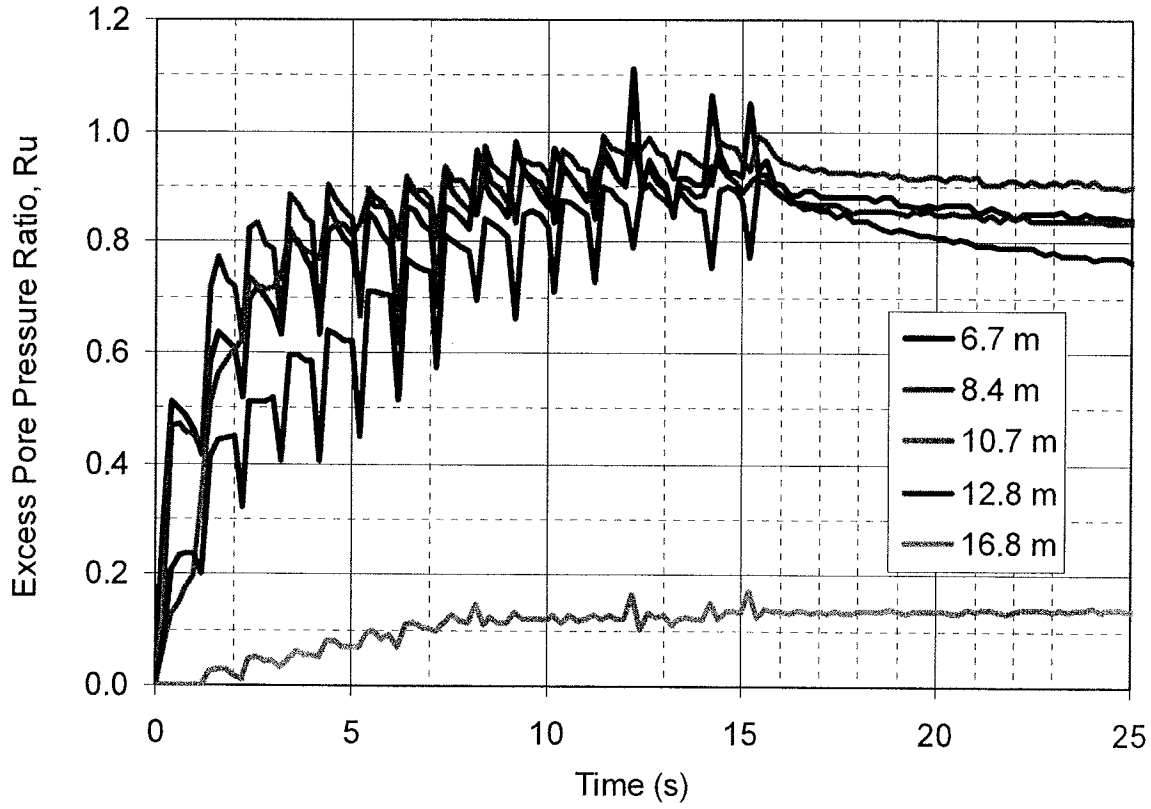

Figure 59 Time history of the generation of excess pore pressure ratios during the first 25 seconds of the second blast test at Site 2.

As occurred during the first blast test, the top three piezometers (those at 6.7, 8.4, and 10.7 m) recorded similar responses. However, the piezometer at 12.8 m showed a somewhat slower rate of pore pressure generation relative to the top three piezometers. After about 12 detonations, the residual excess pore pressure ratio for the piezometers at depths of 6.7, 8.4, 10.7, and 12.8 m was above 90 percent and there was little change in the ratio for the subsequent detonations. As in the first blast test, at a depth of 16.8 m the excess pore pressure ratio remained quite low. In this case, it did not exceed 0.175. The reduced pore pressure ratio at 16.8 m is a result of two factors. First, the soil at this depth is further from the location of the blast charges and second, the sand at this depth has a higher relative density.

Time histories of the dissipation of excess pore pressure ratio for each of the five piezometers following blasting are presented in Figure 60. The pore pressures dissipated more quickly as the depth increased indicating that the sand once again reconsolidated from the bottom to the top. Excess pore pressure dissipation were less than 0.1 after about 25 minutes.

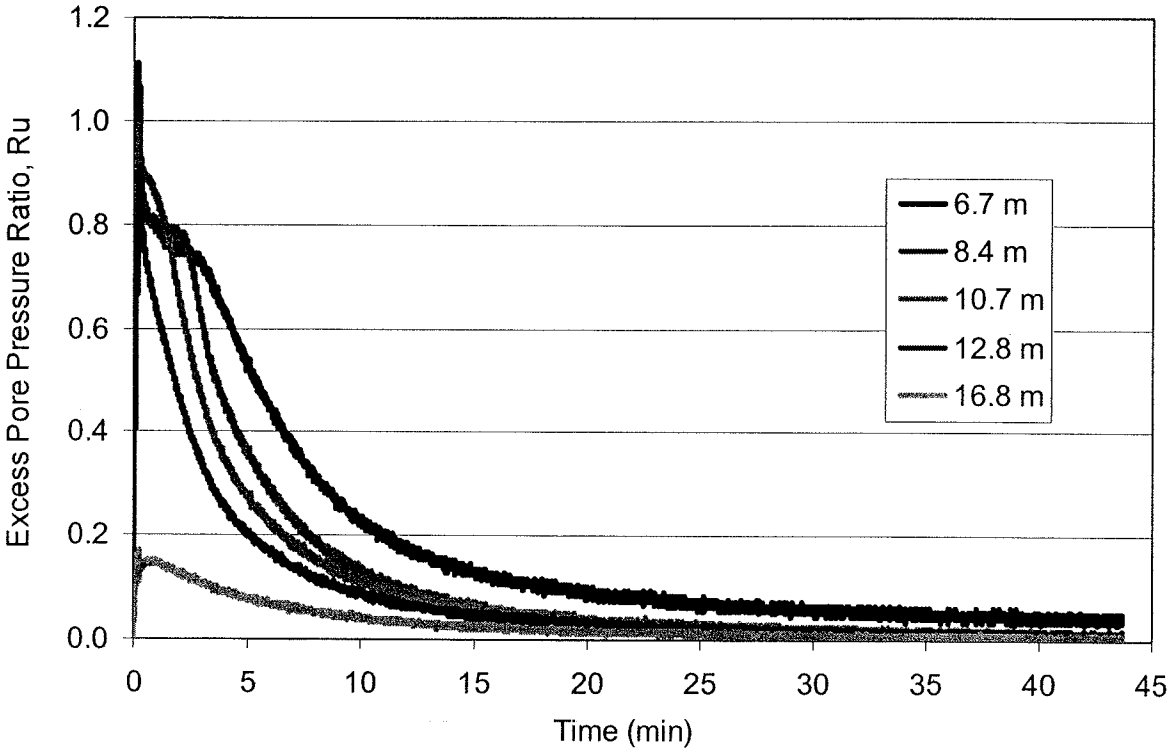

Figure 60 Time histories of the excess pore pressure ratio dissipation for second blast test at Site2.

5.6.2. Blast-Induced Settlement

A color contour plot of the ground surface settlement due to the second blast only is provided in Figure 61. The maximum settlement was approximately 270 mm and this value occurred near the center of the test area. Contours of settlement were generally concentric about the center of the test area.

A plot of the average ground surface settlement with respect to distance from the center of the test area is provided in Figure 62 along with a similar plot from the first blast. Because the excess pore pressures induced in the second blast were much higher than for the first blast, the ground settlement within five meters of the center are typically about 1.7 times greater. On average, settlement was less than 9 mm at distances greater than about 11.5 m from the center of the test area.

A plot of the settlement versus depth obtained from the Sondex tube is provided in Figure 63. According to the level survey data, the ground surface settlement at the location of the Sondex tube was approximately 265 mm, which is similar to the average settlement recorded by the Sondex tube in the top 3.5 m. Settlement was nearly constant from the ground surface to a depth of about 3.5m m and then decreased essentially linearly until it reached zero at a depth of about 13.7 m. This settlement profile indicates that the upper 3.5 m settled as a block on top of an underlying liquefied layer extending from 3.5 m to about 13.6 m. However, the liquefiable sand layer begins at a depth of about 5.m.

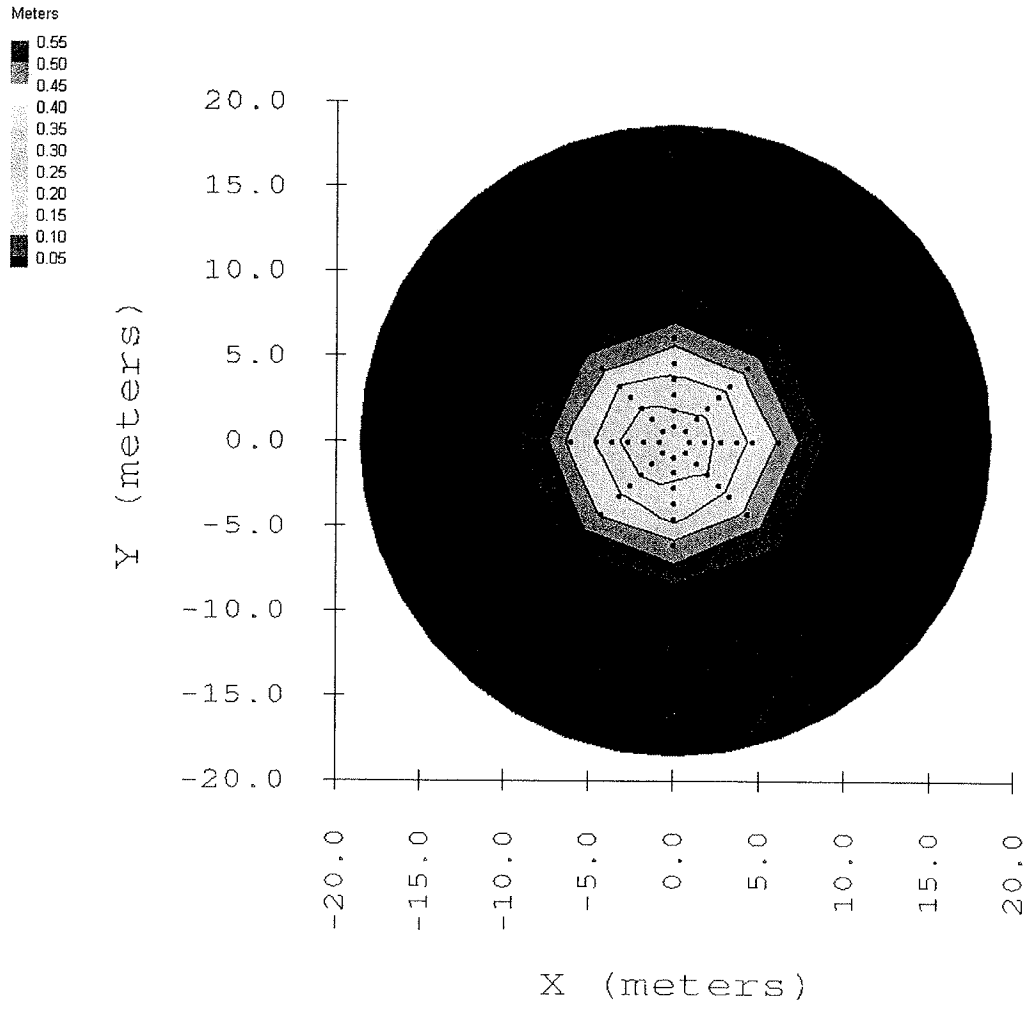

Figure 61 Contour plot of settlement caused by the second test blast at Site 2.

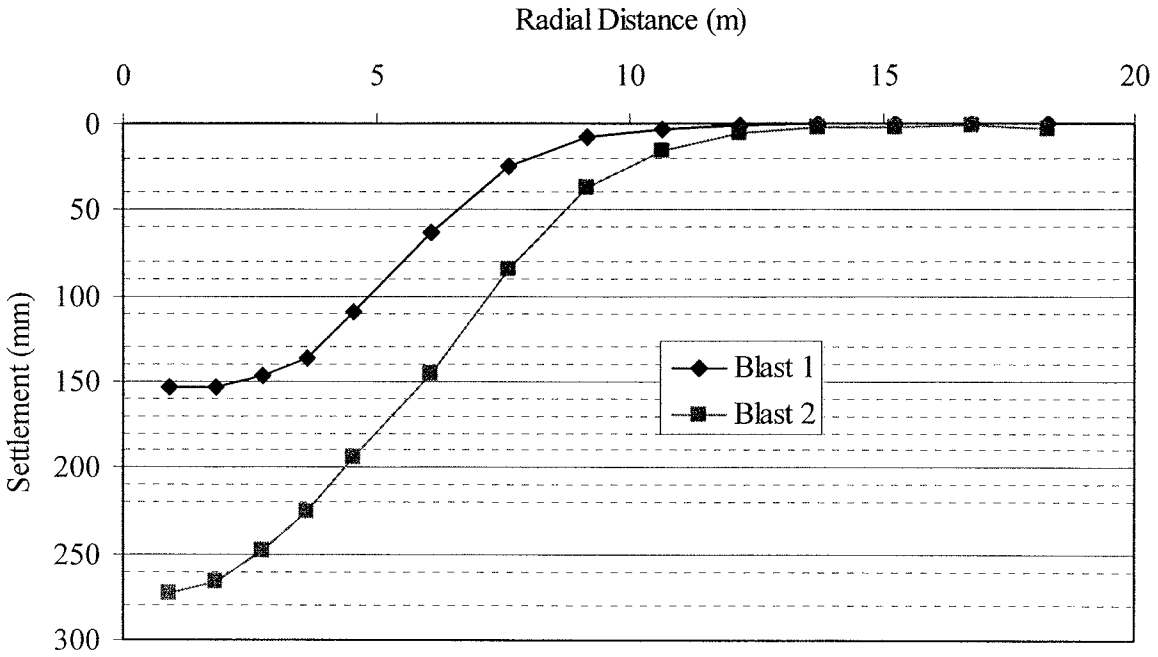

Figure 62 Comparison of average ground surface settlement with distance from center of test site at Site 2.

This discrepancy could be attributed to either slippage of the Sondex pipe within the clayey silt layer or settlement in the silt layer due to liquefaction. Recent studies do indicate that fine-grained soils can settle similar to liquefiable sands (Boulanger and Idriss, 2004).

The average volumetric strain of the target zone (6 m to 13 m) is approximately 2.3percent. However, the possibility exists that the Sondex pipe could have slipped inside the sandy silt/clay zone from 3.5 to 5 m below the ground surface. For example, the settlement plot from the pilot liquefaction test (see Figure 37) did not show any appreciable settlement in this zone. If settlement is assumed to be negligible in this layer, then the average volumetric strain in the liquefied layer for test site 2 would be approximately 3.1 percent. Based on the Tokimatsu and Seed (1988) method, the expected liquefaction induced settlement in this zone would be approximately 3 percent.

Real-time settlement was measured using four string potentiometers and is shown in Figure 64. As can be seen, settlement occurs rapidly following blasting. Approximately 80 percent of the settlement has occurred within three minutes after the onset of blasting.

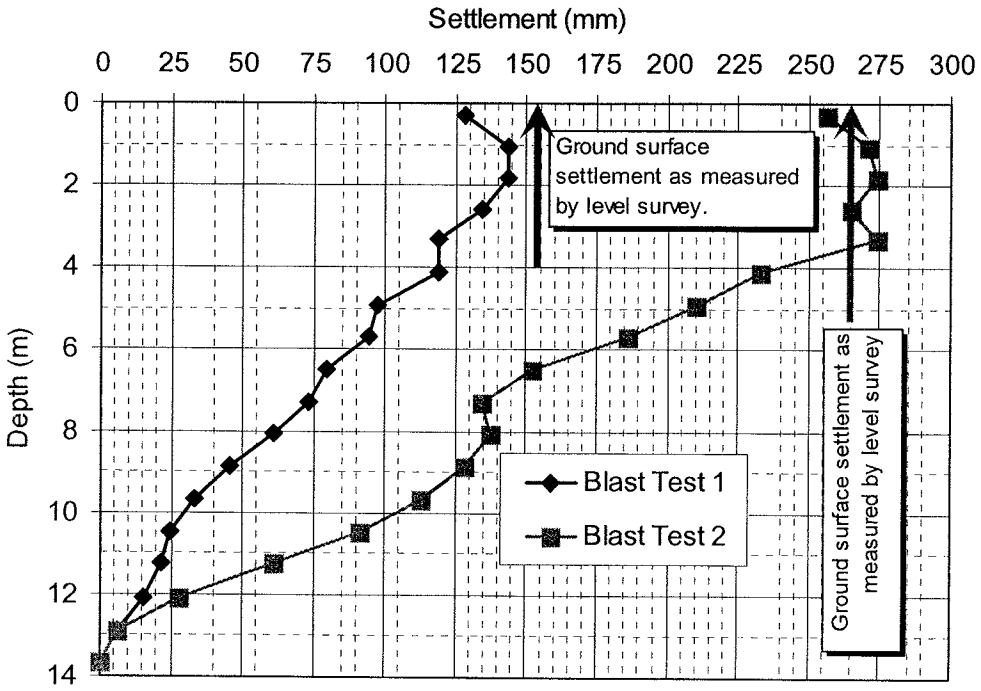

Figure 63 Comparison of settlement measured by the Sondex tube at Site 2 for both blast

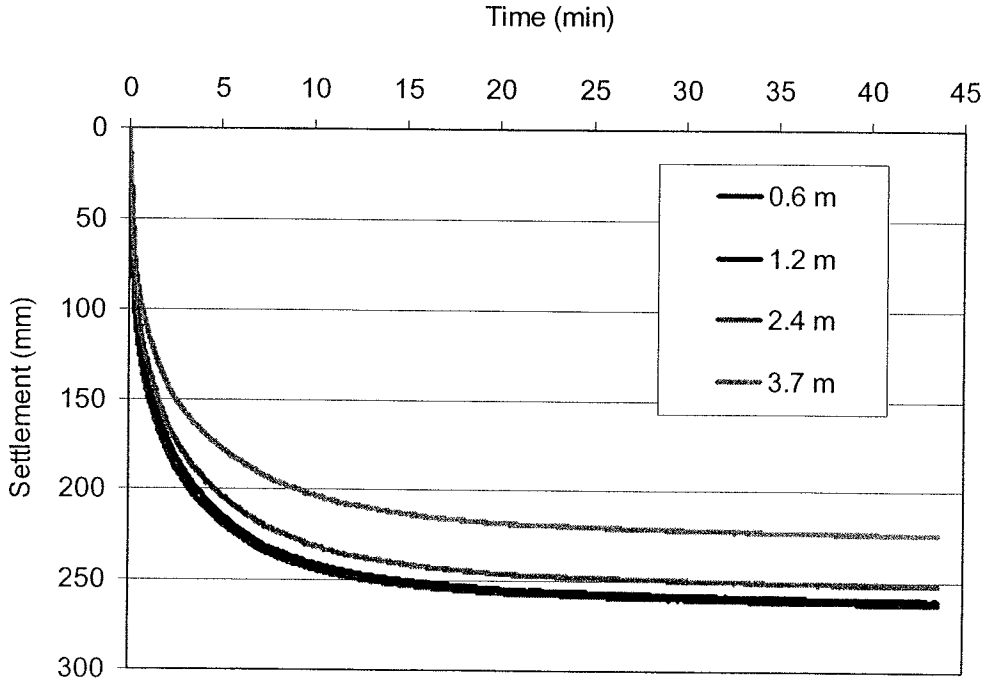

Figure 64 Real-time settlement recorded by the string potentiometers during the second blast test at Site 2.

5.6.3. Pile Load Transfer Variations Due to Liquefaction

Measurements made with the strain gauges attached to the test pile were used to calculate the load carried by the pile as it varied with depth. Figure 65 shows the variation of load in the test pile with respect to depth at three distinct times: immediately before blasting, immediately after blasting, and at the point that surface settlement had essentially ended. Figure 66 shows the load applied to the test pile as it varied with time throughout the test. The onset of blasting was set at time zero, therefore, negative time values indicate the time before blasting.

Immediately before blasting, a load of approximately 536 kN was applied to the test pile. The roughly linear decrease in pile load versus depth shown in Figure 65 indicates that the transfer of load out of the pile and into the soil through skin friction was fairly constant with depth.

At the onset of blasting, the test pile settled slightly so that the load applied by the hydraulic jacks dropped to a low of 380 kN, or about 29% of the applied load at the beginning of blasting. This load was reapplied by the end of the blasting and appears to have been transferred by skin friction to the upper section of the pile. As a result, the pile load vs. depth curve in the upper 6 m of the profile is about the same as before the blast.

Immediately following blasting, the load in the pile became relatively constant throughout the liquefied zone from a depth of about 6 m to 13.5 m indicating that skin friction in that zone had dropped to near zero. The load originally carried by skin friction in the liquefied zone was then transferred to the lower end of the pile where liquefaction had not developed. This additional load was carried by skin friction which had yet to be fully mobilized in this somewhat denser sand. At this stage in the test, the ground around the pile had settled over 100 mm while the pile itself had settled 7 mm. The settlement of the pile developed due to the loss of skin friction at the top of the pile and the movement necessary to mobilize skin friction in the bottom segment of the pile.

Once the excess pore pressure had dissipated and the settlement had stopped, the load vs. depth curve in the previously liquefied zone developed a negative slope as shown in Figure 65. This indicates that negative skin friction had developed in this zone and was causing downdrag on the pile. However, the negative skin friction due to reconsolidation settlement in the liquefied sand is only about one-half of the positive skin friction in this layer prior to blast-induced liquefaction.

Although the ground settlement at this point was now over 270 mm near the test pile, the strain gauges do not indicate any significant downdrag in the soil above the liquefied zone. In fact, the load transfer curve at the end of ground settlement is almost identical to that immediately before blasting.

The lack of downdrag in the upper 6 m may be due to the variation of applied load during the time of pore pressure dissipation. Once all the explosive charges had been detonated, the load applied to the test pile was to be held constant. However, the pressure in the hydraulic jacks would slowly bleed off, reducing the applied load. Therefore the hydraulic pump was turned on momentarily to restore the desired load applied to the test pile. This variation in applied load is recorded as the "saw-tooth" patterns in Figure 66. It is possible that the settling ground surface caused downdrag forces on the upper 6 m of the test pile during the times of hydraulic pressure bleed-off. When the hydraulic pump was turned back on to restore the pressure, the test pile would settle slightly relative to the soil, reversing the frictional forces on the pile.

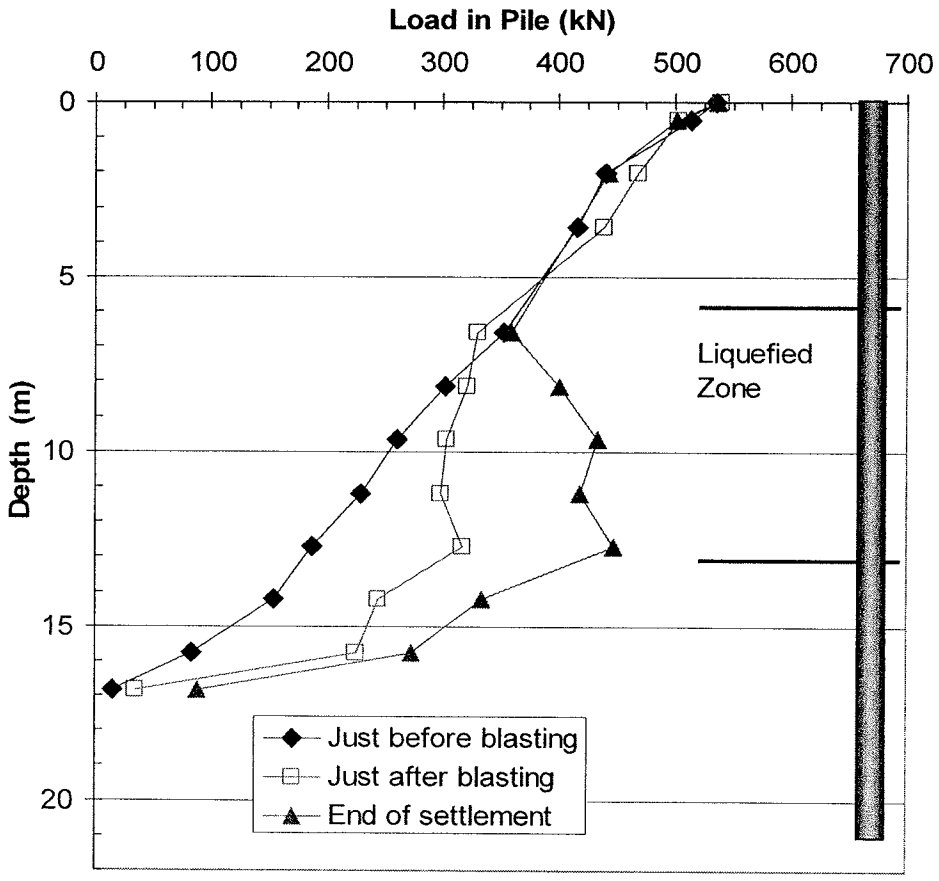

Figure 65 Variation of load transfer during liquefaction.

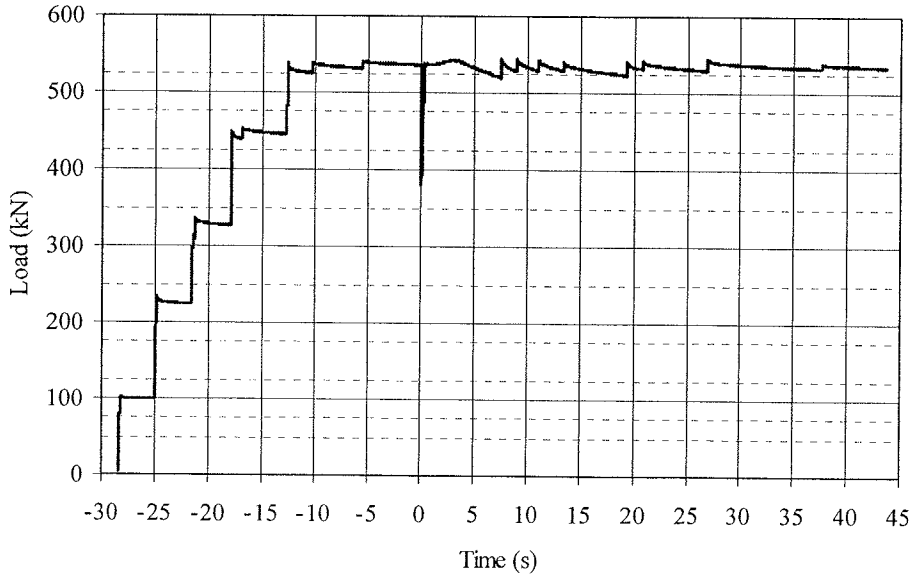

Figure 66 Time history of axial load applied to test pile during second blast test

5.7. *Post-Blast Site Characterization*

To evaluate potential changes in the sand density due to the blast testing, an addition CPT sounding was performed shortly after the second blast test (July 28, 2006). The cone sounding was performed within a meter of the CPT sounding performed before blast testing. Plots of the measured cone tip resistance, friction ratio, and pore pressure are provided in Figure 67 along with curves from the previous CPT soundings at the site along with the interpreted soil profile. A plot of the relative density versus depth was also developed using (1) and is compared with the plots from the previous sounding. Despite the fact that significant settlement (>500 mm) had occurred, there are only minor increases in the tip resistance and relative density.

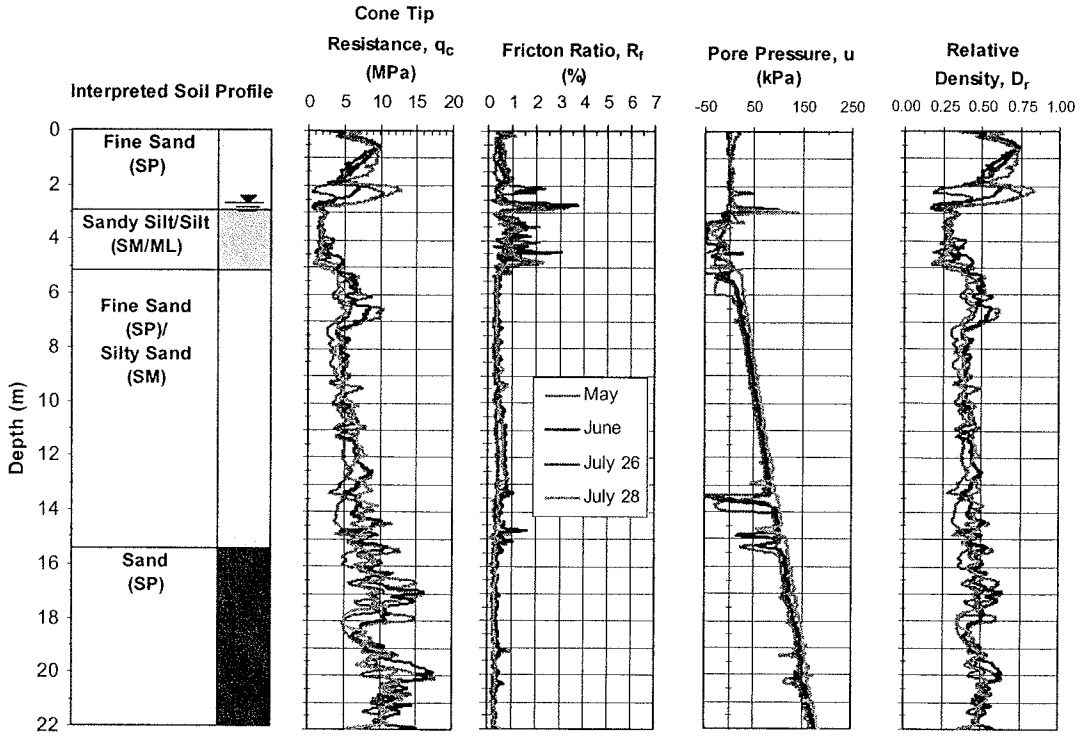

Figure 67 Comparison of CPT data for all soundings performed at Site 2.

6. Earthquake Drains

As mentioned in the introduction, one of the major objectives of this study was to evaluate the effectiveness of EQ drains in preventing liquefaction. Presumably the EQ drains would be able to dissipate the excess pore pressure quickly enough to prevent liquefaction. Drains were installed at Site 3 for full-scale blast testing and Site 2 remained untreated to act as the control. The same sequence of explosive charges which produced liquefaction at Site 2 was then repeated at Site 3. The time-rate of excess pore pressure generation and dissipation at each site was then compared to determine the effectiveness of the EQ drains.

6.1. *Drain Properties*

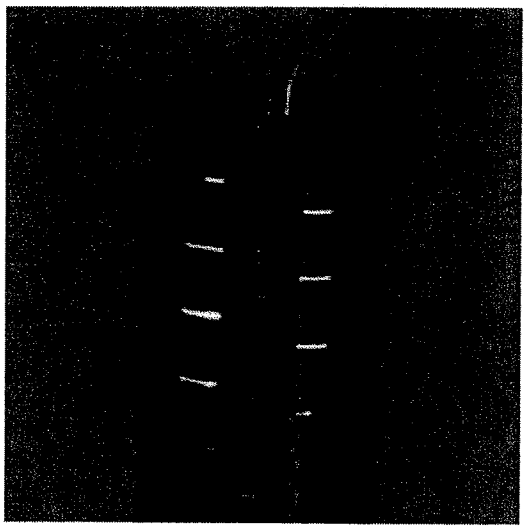

Figure 68 Section of EQDrain. Light suspended on the inside illuminates the slots (after Rollins and Anderson, 2002).

The EQ drains consisted of corrugated, perforated drain pipe covered by a geosynthetic sleeve. The drain pipe used in the test had an inner diameter of 10.2 cm and an outer diameter of 12.1 cm, with corrugations 9.5 mm deep. The flow area was 81.7 cm^2. Three slots, approximately 25 mm long, were cut into each corrugation producing an orifice area of approximately 40.2 cm^2/m of length (see Figure 68). Each drain was cut to a length of 12.8 m before installation and a hemispherical cap was fitted to the bottom end of each drain to prevent sand from plugging the end of the drain.

Each length of hose (with end cap) was slipped into a sleeve of geosynthetic fabric (model SB-252) manufactured by Synthetic Industries. The geosynthetic fabric was a polypropylene spunbond material with an apparent opening size of 50 microns. The grab tensile strength determined according to ASTM D-4632 was 40 lbs. in the machine direction and 50 lbs. in the cross machine direction.

6.2. *Drain Installation*

Between May 9 and 11, 2005, 34 earthquake drains were installed to a depth of 13.4 m with a pipe mandrel clamped to an ICE Model 44 vibratory hammer (500 N-m energy) suspended from a 70-ton mobile crane (see Figure 69). The mandrel consisted of a 165 mm diameter steel pipe with 25 mm thick walls. Three "cleated" fins equally spaced about the circumference of the mandrel transferred vibration from the mandrel to the surrounding soil (see Figure 70). The drains were installed in a triangular pattern with a spacing of 1.22 as shown in Figure 72.

The drain assemblies were "bottom loaded" into the mandrel using a rope attached to the top of the drains. The rope traveled up through the mandrel and out the side of the mandrel over a pulley positioned within the wall of the mandrel. With the bottom of the mandrel suspended approximately 1.5 meters above the ground a workman on the ground would haul the drain up into the mandrel as another workman guided the drain. The drains were pulled up tight into the mandrel to ensure that the anchor plate fit flush with the bottom of the mandrel.

Once the drain was pulled into the mandrel, the hammer was turned on and the mandrel lowered slowly into the ground. After the drains reached the design depth of 12.8 meters, the hammer was turned off. As the mandrel was removed, the hammer was turned back on for a few moments, the vibrations causing the surrounding soil to collapse around the drain, anchoring it firmly in the ground.

The anchors used during the installation of the blast holes consisted of a 150 mm x 150 mm x 12.5 mm steel plate with a loop formed from approximately 8 mm diameter steel rod to which the filter sock was tied (see Figure 71). This type of anchor proved difficult to use as they often did not anchor properly in the soil. It was discovered that the mandrel had to be lowered

Figure 69 Drain installation was accomplished with the use of a 70 ton crane and a vibratory hammer and mandrel.

twice in the same hole to install the drains. The first time the mandrel was lowered with only an anchor plate to prevent the mandrel from plugging with soil. The second time the mandrel was lowered with the drain as described above. This "double penetration" approach required up to approximately 8 minutes to install one drain.

Because of difficulties encountered in anchoring the earthquake drain casings for the blast holes, a larger anchor was used for the earthquake drains. The anchor consisted of a conical section attached to a plate approximately 305 mm x 305 mm square. This anchor was successful in efficiently anchoring the drains into the loose sand so that the installation time for a 12.8 m long drain was approximately 3 minutes.

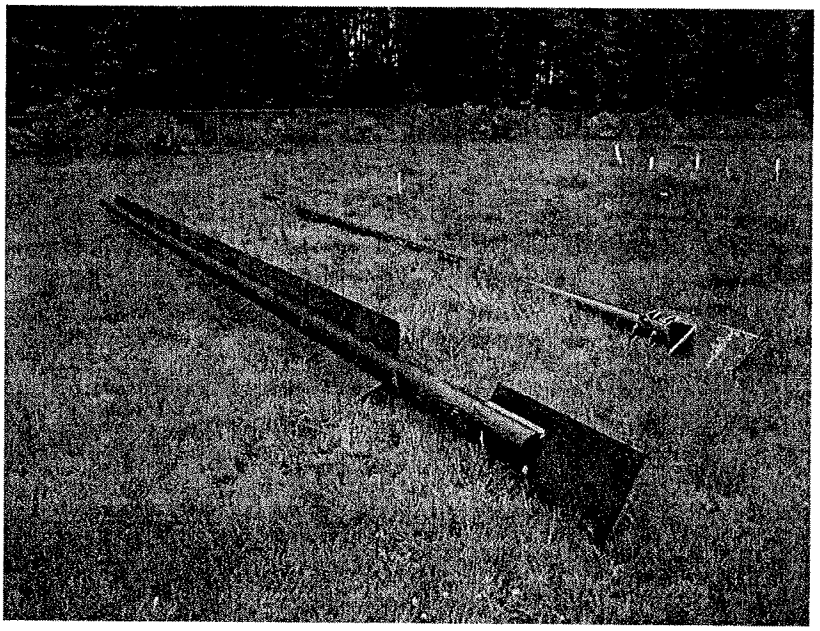

Figure 70 Mandrels used in EQDrain and blast hole installation. Mandrel on left has three "fins" designed to transfer vibrational energy to surrounding soil. Mandrel on right is smooth.

Figure 71 Photograph of an EQ Drain tied to an anchor. Anchors measured 150 mm x 150 mm x 12.5 mm. Generally, the anchors had the corners bent over; this

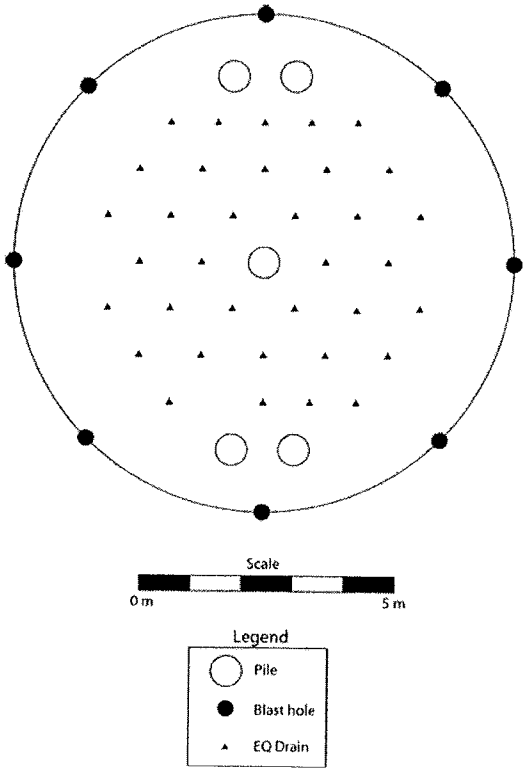

Figure 72 Layout of EQ Drain at Site 3.

6.3. *Drain Installation and Influence on Surrounding Soil*

Inasmuch as the EQ drains are designed to mitigate against liquefaction in real-world use, it is probable that they would be used in conjunction with other anti-liquefaction measures. Accordingly the drains were installed using a finned mandrel that caused soil densification during drain installation.

To evaluate changes in the sand density due to earthquake drain installation the ground settlement was measured approximately one month after installation (June 6, 2005) and an additional CPT sounding was performed at that same time. Color contours of the drain installation induced settlement are plotted in Figure 73. At one location near the center of the test area the settlement measured over 300 mm, however the average settlement within the treated area was approximately 200 mm. If it is assumed that this settlement was uniformly distributed along the length of the drain (13.7 m) then the average volumetric strain produced by installation would be approximately 1.5 percent. However, if the settlement is assumed to occur only within the liquefiable zone from 6 m to 13 m, then the average volumetric strain would be approximately 2.9 percent.

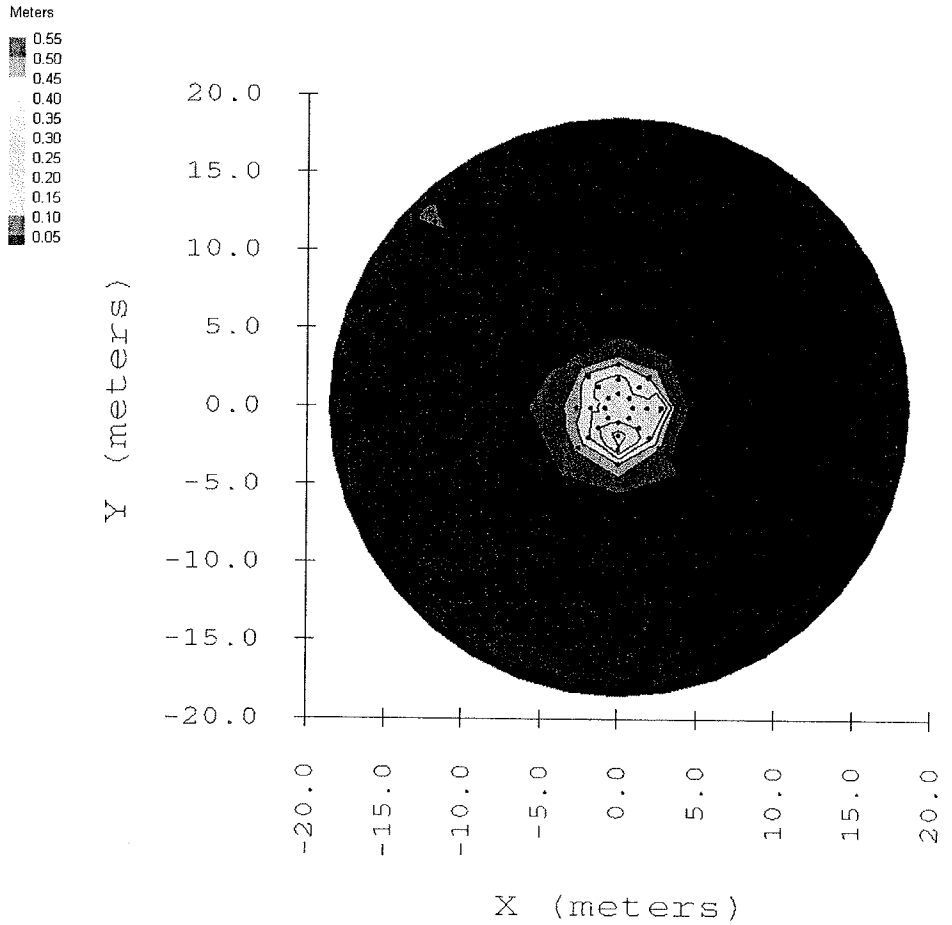

Figure 73 Contour plot of ground surface settlement caused by installation of Earthquake drains at Site 3.

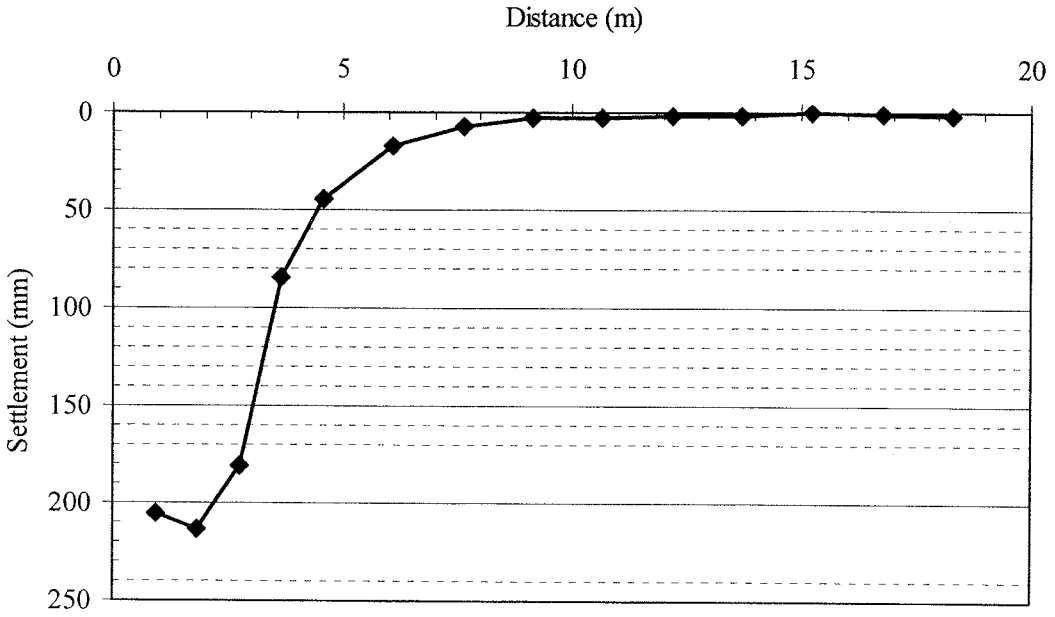

Figure 74 Average ground surface settlement caused by installation of earthquake drains and blast holes at Site 3.

A plot of the average settlement versus distance from the center of the test area is provided in Figure 74. The settlement within about 3 m of the center is relatively constant and would likely be representative of what would be expected after treatment of a large area. Beyond 3 m the settlement decreased significantly and was less than 3 mm beyond a distance of about 9 m from the center of the test area.

The cone sounding after blast hole installation was performed within a meter of the original CPT sounding. Plots of the measured cone tip resistance, friction ratio, and pore pressure are provided in Figure 75 along with average curves from the previous CPT sounding at the site along with the interpreted soil profile. A plot of the relative density versus depth was also developed using Equation (1) and is compared with the average plot from the previous sounding. Despite the fact that settlement occurred and clearly produced increased density in the liquefiable layer, there was no consistent increase in tip resistance, friction ratio or relative density. Apparently the disruption to the structure of the sand produced by the drain installation process decreased the penetration resistance more than the increased density increased the penetration resistance.

The finned mandrel caused localized settlement to occur within a circular area approximately 280 mm in diameter concentric about the center of the drain (see Figure 76). Settlement in this zone could approach 30 cm or more than the surrounding ground surface. It appears that the vibration of the mandrel as it was removed caused the surrounding soil to compact in a localized manner around the drains, causing the settlement.

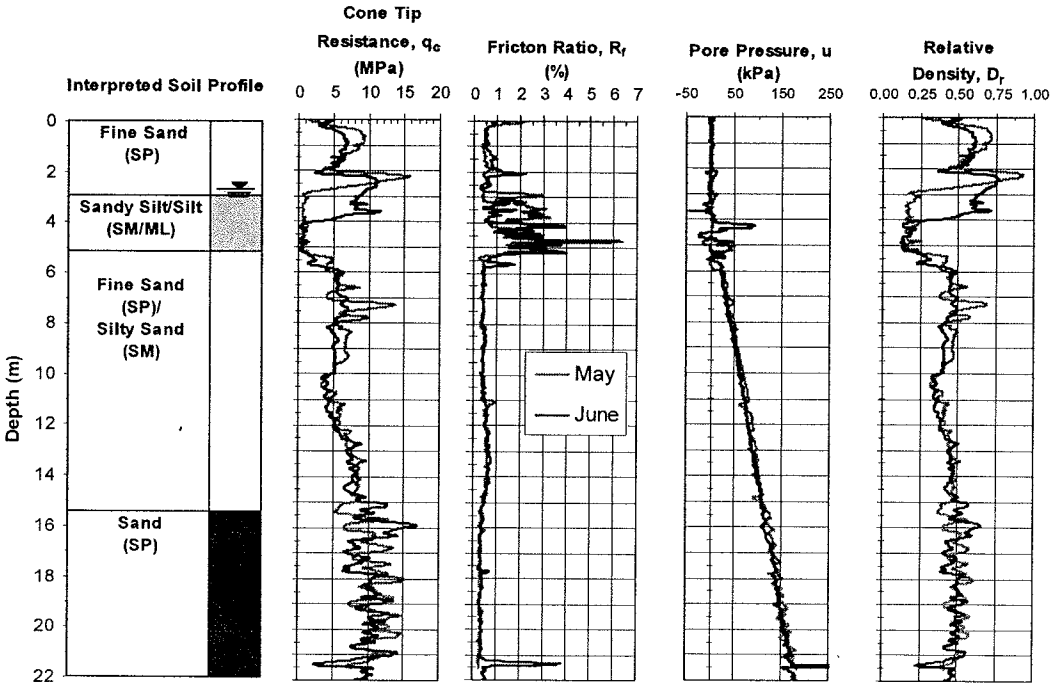

Figure 75 Comparison of CPT results at Site 3.

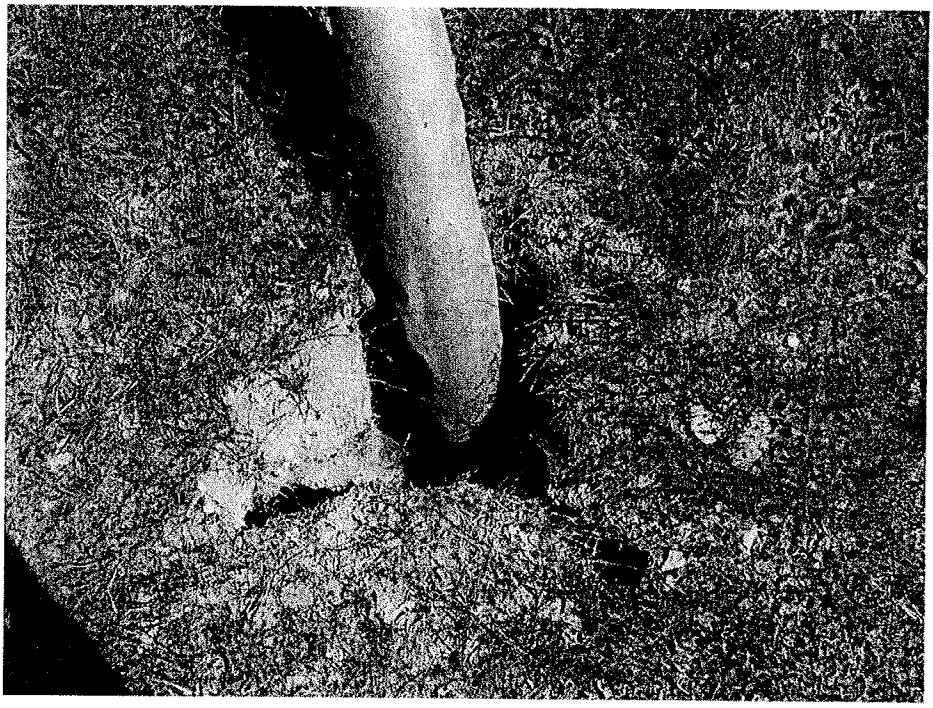

Figure 76 View of localized settlement surrounding the EQ Drain. Localized settlement immediately surrounding the drain commonly exceed 30 cm.

7. Site 3—Treated Area Pile Testing

7.1. Test Layout and Instrumentation

Plan and profile views of the layout of the test pile relative to the blast holes and instrumentation are shown in Figure 77 and Figure 78 respectively. Once again, the test pile was a 324 mm outside diameter steel pipe pile with a 19 mm wall thickness and was driven closed-ended to a depth of 21.3 m as shown in Figure 78. The test pile was instrumented with strain gauges at 1.5 m intervals from the ground surface to a depth of approximately 17.3 m as shown in Figure 77

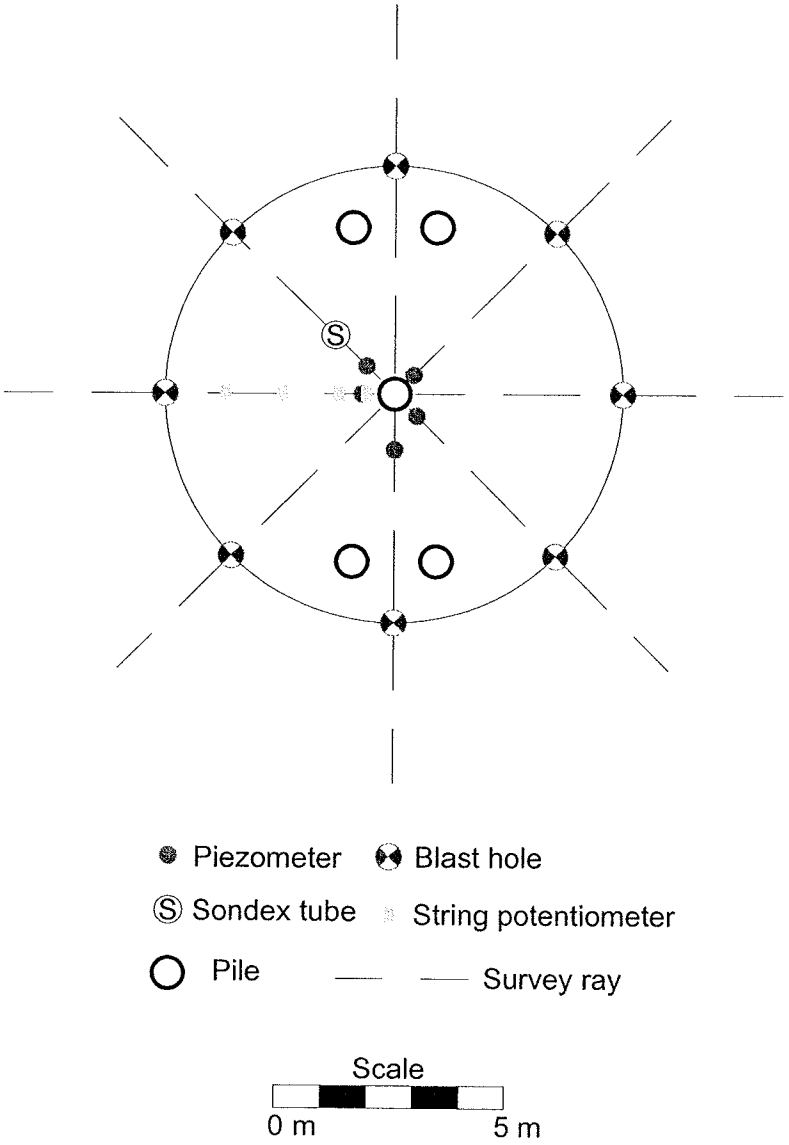

Figure 77 Plan view of pile foundation and instrumentation layout at

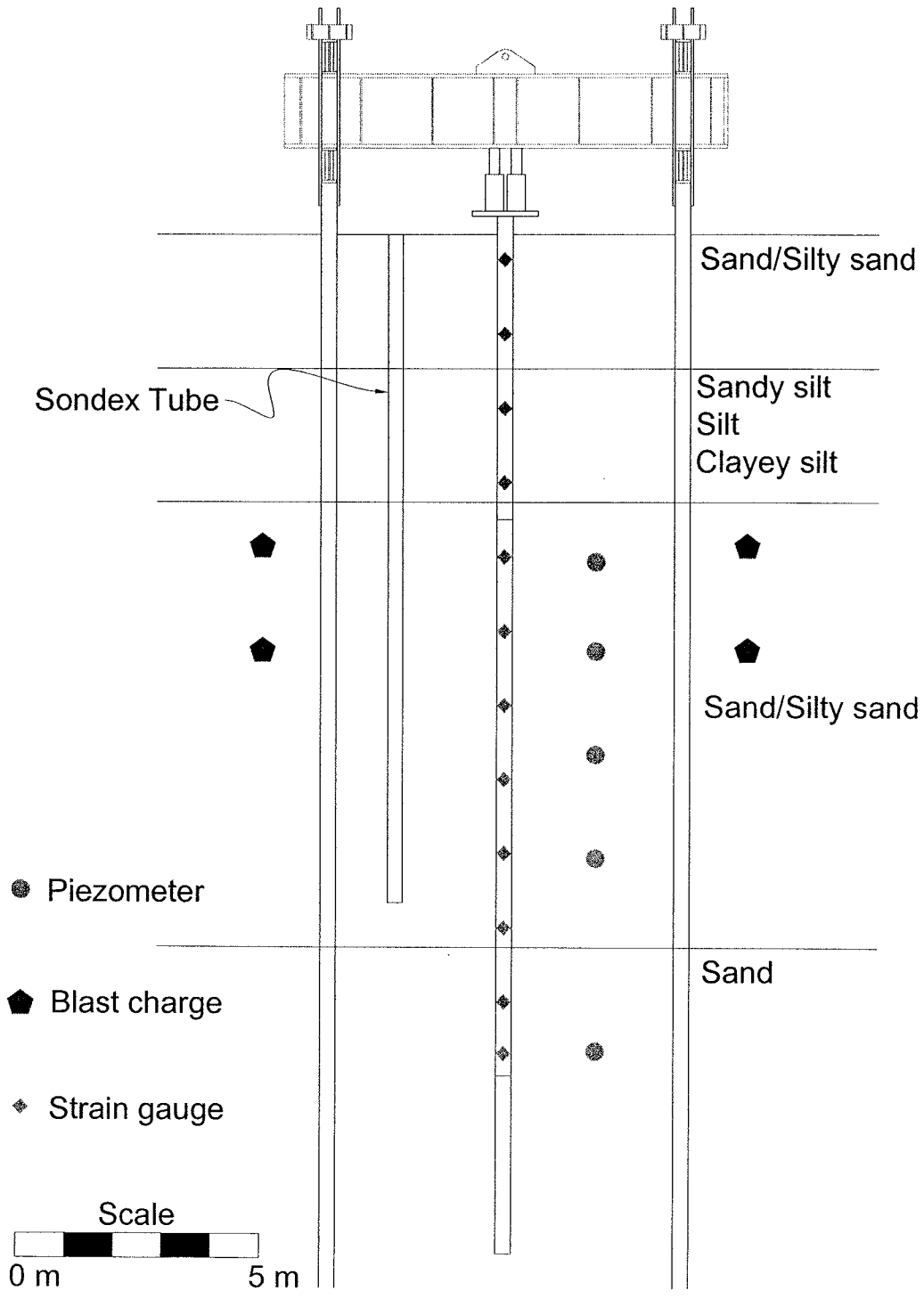

Figure 78 Profile view of pile foundation and instrumentation layout at Site 3.

the second test, the failure load was approximated). In comparison, the failure load for the test pile at Site 2 was 650 kN for the first test (performed one day after pile driving) and 1030 kN for the second test (performed one and a half months after pile driving). The difference in failure load between the two sites is 32 percent for the first tests, but only 4 percent for the second tests. The discrepancy in the failure loads for the first two tests appears to be due to set-up. The agreement for the second set of tests is very good and suggests that the two piles can be used for comparative studies.

The first load test was continued until the pile began to plunge and the maximum settlement reached approximately 69 mm, matching the deflection reached during the first test at Site 2 (approximately 67 mm). The residual displacement at the end of this initial load test was approximately 62 mm. The strain measurements at the end of the load test indicated that residual strain in the pile following the load test was very minor.

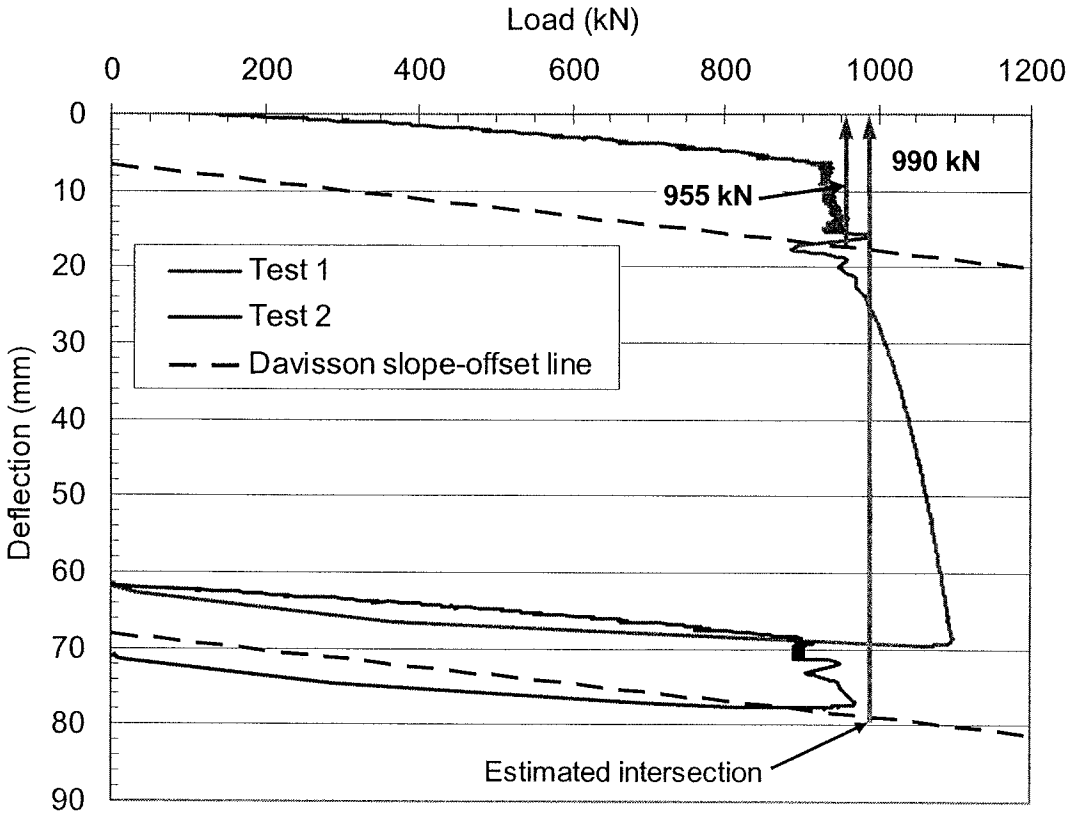

Figure 80 Pile-head-load vs. pile-head-deflection curves from the two static axial load tests performed on the test pile at Site 3.

A comparison of the load versus deflection curves for the second set of pile load tests at Sites 2 and 3 is provided in Figure 81. The results for the second tests conducted at both sites are generally quite consistent with each other. These results suggest that the increased resistance after one month relative to that one day after pile driving is a result of reconsolidation and redevelopment of the sand structure or set-up.

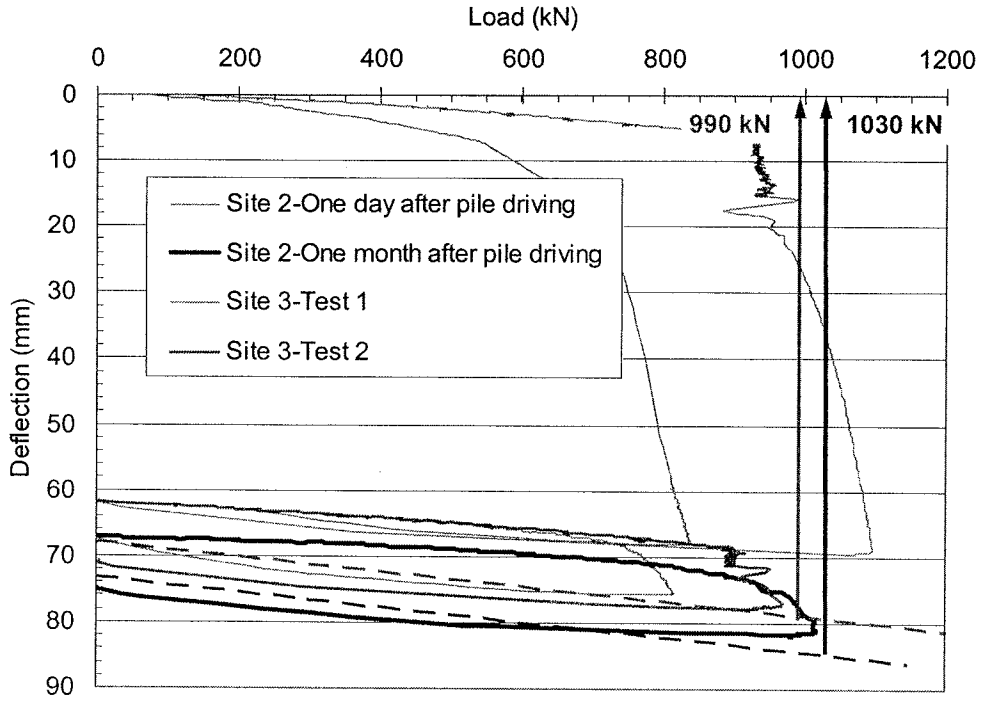

Figure 81 Comparison of pile-head-load vs. pile-head-deflection curves for all static load tests performed at Sites 2 and 3.

Based on the strain gauge data, the load in the pile during the first static test was plotted as a function of depth for a number of load increments as shown in Figure 82. A similar plot was produced for the second load test and is plotted in Figure 83.

7.4. Blast Test

For the blast test, a total of 16, 1.36 kg (3 lb) explosive charges (Pentex) were detonated sequentially with a one second delay between detonations. Charges were located at depths of 6.4 and 8.5 m below the ground surface in each of eight drill holes spaced evenly around a 10 m diameter circle centered about the test pile. The eight explosive charges at 8.5 m were detonated first followed by the eight charges at 6.4 m. This blasting pattern was identical to that used for the second blast test in the untreated test area at Site 2.

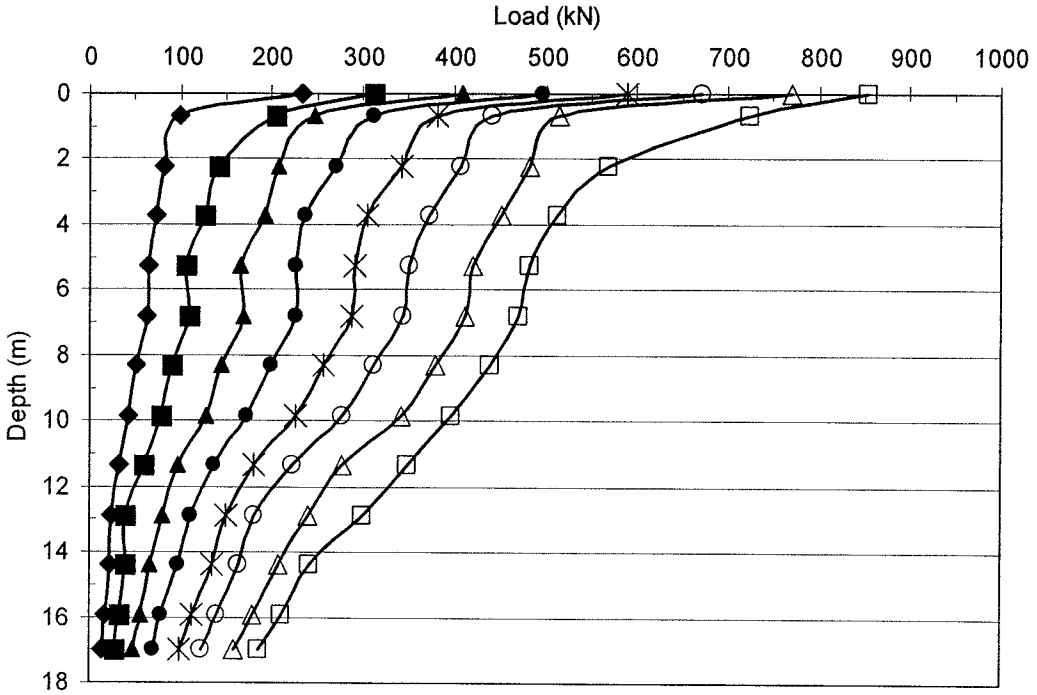

Figure 82 Load vs. depth curves for the first static load test performed at Site 3.

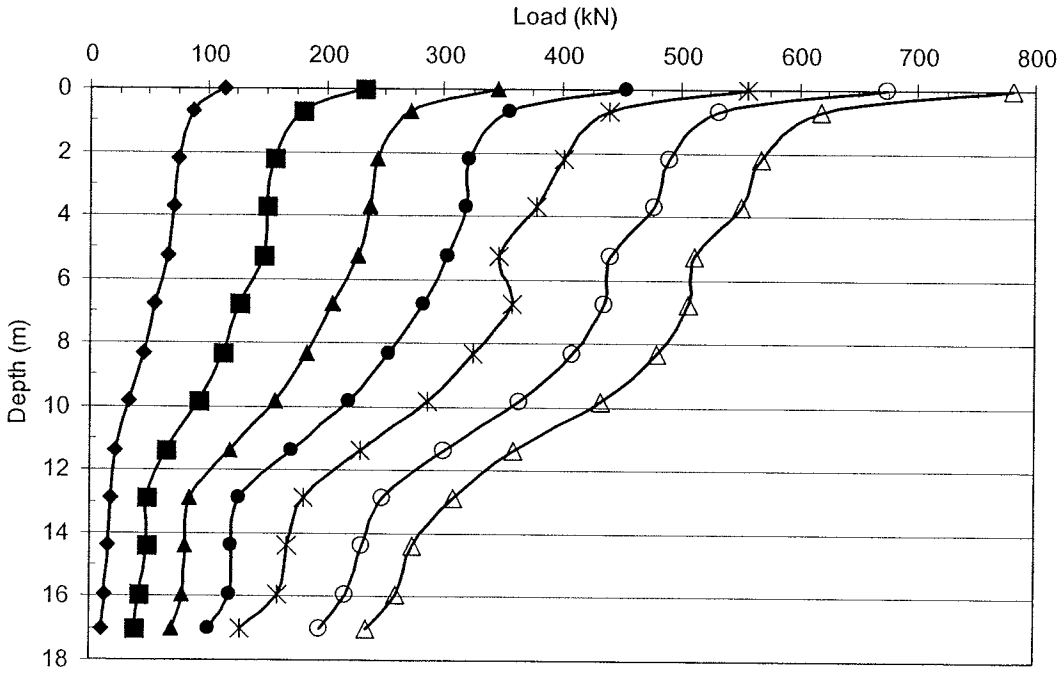

Figure 83 Load vs. depth curves for second static load test performed at Site 3.

7.4.1. Excess Pore Pressure Generation and Dissipation

Time histories showing the generation of excess pore pressure ratio for each of the five piezometers during the blast tests at Site 2 (untreated) and Site 3 (treated) are plotted in Figure 84 through Figure 88. A comparison of the piezometers at a depth of 6.5 m (6.4 m and 6.7 m) (Figure 84) the drains initially reduced the rate of pore pressure generation by about half relative to the untreated site; however, after 16 detonations, the excess pore pressure ratio at Site 3 (the treated site) still reached 90 percent indicating that the soil was essentially liquefied. A comparison of the piezometers at about 12.5 m depth indicates that the drains were successful in limiting the excess pore pressure ratio to about 0.60 in comparison to the untreated site where liquefaction was produced. This is the location where the rate of pore pressure generation was somewhat smaller than that at the other depths as discussed in section 5.6. This result suggests that the drains can be successful if the load rate is not quite as severe as that produced with the larger charge weights. At the other piezometer depths, evidence of increased pore pressure dissipation was apparent during the one second interval between detonations; however, the difference in excess pore pressure ratio between the treated and untreated sites was typically less than 0.20 and liquefaction was still produced by the sequence of blast detonations. Of course, the piezometers at a depth of 16.8 were located below the zone treated with drains and the pore pressure response is almost identical at both sites.

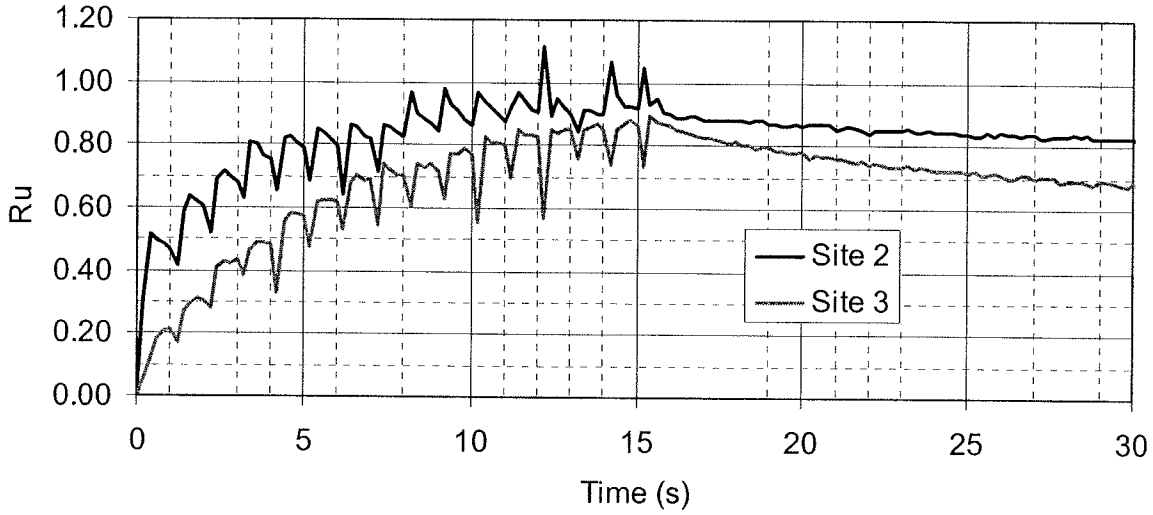

Figure 84 Comparison of excess pore pressure ratio generation at Sites 2 and 3 recorded at 6.7 m and 6.4 m depth. The piezometer at Site 2 was located at 6.7 m and the piezometer at Site 3 was located at 6.4 m depth.

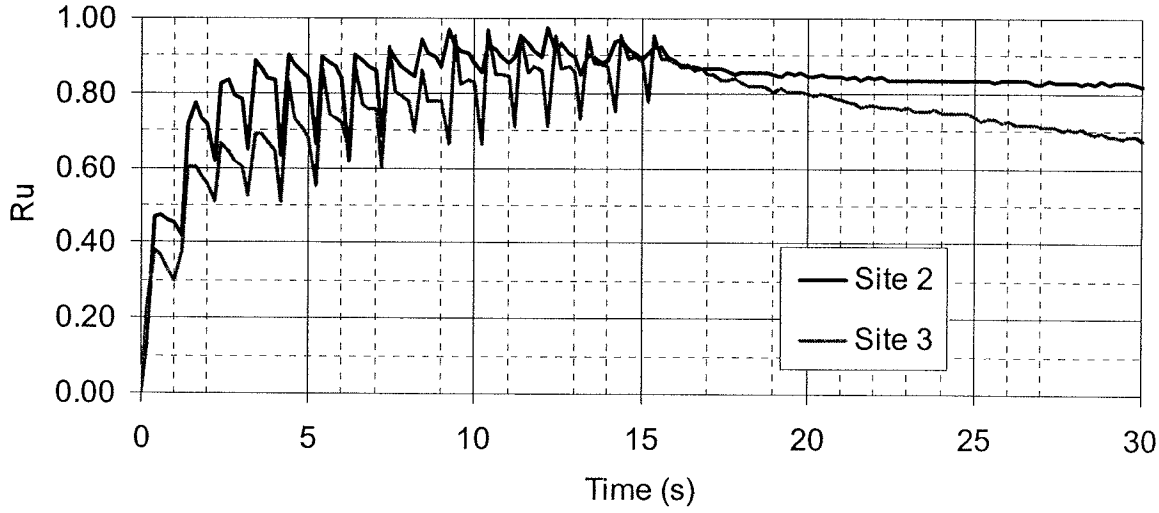

Figure 85 Comparison of excess pore pressure ratio generation at Sites 2 and 3 recorded at 8.5 m depth.

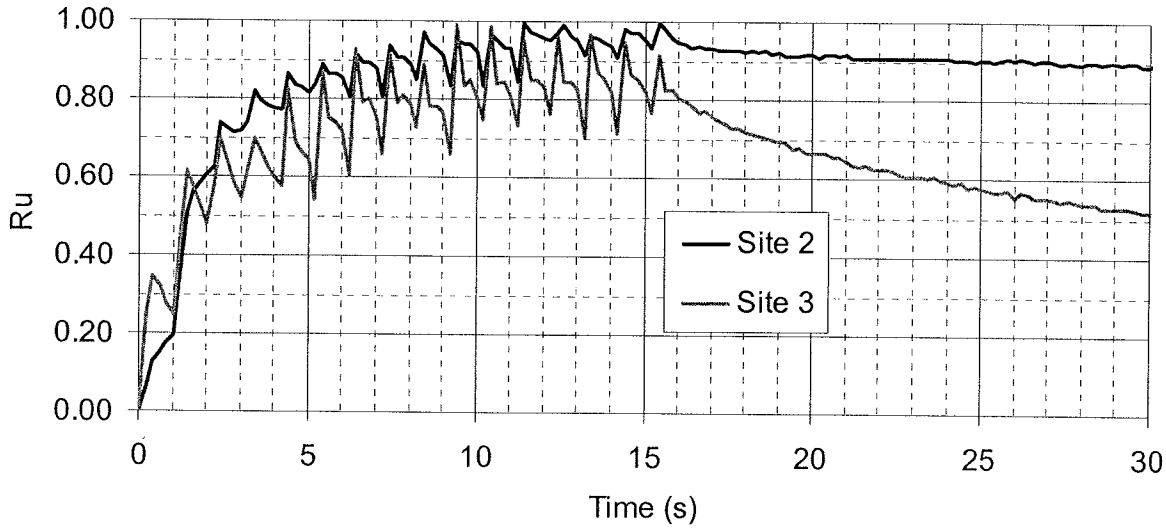

Figure 86 Comparison of excess pore pressure ratio generation at Sites 2 and 3 recorded at 10.7 m depth.

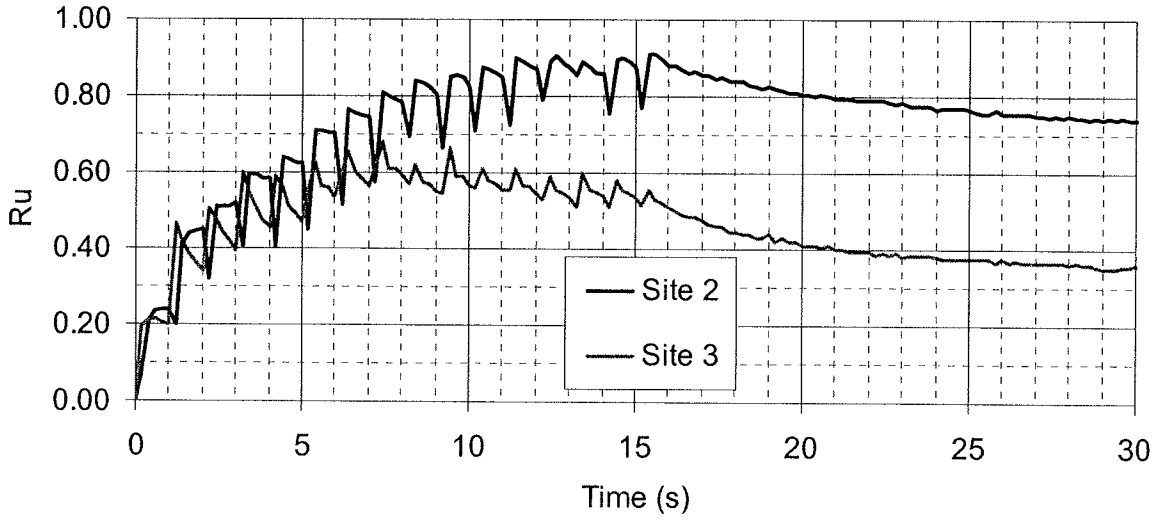

Figure 87 Comparison of excess pore pressure ratio generation at Sites 2 and 3 recorded at 12.8 m and 12.5 m depth. The piezometer at Site 2 was located at 12.8 m depth and the piezometer at Site 3 was located at 12.5 m depth.

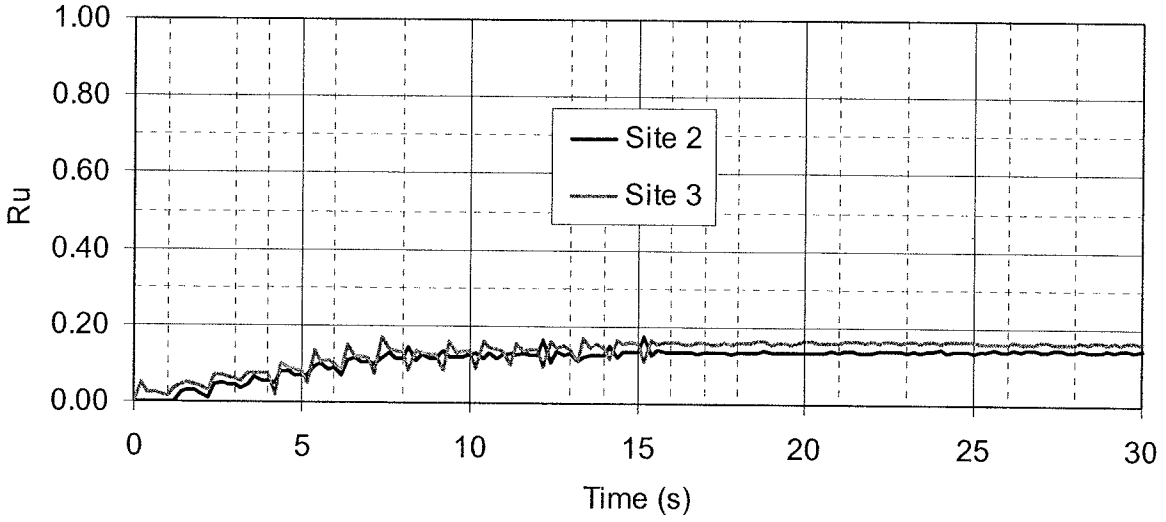

Figure 88 Comparison of excess pore pressure ratio generation at Sites 2 and 3 recorded at 16.8 m depth.

Time histories of the dissipation of excess pore pressure ratio for each of the five piezometers following blasting are presented in Figure 89 through Figure 93. Each of the piezometers at Site 3 clearly demonstrate that the drains produced substantial increases in the rate of pore pressure dissipation relative to Site 2 where drains were not used. In contrast, the rate of dissipation was almost identical for the piezometers at 16.8 below the depth treated with drains. The difference in dissipation rate is particularly pronounced for the top three piezometer locations. In this region upward water flow and the restriction to drainage provided by the upper silty clay layer resulted in a significant lag in pore pressure dissipation for the untreated site. In

contrast, all the piezometers in the area treated with drains show rapid decreases in pore pressure at the end of blasting.

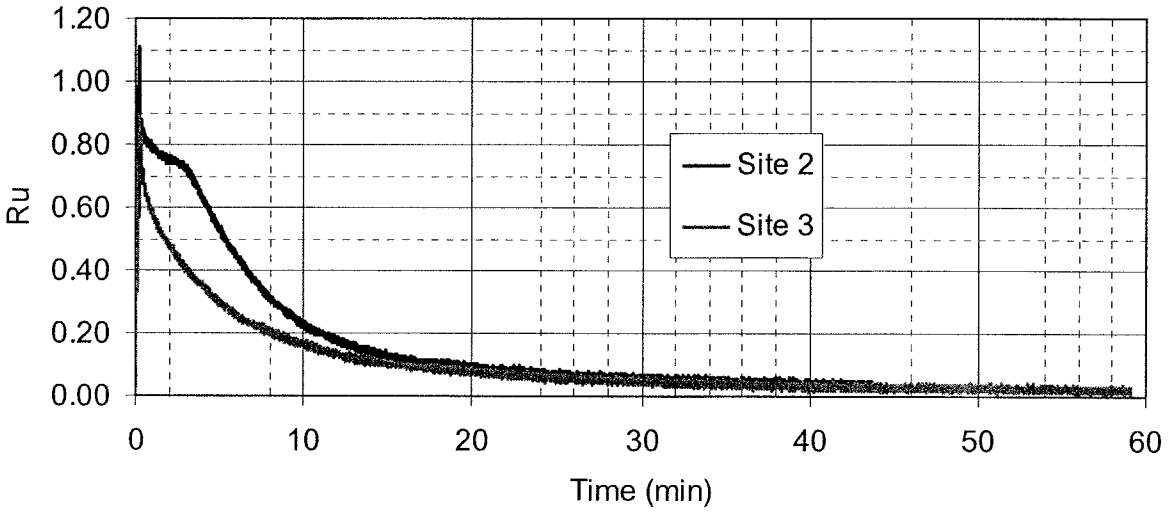

Figure 89 Comparison of excess pore pressure ratio dissipation at Sites 2 and 3 recorded by piezometers located at 6.7 m and 6.4 m depth. The piezometer at Site 2 was located at 6.7 m and the piezometer at Site 3 was located at 6.4 m depth.

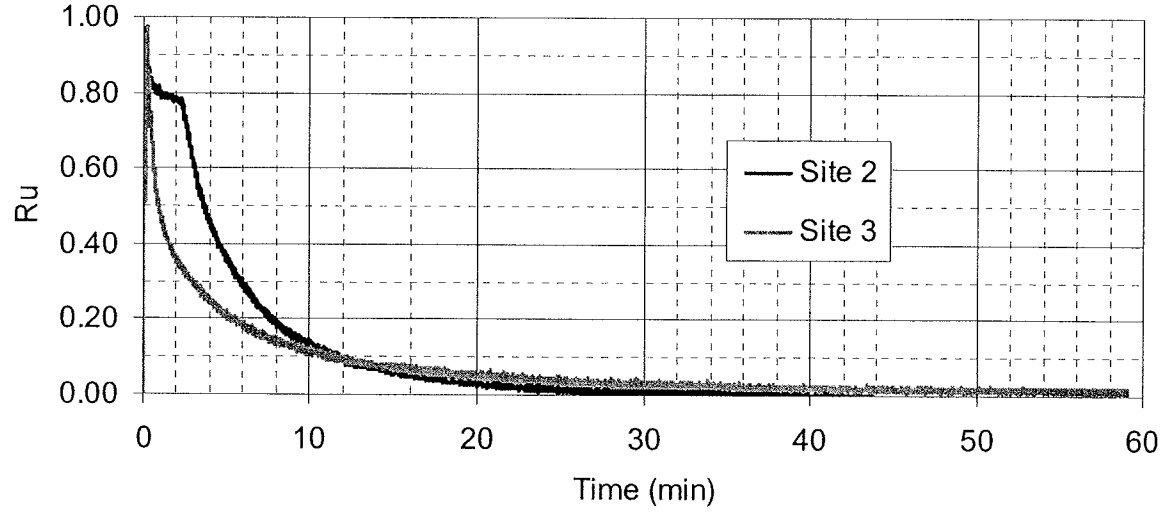

Figure 90 Comparison of excess pore pressure ratio dissipation at Sites 2 and 3 measured by piezometers located at 8.5 m depth at both sites.

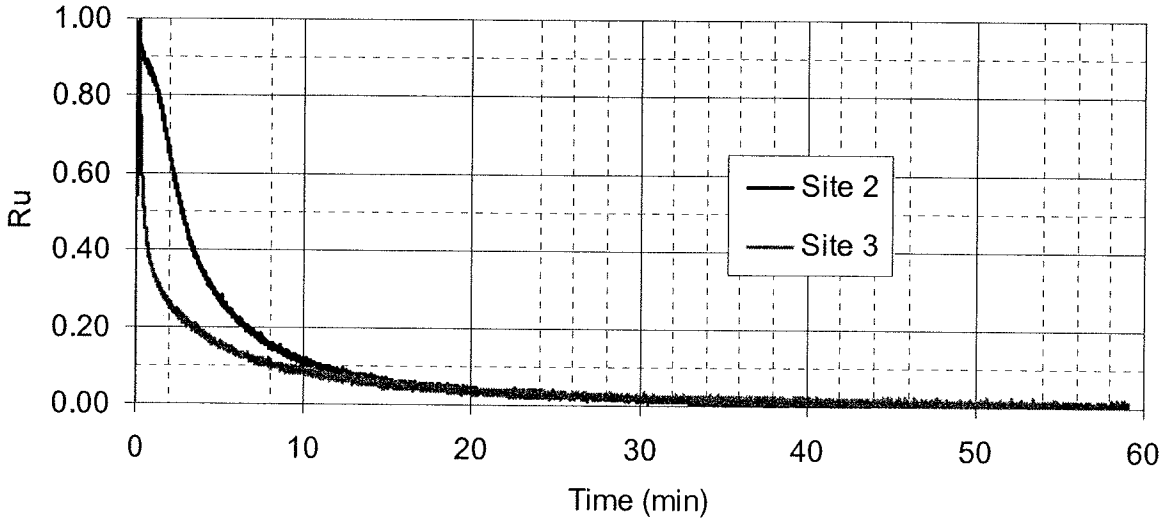

Figure 91 Comparison of excess pore pressure ratio dissipation measured by piezometers located at 10.7 m depth at both sites.

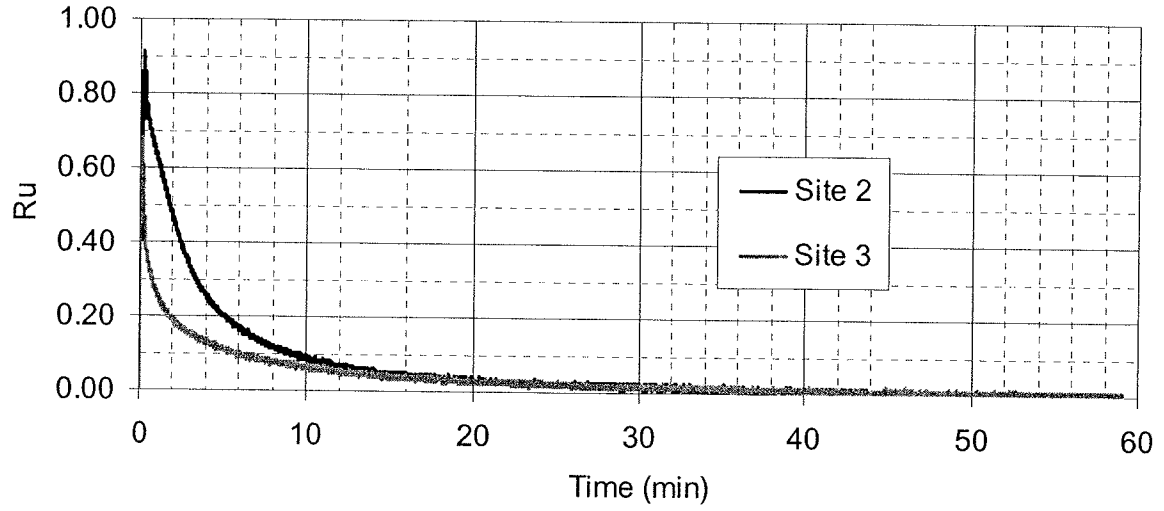

Figure 92 Comparison of excess pore pressure ratio dissipation at Sites 2 and 3. The piezometer at Site 2 was located at 12.8 m depth and the piezometer at Site 3 was located at 12.5 depth.

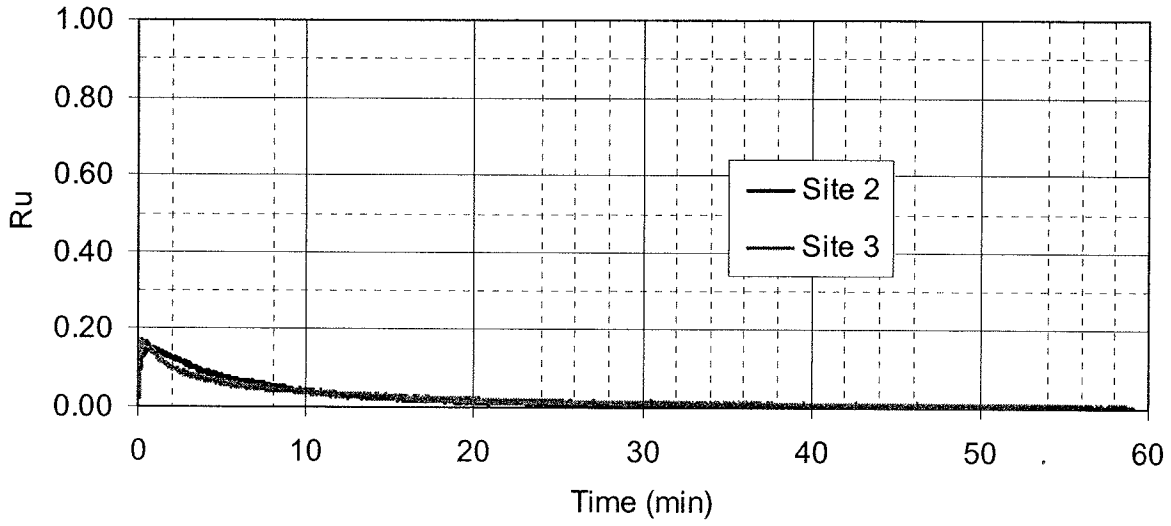

Figure 93 Comparison of excess pore pressure ratio dissipation at Sites 2 and 3 measured at 16.8 m depth at both sites.

The results of this test clearly indicate that the drains are increasing the rate of dissipation at the treated site. However, the increased drainage was apparently insufficient to prevent liquefaction at all but the 12.5 m depth. This situation could potentially be remedied by using larger drains or placing the drains at closer spacings. Evaluation of these possibilities will be examined in subsequent sections of this report.

7.4.2. Blast-Induced Settlement

A color contour plot of the ground surface settlement following the test blast is provided in Figure 94. The maximum settlement was approximately 270 mm which occurred approximately 3.5 meters east of the center of the site. However, the settlement is relatively uniform throughout most of the area covered by drains. Contours of settlement were generally concentric about the center of the test area

A plot of the average ground surface settlement with respect to distance from the center of the test area is provided in Figure 94 along with a similar curve of settlement for the second blast test at the untreated area. In general, ground surface settlement was almost identical outside the area treated with drains. The major differences occurred within a circular area within four meters of the center of the test site which corresponds with the treated area. On average, the settlement in the treated area was about 17 percent lower than settlement in the untreated area. In addition, the settlement in the drained area is much more uniform than that in the untreated area, which would be beneficial in minimizing differential settlements to structures over these treated areas.

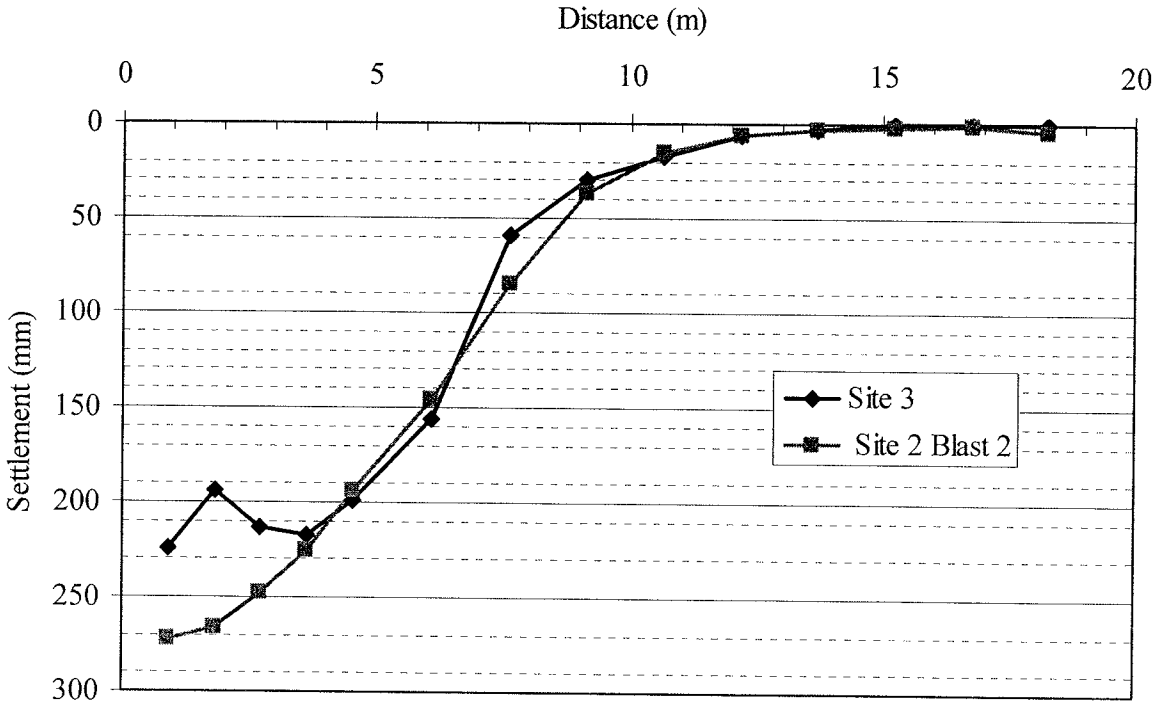

Figure 94 Comparison of average settlement caused by blast testing at Sites 2 and 3.

A plot of the settlement versus depth obtained from the Sondex tube is provided in Figure 96. Once again the top layer appears to settle as a block over the liquefied sand, although the effect was less pronounced than at Site 1 or Site 2. Settlement in the liquefied zone is relatively linear and decreases to essentially zero at a depth of about 14 m. Based on the measurements the average volumetric strain in the sand layer from 6 m to 13 m was approximately 1.6 percent. This volumetric strain is 50 percent less than the 2.4 percent volumetric strain measured for the second test blast in the untreated liquefied sand at Site 2.

Plots of settlement versus time are shown in Figure 96 for the string potentiometers installed on the ground surface located 1.2 m, 2.4 m, and 3.7 m from the center of the test site. The settlement patterns measured by the string potentiometers were as expected. Maximum settlement occurred near the center and decrease somewhat with increasing distance from the center of the test area. In general, the settlement occured very rapidly after blasting. About 60% of the settlement occurred within 23 seconds of the onset of blasting, corresponding to an average R_u of 85 percent in the liquefied zone. About 90 percent of the settlement was complete within four minutes of blasting corresponding to an average excess pore pressure ratio of 40 percent in the target zone (6 to 13 m). The remaining 10 % of the settlement took approximately 55 minutes to complete.

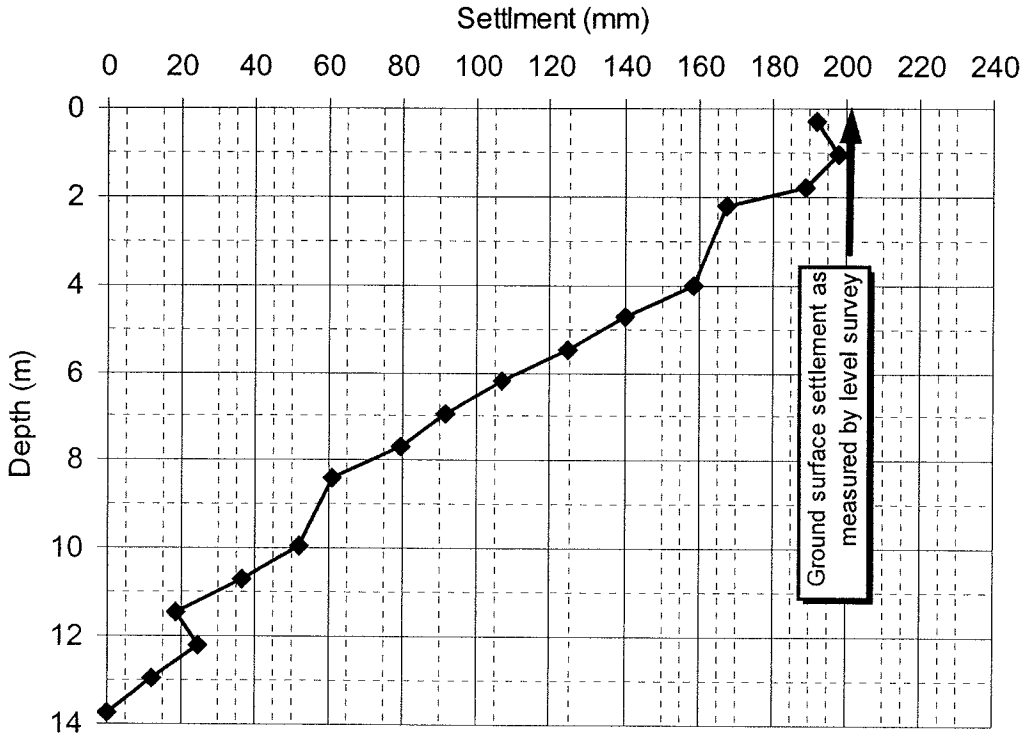

Figure 95 Settlement vs depth as measured by the Sondex tube at Site 3.

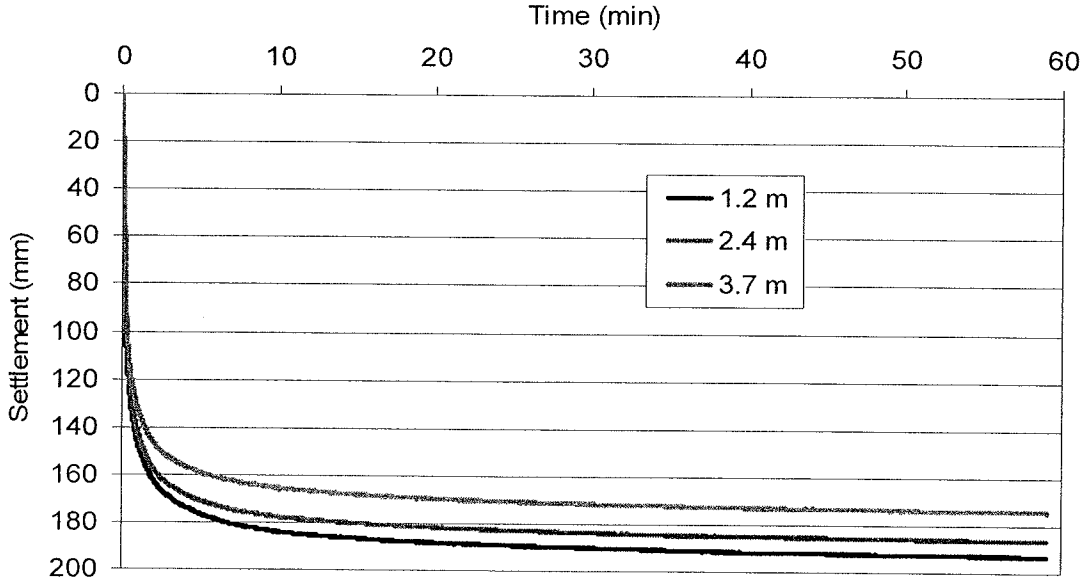

Figure 96 Time histories of real-time settlement measured by string potentiometers located at 1.2 m, 2.4 m, and 3.76 meters from the center of Site 3.

A plot of the normalized settlement versus time curves for string potentiometers located 1.2 m from the center of the test areas at Sites 2 and 3 is provided in Figure 97. These curves clearly show that settlement occurs much more rapidly at Site 3 due to the increased rate of dissipation provided by the drains relative to the untreated site. This plot provides additional evidence of the efficacy of the drains in increasing the pore pressure dissipation rate.

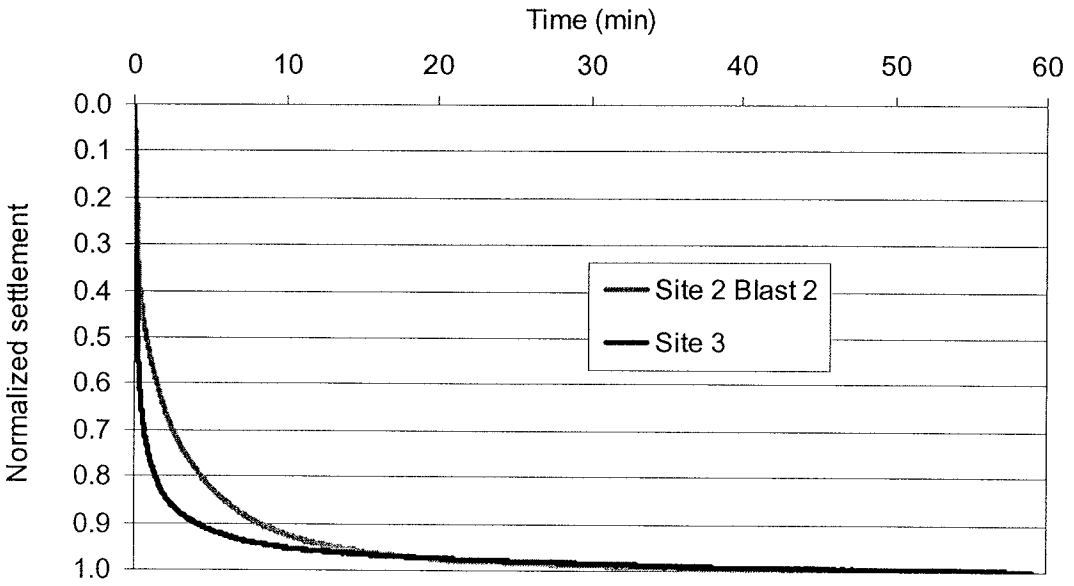

Figure 97 Comparison of normalized settlement at Sites 2 and 3.

7.4.3. Pile Load Transfer Variations Due to Liquefaction

Figure 99 provides a plot showing the load in the test pile versus depth for the blast test at Site 3 based on strain gauge measurements. As was done for Site 3, load versus depth curves are provided for the case immediately prior to the blasting sequence, immediately after blasting, and at the end of settlement. Immediately prior to blasting with a load of approximately 500 kN was applied to the test pile and this load was resisted primarily by positive skin friction with a minor contribution from end-bearing. Just after the blast, the load at the pile head dropped to about 450 kN because of settlement of the pile relative to the reaction frame and the pump was activated to bring the load back up to the original value. At this stage, the load versus depth curve still indicates positive skin friction down to the top of the liquefied zone, but negative skin friction in the liquefied zone. The rapid development of negative skin friction in this case relative to that observed at Site 2 is likely due to the drainage provided by the drains which accelerated the settlement process. At the end of settlement, skin friction still appears to be positive in the soil above the liquefied zone, although attrition of the strain gauges makes a detailed assessment difficult. The negative skin friction in the zone that liquefied has become greater and is equal to

or somewhat higher than the positive skin friction in this zone prior to blasting. The increase in negative skin friction appears to have been resisted by a combination of increased skin friction as well as some increase in the end-bearing resistance relative to the conditions before blasting.

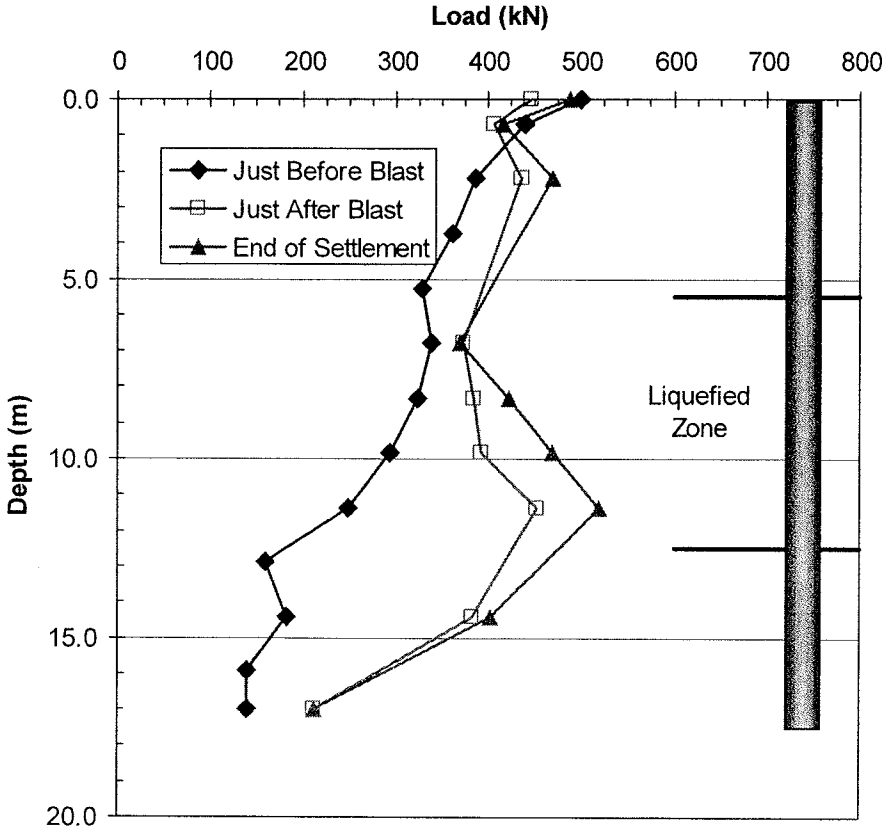

Figure 98 Plot of load in pile immediately before the blast, immediatley after blast and at the end of settlement.

Figure 100 provides a comparison plot of the load versus depth curves for the test piles at Site 2 and Site 3 just before blasting, just after blasting and at the end of settlement. The load versus depth curves before blasting appear to be reasonably comparable, although the curve at Site 3 appears to indicate greater end-bearing resistance. Just after blasting the curves in the liquefied zone show greater negative skin friction at Site 3 relative to Site 2, presumably due to the increase in the drainage rate. In fact, at this stage the negative skin friction is similar to that at the end of settlement for Site 2. At the end of settlement, the negative skin friction in the

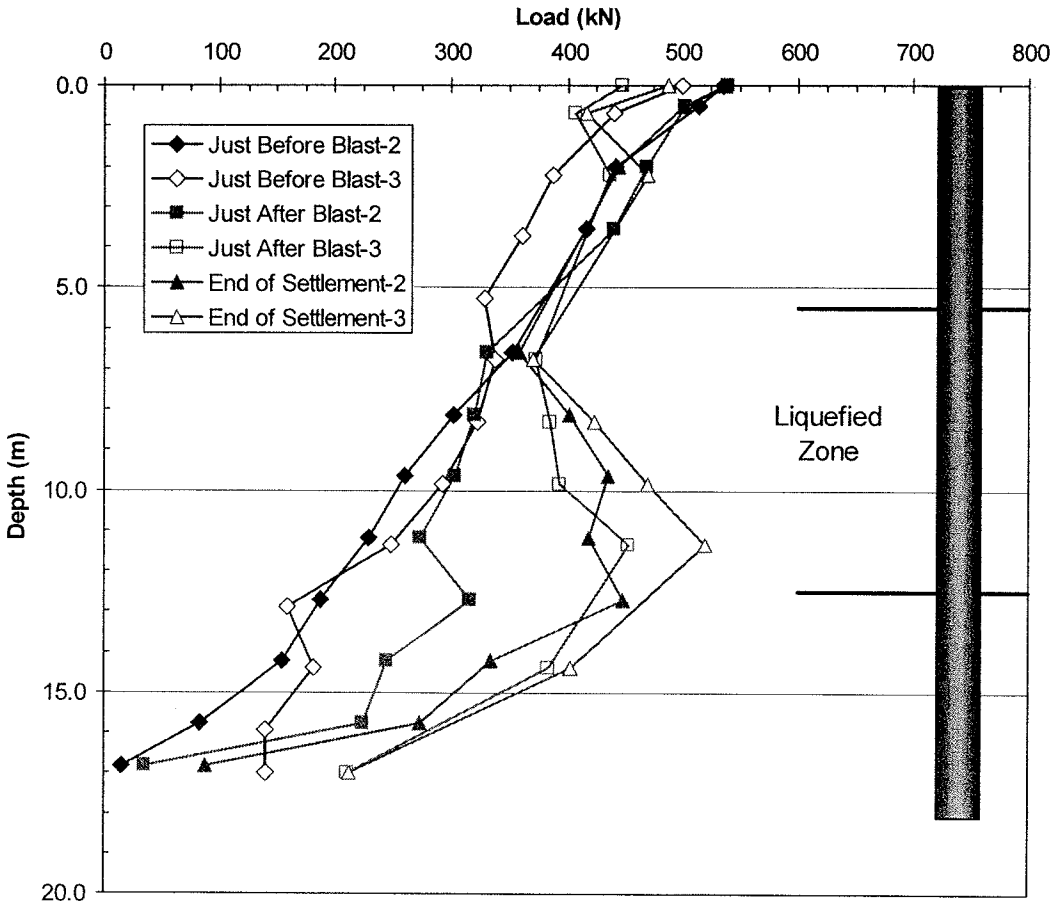

Figure 99 Comparison of the load versus depth curves measured at Sites 2 and 3 immediately prior to blasting, immediately after blasting and at the end of blasting.

liquefied zone is higher for Site 3 than for Site 2. The higher negative skin friction could result from the increased rate of pore pressure dissipation which would allow the liquefied sand to return to a semi-solid state more rapidly.

8. Computer Analysis of Blast Liquefaction Tests

Although the blast liquefaction tests clearly indicated that pore pressure dissipation rates were significantly increased with the use of EQ drains, the drains in their present configuration were insufficient to prevent liquefaction. To provide increased understanding of the behavior of the drains for different drain configurations (spacing and diameter) along with less demanding analyses were performed using the computer program FEQDrain (Pestana et al, 1997). During this study, the computer model was first calibrated using the measured settlement and pore pressure response from the blast test at Site 3. Then, the calibrated soil properties were held constant while the drain configuration was varied. Similar analyses could be performed to evaluate variation in the rate of loading from earthquake events (amplitude of shaking and number of cycles),

FEQDrain uses an axi-symmetric finite element model of the soil profile and composite drain system. The program models an individual drain within a grid of drains using a "radius of influence" concept based on the drain spacing. The computer program calculates the excess pore pressure ratio in each soil layer within the radius of influence. This is done by accounting for the generation of pore pressure produced by the earthquake and the dissipation of pore pressure provided by flow to the drains.

The program is capable of accounting for head loss in the drain and storage in the drain as water levels change during pore pressure build-up. FEQDrain can also account for non-linear increases in the modulus of compressibility of the soil as the excess pore pressure ratio increases. In addition to computing pore pressure response, the program can compute the settlement due to the dissipation of excess pore pressures.

8.1. Calibration of Computer Model

8.1.1. Selection of Soil Input Parameters

The basic soil profile and layer thickness values used in the analysis of the EQ drain test area (Site 3) was based on the CPT profiles previously shown in Figure 79. The soil profile was divided into 6 separate layers: the top two layers representing the silty sand layer and the clayey silt layers respectively (see Figure 15). The boundaries of the bottom four layers were located such that the piezometers were located at the center of each layer. This allowed the soil properties to be varied individually for each piezometer to assist in the calibration of the FEQ Drain model.

The five most important soil properties in matching the pore pressure history and settlement are the horizontal hydraulic conductivity (k_h), vertical hydraulic conductivity (k_v), modulus of compressibility (M_v), relative density (D_r), and the number of cycles required to cause liquefaction (N_L). The determination of each of these properties is discussed in the following section.

Hydraulic Conductivity

The horizontal hydraulic conductivity is perhaps the most important factor governing the rate of dissipation. As k_h increases, the rate of dissipation increases. In general, the vertical hydraulic conductivity does not greatly influence the response since most of the drainage is radial or horizontal. For example, Seed and Booker (1977) used $k_v = 0$ in original computations for their design charts. In relatively uniform sands, k_v has little effect as shown by Pestana et al (1997); however, in layered soil strata, k_v can sometimes be important. Typical ranges of k_h as a function of soil type are provided by Pestana et al (1997) based on recommendations from Terzaghi and Peck (1948) in Table 5. A review of the data in the Table 5 indicates that significant variation can occur within a given soil type due to minor variations in fines content and density. Other investigators have indicated that the variation in k_h within a given soil type could be as much as two orders of magnitude (Freeze and Cherry, 1979).

Table 5 Typical values for horizontal hydraulic conductivity (k_h) from Pestana et al, 1997 (after Terzaghi and Peck, 1948).

Soil Type	Particle Size (mm)	Coefficient of hydraulic conductivity (cm/s)
Very fine sand	0.05-0.10	0.001-0.005
Fine sand	1.10-0.25	0.005-0.01
Medium sand	0.25-0.50	0.01-0.1
Coarse sand	0.50-1.00	0.1-1.0
Small pebbles	1.00-5.00	1.0-5.0

Due to layering effects and soil structure orientation under stress, the horizontal hydraulic conductivity is typically higher than the vertical hydraulic conductivity. Typical ratios of the horizontal to vertical hydraulic conductivity for various soil conditions are given in Table 6.

Table 6 Relationship between k_h and k_y from Pestana et al (1997).

Description	k_h/k_y
Uniform (clean sands)	1.5-2.0
Moderately anisotropic (silt seams)	4.0-5.0
Highly anisotropic	10-100

The horizontal hydraulic conductivity used in this study was initially selected based on the value measured in-situ by the packer tests as shown previously in Figure 18. The ratio of k_h/k_v was generally assumed to be 10. In an iterative process, adjustments were made to the k_h values used in FEQ Drain to improve the agreement between the computed and measured pore pressure response in the various soil layers. The final profiles of k_h versus depth for Site 3, the EQ Drain Test Area is shown in Figure 101. The range of measured/expected values of k_h, as measured by Rollins and Anderson (2002) at a site approximately 30 m south of the current test location is also shown in Figure 101. Although the k_h values for the two lowest layers remained within the expected range, the values of k_h in the two upper liquefiable layers fell outside the measured range range, but still within a reasonable upper bound for permeability selection.

Modulus of Compressibility

The modulus of compressibility (M_v) is a measure of the vertical strain produced by a change in vertical stress. This parameter is roughly equivalent to the inverse of the elastic or Young's modulus. Although M_v is often measured for clays while pore pressures dissipate, very few studies have made measurements of M_v for sands during pore pressure dissipation. Based on studies by Pestana et al (1997), M_v for sand typically lies within a fairly narrow band ranging from 2.05×10^{-7} to 1.0×10^{-8} m^2/kN and is not sensitive to highly relative density. However, as the excess pore pressure ratio (R_u) increases beyond about 0.60, the M_v can increase significantly as shown in Figure 102. In these cases, M_v is dependent on both the relative density and the excess pore pressure ratio. Seed et al (1976) developed a relationship to account for the variation in M_v with D_r and R_u as shown in Figure 102. This relationship is used in the computer model FEQDrain.

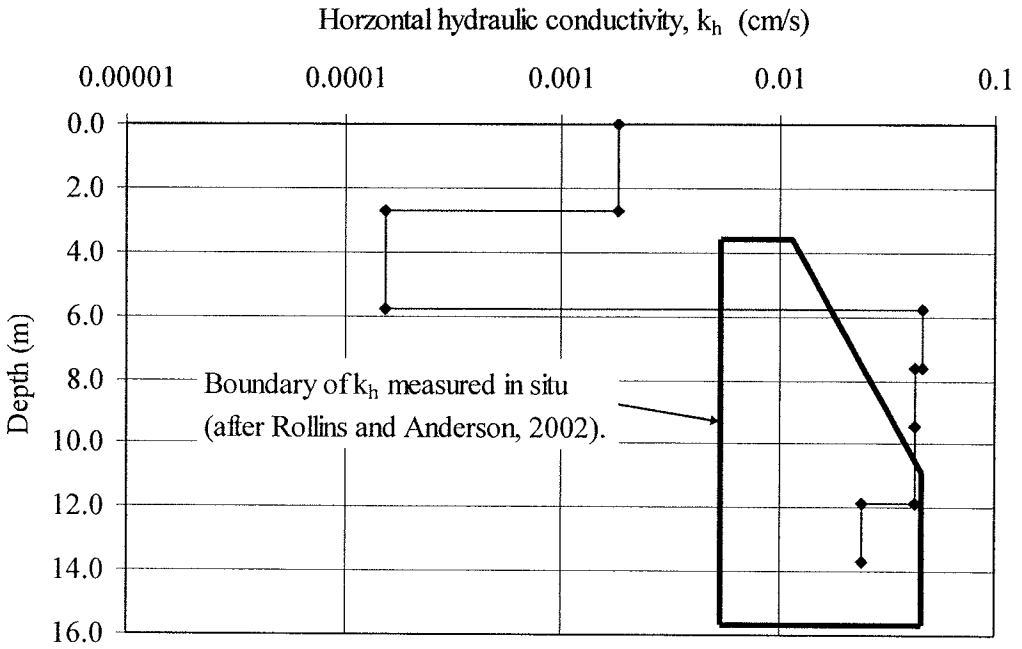

Figure 100 Comparison of calibrated values of horizontal hydraulic conductivity (k_h) versus depth with values measured in situ by Rollins and Anderson (2002).

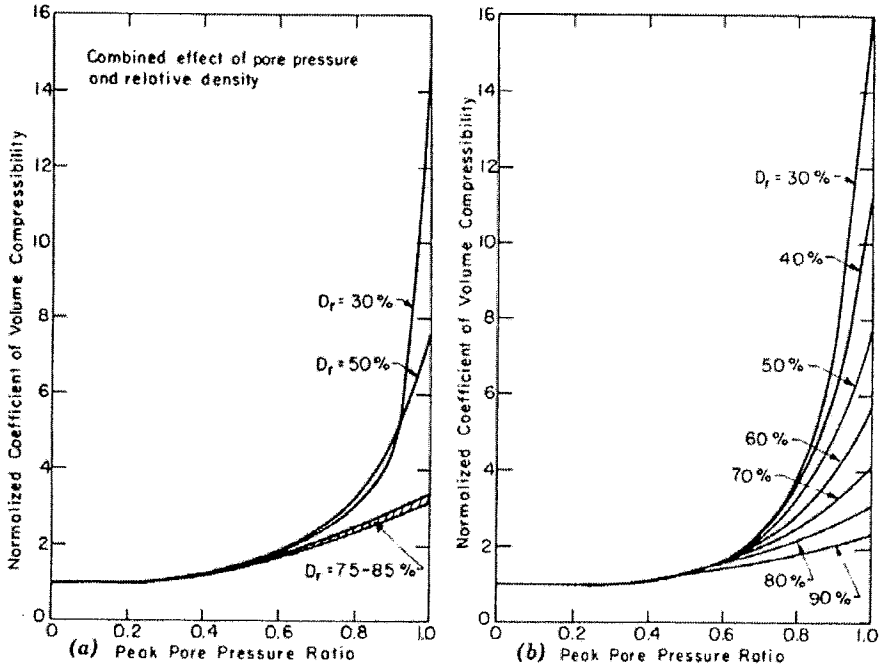

Figure 100 Variation in normalized coefficient of compressibility (M_v/M_{vi}) versus peak pore pressure ratio (R_u) for sands of various relative densities (D_r) from (a) laboratory tests, and (b) as modeled in FEQDrain (Seed et al, 1976).

It was impossible to calibrate the FEQ Drain model such that both the measured and calculated values of R_u and settlement matched at the same time. Because the settlement calculations used in FEQ Drain are based on the poorly understood and difficult to measure M_v parameter, it was decided to calibrate the FEQ Drain model based on excess pore pressure ratios only. The validity of this decision will be shown in a later. The disregard of the coefficient of compressibility did not add significantly to the error in calibrating the model.

Relative Density

The estimates of relative density were made based on the initial values provided by the CPT soundings. This parameter was not modified greatly during the investigation.

Number of Cycles to Cause Liquefaction

Another important characteristic of the soil is the number of cycles required to cause liquefaction (N_L). The N_L for the blast simulation was obtained by determining the time at which liquefaction occurred using the pore pressure ratio versus time plot measured at Site 2 as shown in Figure 59. As can be seen, the upper three liquefiable layers liquefied after 10 to 12 blasts while the bottom layer never fully liquefied. For the analyses conducted in this study, the best agreement with the measured response was obtained when N_L was assumed to be 11 for the upper three layers and 16 for the bottom layer.

Summary of calibrated values

The final, calibrated soil properties for Site 3 (EQ Drain Test Area) obtained by trial and error with FEQDrain are shown in Figure 103.

8.1.2. Drain Input Properties

The outside radius of the drain was 12.1 cm which corresponds to a drain area of 115.0 cm^2. The radius of the area of influence was 0.64 m which represents a drain spacing of 1.22 m in a triangular grid. The area of openings per unit length in the perforated pipe was 0.004 m^2/m of length and the constant associated with head loss through the perforations was taken as 1.0.

The equation for head loss due to vertical resistance in the drain (H_{drain}) was given by

$$H_{drain} = 0.5(Q * z)^2 \tag{8}$$

where Q is flow rate and z is depth.

	Layer thickness	Depth to sublayer (m)	Calibrated soil properties
Layer 1	2.744 m 9 sublayers	0.3049 0.6098 0.9146 1.2195 1.5244 1.8293 2.1341 2.4390 2.7439	Sand/Silty sand Kh = 1.83 x 10^{-4} cm/s Kv = 1.83 x 10^{-5} cm/s Mv =2.099 x 10^{-5} m^2/kN Dr =0.6
Layer 2	3.049 m 10 sublayers	3.0488 3.5370 3.6585 3.9634 4.2683 4.5732 4.8780 5.1829 5.4878 5.7927	Sandy silts/Silts/Clayey silts Kh = 1.524 x 10^{-5} cm/s Kv = 1.524 x 10^{-6} cm/s Mv =8.359 x 10^{-5} m^2/kN Dr =0.7
Layer 3	1.829 m 6 sublayers	6.0976 6.4024 6.7073 7.0122 7.3171 7.6220	Sand/Silty sand Kh = 4.572 x 10^{-3} cm/s Kv = 4.572 x 10^{-4} cm/s Mv =1.045 x 10^{-4} m^2/kN Dr =0.3
Layer 4	1.829 m 6 sublayers	7.9268 8.2317 8.5366 8.8415 9.1463 9.4512	Sand/Silty sand Kh = 4.267 x 10^{-3} cm/s Kv = 4.267 x 10^{-4} cm/s Mv =1.045 x 10^{-4} m^2/kN Dr =0.3
Layer 5	2.439 m 8 sublayers	9.7561 10.061 10.366 10.671 10.976 11.280 11.585 11.890	Sand/Silty sand Kh = 4.267 x 10^{-3} cm/s Kv = 4.267 x 10^{-4} cm/s Mv =1.045 x 10^{-4} m^2/kN Dr =0.3
Layer 6	1.83 m – 6 sublayers	12.195 12.500 12.805 13.110 13.415 13.720	Sand/Silty sand Kh = 2.408 x 10^{-3} cm/s Kv = 2.408 x 10^{-4} cm/s Mv =1.045 x 10^{-4} m^2/kN Dr =0.3

Figure 102. Summary of input properties for FEQDrain analyses.

8.1.3. Other Required Input Parameters

To simulate the blast detonation series as an earthquake event in FEQDrain, the equivalent number of cycles (N_q) due to the "earthquake" loading that occurred as a result of the detonations and the duration of the "earthquake" event needed to be determined. This was accomplished by counting pulse peaks recorded by the piezometers. Sixteen detonations with a delay of 1.0 seconds between each detonation produced sixteen relatively distinct peaks. These were taken to be the cycles for the blast simulation in FEQDrain. The duration (t_d) of the explosions was pulled from the same plot of pore pressure generation. The event lasted approximately 15.5 seconds so 16 seconds was used for t_d.

The hydraulic head boundary at the top of the drain is set equal to the ground elevation because water could flow away from the drain above this level. The volume of water necessary to raise the water level above the ground water surface was specified as a "reservoir". The

reservoir volume was set equal to the inside area of the drain multiplied by the depth to the static water table.

8.1.4. Comparison of Measured and Computed Pore Pressure and Settlement

A comparison of the measured and computed excess pore pressure ratios for 300 second time histories at depths of 6.7, 8.5, 10.8 and 12.8 m at Site 3 are presented in Figure 104 through Figure 107 respectively. The computed response does not account for the peaks and troughs in the time history produced by each blast detonation, but the average or residual pore pressure is reasonably well captured. In general, the agreement between measured and computed pore pressure response is reasonable. While the portion of the calculated curves representing the generation of pore pressures do not match precisely the measured curves, in general the peak excess pore pressure ratios were successfully matched. Additionally, reasonable matches were found for the dissipation of pore pressures out to times between 150 and 200 seconds.

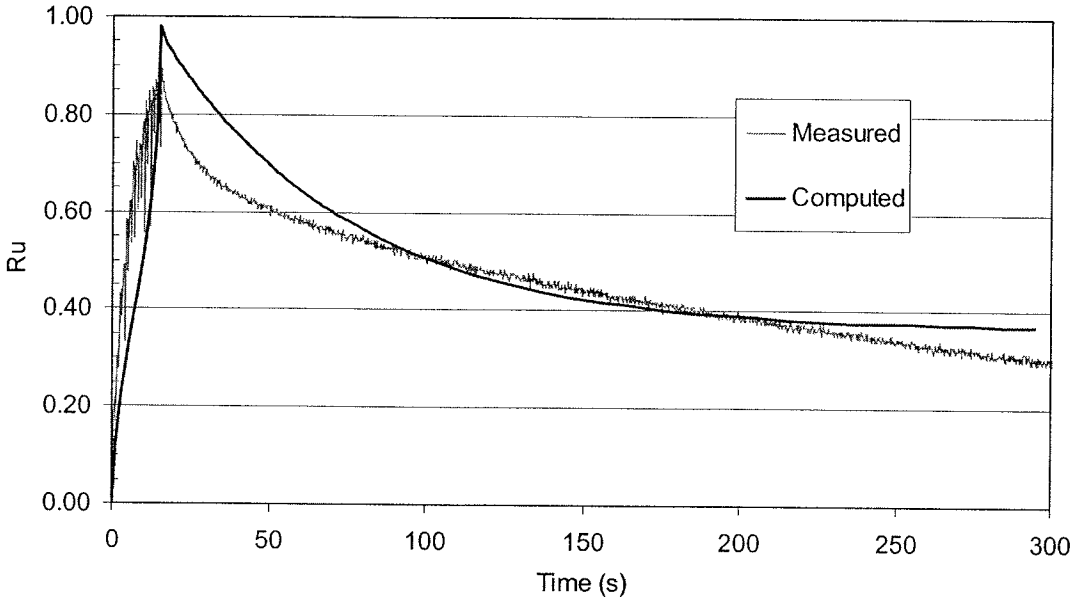

Figure 101 Comparison of measured and computed excess pore pressure ratios for the blast test at Site 3 at a depth of 6.7 m.

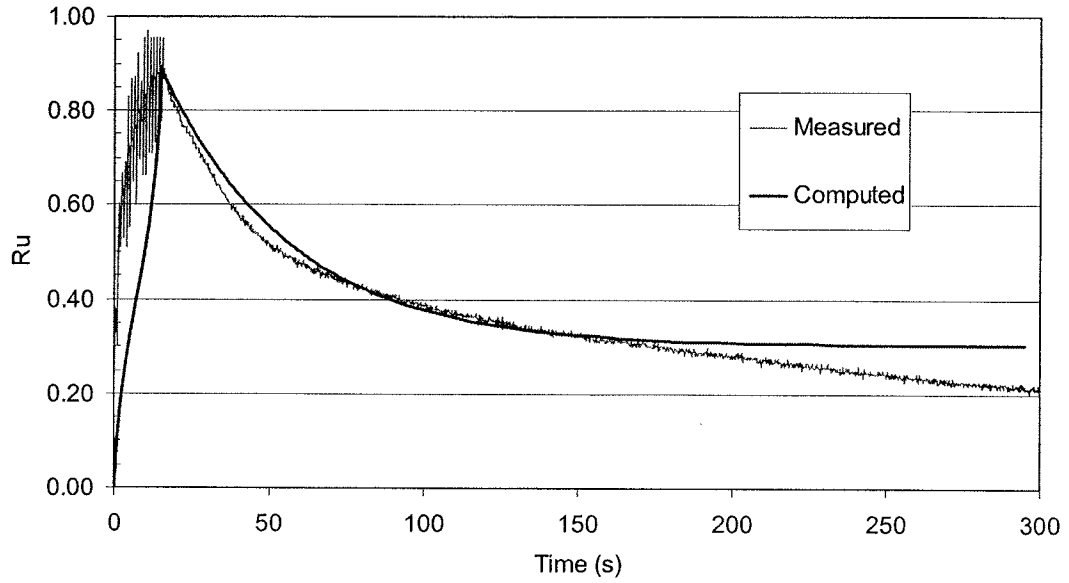

Figure 102 Comparison of measured and calculated excess pore pressure ratios for the blast test at Site 3 at a depth of 8.5 m.

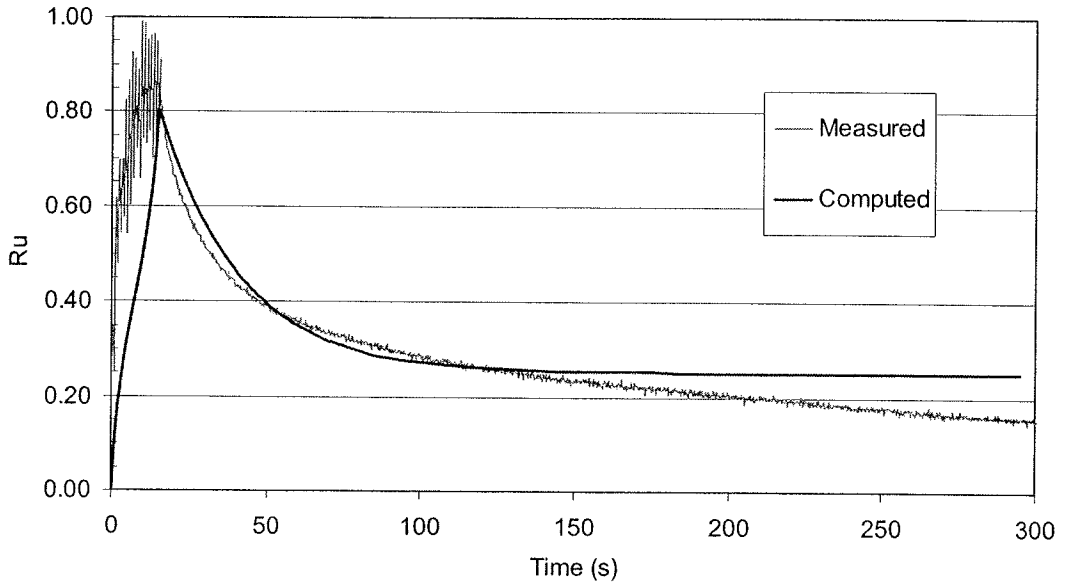

Figure 103 Comparison of measured and calculated excess pore pressure ratios for the blast test at Site 3 at a depth of 10.8 m.

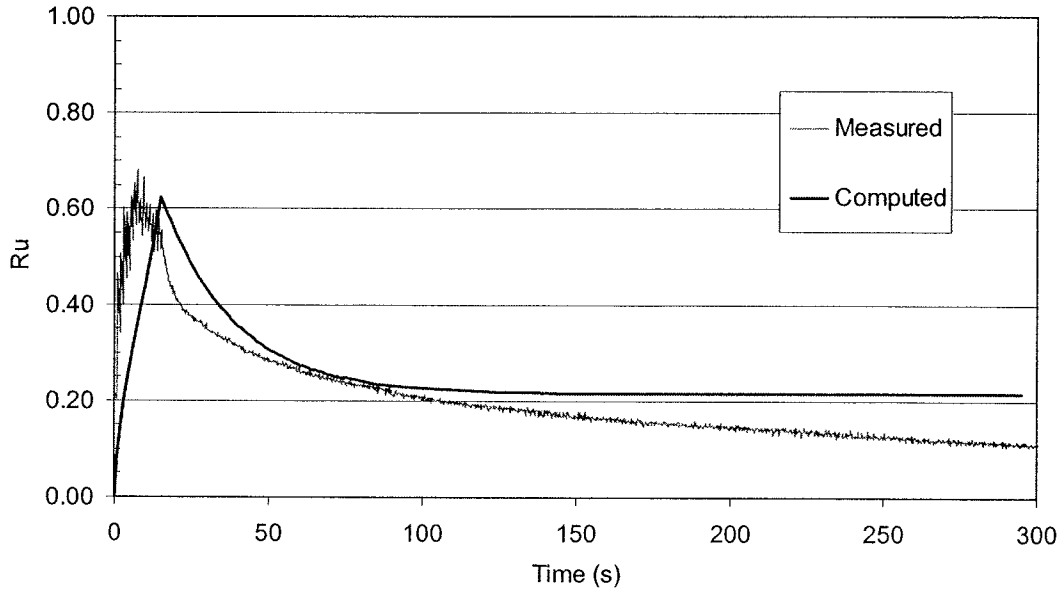

Figure 104 Comparison of measured and calculated excess pore pressure ratio for the blast test at Site 3 at a depth of 12.8 m.

8.2. EQ Drain Performance with Different Drain Arrangements

Once a reasonable match was obtained with the pore pressure response for the blast events using FEQDrain, various drain size and spacing configurations were simulated to measure the efficacy of the EQ Drains in preventing liquefaction. Table 7 provides a summary of the simulations performed. In all, three configurations were simulated: Simulation 1 used a smaller drain spacing; Simulation 2 used a larger drain diameter; and Simulation 3 used both a smaller drain spacing and larger drain diameter. Maximum calculated R_u and settlement are also included in Table 7. In all three simulations, the maximum R_u calculated by FEQ Drain occurred in the non-liquefiable silty layer directly above the liquefiable sand layer where the piezometers were located. Therefore, the maximum R_u that occurred within the liquefiable zone is reported in Table 7. The drain configuration used in the blast testing is also included for comparison.

Table 7 Summary of results for various drain size and spacing configurations simulated with FEQ Drain.

Simulation/Test	Nominal drain diameter (cm)	Triangular drain spacing (m)	Maximum Ru	Maximum settlement (mm)
Blast test	10	1.22	0.98	156
Simulation 1	10	0.91	0.56	58
Simulation 2	15.25	1.22	0.63	66
Simulation 3	15.25	0.91	0.39	38

Calculated R_u time histories of the three simulations are compared with measured R_u time histories from the blast testing at Site 3 for depths of 6.7, 8.5, 10.8, and 12.8 m depth in Firgures 108 through 111, respectively.

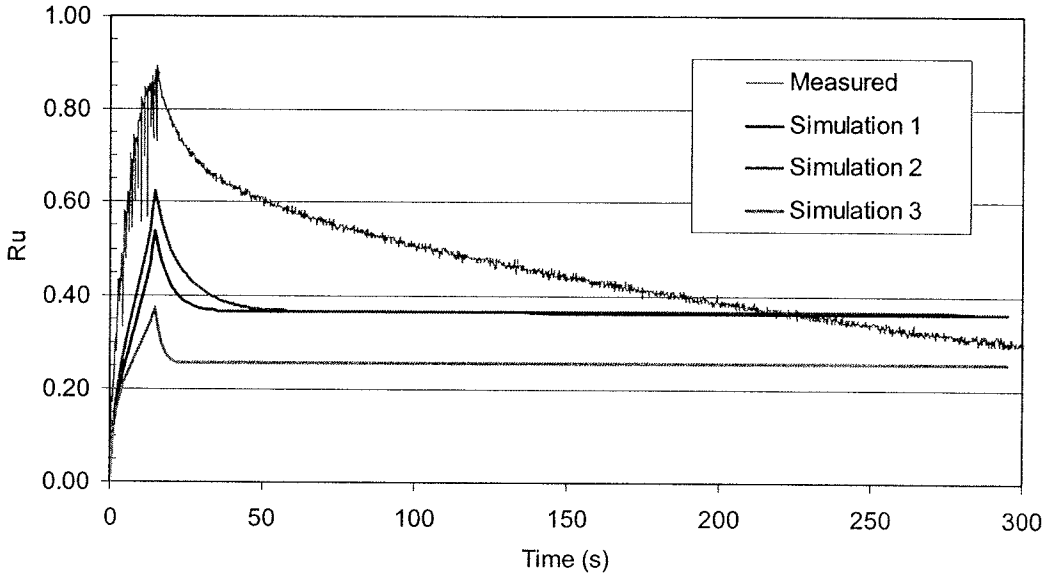

Figure 105 Comparison of R_u values measured during blast testing and calculated values for Simulations 1 through 3 at 6.7 m depth.

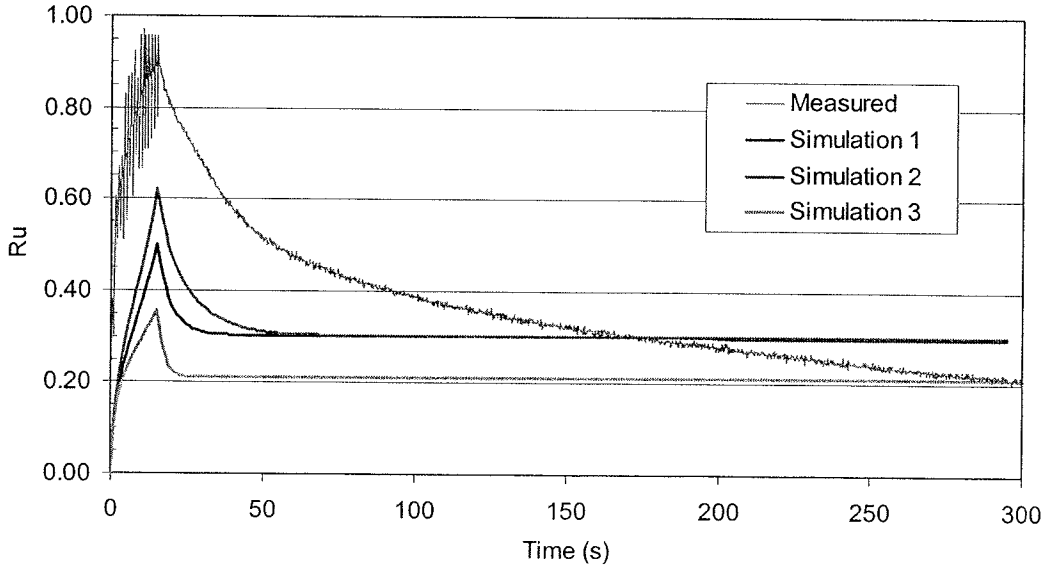

Figure 106 Comparison of values of R_u measured during blast testing and values calculated by FEQ Drain for Simulations 1 through 3 for a depth of 5.8 m.

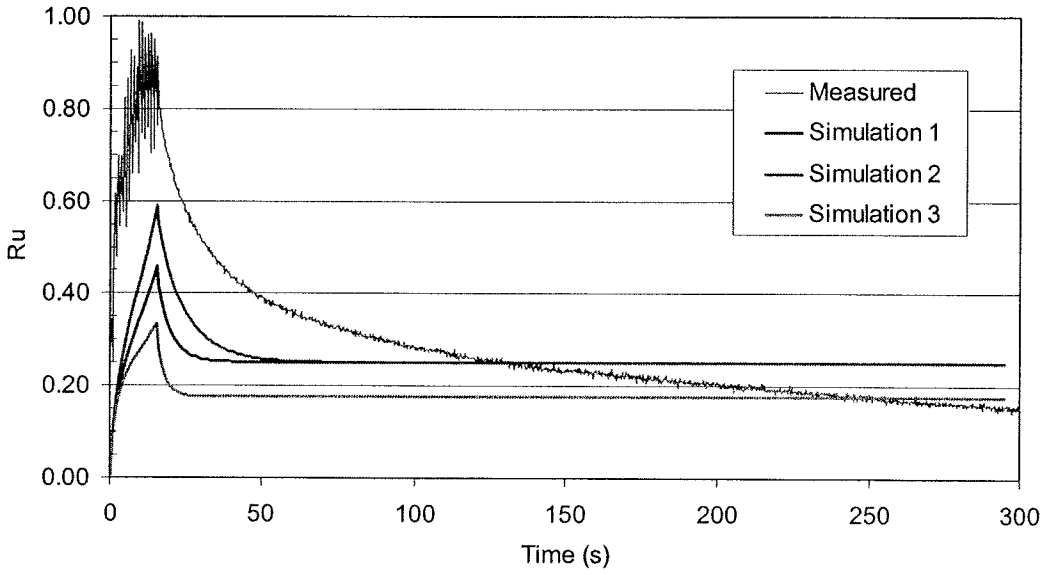

Figure 107 Comparison of values of R_u measured during blast testing and values calculated by FEQ Drain for Simulation 1 through 3 at a depth of 10.8 m.

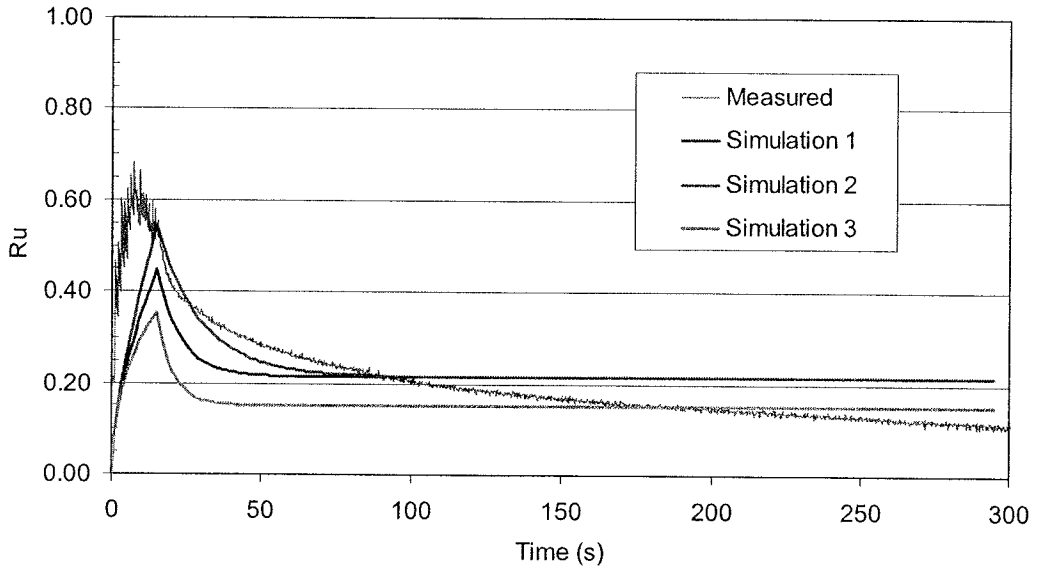

Figure 108 Comparison of R_u values measured during blast testing and values calculated by FEQ Drain for Simulations 1 through 3 at a depth of 12.8 m.

As can be noted in the table and figures representing the three trial simulations, all three configurations of drain size and spacings were successful in limiting the generation of pore pressures sufficiently to prevent liquefaction. As expected, Simulation 3 was the most successful inasmuch as it used a combination of smaller drain-to-drain spacings and a larger diameter

drain.. Simulation 2, using just a smaller drain-to-drain spacing was the next most successful in limiting pore pressure generation. The least effective simulation was Simulation 2, which used just a larger drain diameter.

8.3. Considerations in Design of Drain Spacing

The results of the testing and analysis clearly indicate the need for an accurate assessment of the horizontal permeability (hydraulic conductivity) of the soil in the profile when determining the required drain spacing. Perhaps the simplest and most reliable means of obtaining this information is to conduct borehole permeability tests at the site using a double packer approach as outlined in Designation E-18 in the Earth Manual published by the US Bureau of Reclamation (1974). This procedure makes it possible to evaluate the permeability in 5 to 10 ft intervals along the length of the borehole. Alternatively, these permeability tests can also be performed inside one of the drains during installation to verify design assumptions. Although correlations can be used to estimate permeability coefficients, they must be chosen conservatively. Use of conservative permeability values can easily lead to a design with an increased cost that greatly exceeds the cost of a simple in-situ permeability test.

The analysis also indicates the importance of evaluating the drain performance for a range of soil conditions rather than just a mean value to assure that performance will be satisfactory. Improved drain performance can be achieved by decreasing the drain spacing or increasing the drain diameter; however, these actions have cost consequences. For example, decreasing the drain spacing from 4 ft spacing to 3 ft spacing will increase the number of required drains by a factor of about 75% which will significantly increase the cost of the treatment.

Finally, the computer analysis highlights the importance of having a flexible numerical model which can easily incorporate variations in soil layer, soil properties and drain properties. Although simplified charts for selecting drain diameter and spacing have been developed by Seed and Booker (1977) and Onoue (1988), they generally do not allow an engineer to account for layered soil profiles and more complex boundaries which are often encountered in real-life applications. Because FEQDrain is available at no cost from Nilex, Inc. and can easily be run on typical personal computers, we recommend that this numerical model be used in optimizing the drain spacing and diameter.

9. Conclusions

1. Besides providing drainage, EQ Drains provide a side benefit of inducing significant settlement during installation. This leads to increased density and a lower compressibility which both reduce the amount of settlement and increase the rate of pore pressure dissipation relative to untreated sites. Drain installation using vibration produced volumetric strain of about 2.9%.

2. The presence of earthquake drains (1.22 m drain spacing and 100 mm drain diameter).significantly increased the rate of excess pore water pressure dissipation relative to an untreated area but did not prevent liquefaction for the blast sequence. Nevertheless, liquefaction induced settlement was reduced from about 270 mm at the untreated site to 220 mm at the site with drains, a reduction of 17%

3. Computer analyses using FEQDrain, back-calculated from the measured response, indicate that the vertical drains could successfully limit pore pressure buildup and settlement for blast sequence with somewhat smaller drain spacing (0.9 m) or larger drain diameter (150 mm).

4. Liquefaction at the site without drains initially reduced the side friction in the liquefied zone to approximately zero; however, as pore pressures dissipated and the sand settled, negative skin friction developed with a maximum value about one-half of the initial positive skin friction. The semi-fluid nature of the sand during reconsolidation apparently prevented higher negative skin friction from developing.

5. Because of the high rate of pore pressure dissipation, negative skin friction developed in the liquefied zone almost immediately after the blasting ended at the site with drains. The negative skin friction had a magnitude approximately equal to the positive skin friction prior to the blasting. The higher negative skin friction values at the site with drains relative to the untreated site is likely a result of the more rapid drainage which led to a more solidified mass during settlement.

6. Negative skin friction was not observed for the non-liquefied soil above the liquefied zone at either test site despite the fact that ground settlement exceeded 220 mm in both cases. This could result from downward movement of the pile at the surface as pile head load was increased to maintain the initial force that was applied to the pile.

7. The increased downdrag load produced by negative skin friction at both test sites was resisted by increased friction and end-bearing resistance in the denser sand below the liquefied zone and settlement of the pile in both cases was limited to less than 7 to 10 mm.

8. Although EQ drains have the potential to mitigate liquefaction hazard, the use of drains around piles to prevent negative skin friction does not generally appear to be a viable option. Analyses suggest that it will be very difficult to reduce settlement sufficiently to prevent negative friction and if negative friction does develop, test results suggest the magnitude could be greater if drains are used.

9. The reduced settlement and pore pressures produced by treatment of liquefiable soils with drains would likely be sufficient to prevent damage to shallow foundations, slopes, embankments, retaining structures and other systems for many earthquake events.

10. Selection of an appropriate drain spacing should be accomplished using a numerical model such as FEQDrain which can account for variations in soil properties and drain properties. Horizontal permeability, which is critical to such analyses, should be measured in-situ to provide reliable designs and avoid unnecessary costs.

10. Appendix

Table 8 Pile driving data for pile foundation installed at Site 2.

Pile:	Test Pile		NE		NW		SE		SW	
Depth (m)	Drop Height (m)	Blows	Drop Height (m)	Blows	Drop Height (m)	Blows	Drop Height (m)	Blows	Drop Height (m)	Blows
0.3	0.6	9					0.6	6		
0.6	0.6	8	0.6	10			0.6	5		
0.9	0.9	8	1.2	4	1.2		0.9	4	0.9	12
1.2	0.9	7	1.2	3	1.2		0.9	5	0.9	4
1.5	0.9	8	1.2	3	1.2	10	1.2	4	1.2	5
1.8	0.9	8	1.2	0	1.2	2	1.2	4	1.2	3
2.1	0.9	6	1.2	4	1.2	2	1.2	4	1.5	4
2.4	1.2	5	1.5	2	1.2	1	1.2	5	1.5	4
2.7	1.2	4	1.5	1	1.2	2	1.2	4	1.2	4
3.0	0.9	7	1.5	2	1.2	2	1.5	3	1.2	3
3.4	0.9		1.5	3	1.2	3	1.5	3	1.5	3
3.7	0.9	8	1.5	2	1.2	2	1.5	3	1.5	3
4.0	0.9	3	1.5	3	1.2	2	1.5	3	1.5	2
4.3	0.9	3	1.5	3	1.5	3	1.5	2	1.5	3
4.6	1.2	4	1.5	4	1.5	3	1.5	3	1.5	4
4.9	1.2	4	1.5	3	1.5	2	1.5	4	1.5	3
5.2	1.2	6	1.5	3	1.5	2	1.5	4	1.5	4
5.5	1.2	8	1.5	3	1.5	3	1.5	6	1.5	5
5.8	1.2	6	1.5	4	1.5	4	1.5	6	1.5	5
6.1	1.8	7	1.5	6	1.5	5	1.5	6	1.5	6
6.4	1.8	6	1.5	6	1.5	5	1.5	7	1.5	8
6.7	1.8	6	1.5	7	1.5	6	1.5	6	1.5	6
7.0	1.8	5	1.5	6	1.5	6	1.5	6	1.5	6
7.3	1.8	4	1.5	6	1.5	7	1.5	6	1.5	5
7.6	2.1	4	1.5	6	1.5	6	1.5	6	1.5	6
7.9	2.1	4	1.5	8	1.5	6	1.5	6	1.5	6
8.2	2.1	4	1.5	8	1.5	8	1.5	7	1.5	7
8.5	2.1	5	1.5	8	1.5	7	1.5	6	1.5	7
8.8	2.1	5	1.5	6	0.6	10	1.5	9	1.5	7
9.1	2.1	5	1.5	6	1.5	7	1.5	9	1.5	8
9.4	2.1	5	1.5	6	1.5	7	1.5	9	1.5	9
9.8	2.1	6	1.5	9	1.5	7	1.5	8	1.5	10
10.1	2.1	6	1.5	10	1.5	5	1.5	9	1.5	10
10.4	2.1	8	1.5	9	1.5	6	1.5	10	1.5	9
10.7	2.1	9	1.5	8	1.8	6	1.5	10	1.5	11
11.0	2.1	7	1.5	10	2.1	6	1.5	12	1.5	13
11.3	2.1	9	1.5	10	2.1	7	1.5	11	1.5	15
11.6	2.1	10	1.5	11	2.1	7	1.5	10	1.5	15
11.9	2.1	9	1.5	0	2.1	7	0.6	10	1.8	0

12.2	2.1	10	2.1	8	2.1	9	1.2	0	1.8	1
12.5	2.1	12	2.1	7	2.1	9	2.4	7	2.1	
12.8	2.1	10	2.4	10	2.1	9	2.4	6	2.1	9
13.1	2.1	11	2.4	4	2.1	10	2.4	7	2.1	5
13.4	2.1	11	2.4	5	2.1	11	3.0	6	2.1	
13.7	2.1	11	2.4	6	2.1	11	3.0	5	2.1	6
14.0	2.1	13	2.4	6	2.1	13	3.0	6	2.1	8
14.3	2.1	13	2.4	7	2.1	12	3.0	0	2.1	
14.6	2.1	12	2.4	7	2.4	13	3.0	6	2.1	
14.9	2.1	14	2.4	7	2.4	13	3.0	0	2.1	9
15.2	2.1	12	2.7	7	2.4	12	3.0	6	2.1	1
15.5	2.1	12	2.7	7	2.4	13	3.0	7	2.1	1
15.8	2.1	11	2.7	7	1.8	15	3.0	6	2.1	9
16.2	2.1	13	2.7	9	1.8	13	3.0	0	2.1	1
16.5	2.1	13	2.7	10	1.8	0	3.0	7	2.1	1
16.8	2.1	14	2.7	8	1.8	0	3.0	6	2.1	1
17.1	2.1	14	2.7	9	1.8	14	3.0	7	2.1	9
17.4	2.1	11	2.7	9	2.4	12	3.0	7	2.1	1
17.7	2.1	12	2.7	9	2.4	13	3.0	8	2.1	1
18.0	2.1	14	2.7	9	2.4	15	3.0	8	2.1	11
18.3	2.1	13	2.7	8	2.4	13	3.0	8	2.1	9
18.6	2.1	12	2.7	9	2.4	15	3.0	9	2.1	9
18.9	2.1	14	2.7	10	2.4	17	3.0	8	2.1	10
19.2	2.1	14	2.7	11	2.7	13	3.0	10	2.1	1
19.5	2.1	15	2.7	11	2.7	14	3.0	12	2.1	1
19.8	2.1	16	2.7	11	2.7	0	3.0	11	2.1	12
20.1	2.1	17	2.7	11	2.7	14	3.0	11	2.1	13
20.4	2.1	15	2.7	12	2.7	16	3.0	9	2.1	1
20.7	2.1	14	2.7	12	2.7	13	3.0	0	2.1	1
21.0	2.1	8	2.7	12	2.7	13	3.0	10	2.1	12
21.3			2.7	15	2.7	12	3.0	11	2.1	1
21.6			2.7	14	2.7	12	3.0	12	2.1	1

Table 9 Pile driving data for the pile foundation installed at Site 3.

Pile:	Test Pile		NE		NW		SE		SW	
Depth (m)	Drop Height (m)	Blows	Drop Height (m)	Blows	Drop Height (m)	Blows	Drop Height (m)	Blows	Drop Height (m)	Blows
0.3	0.6	6	1.5	1			0.6	1	1.2	
0.6	0.6	8	1.5	1	1.2		0.6	1	1.2	1
0.9	0.6	10	1.5	3	1.2	8	0.6	1	1.2	1
1.2	0.6	8	1.5	1	1.2	3	0.6	2	1.2	1
1.5	0.9	8	1.5	6	1.2	4	0.6	2	1.2	1
1.8	0.9	9	1.5	2	1.2	4	0.9	2	1.2	2
2.1	0.9	8	1.5	2	1.2	3	0.9	1	1.2	2
2.4	0.9	6	1.5	2	1.2	3	0.9	4	1.2	3
2.7	0.9	4	1.5	3	1.2	3	0.9	3	1.2	3
3.0	0.9	6	1.5	2	1.2	3	0.9	7	1.2	5
3.4	0.9	4	1.5	3	1.2	2	0.9	5	1.2	5
3.7	0.9	4	1.5	2	1.5	3	1.2	4	1.2	4
4.0	0.9	4	1.5	3	1.5	3	1.2	4	1.2	3
4.3	0.9	4	1.5	2	1.5	2	1.2	3	1.2	2
4.6	0.9	3	1.5	3	1.5	3	1.2	3	1.2	3
4.9	0.9	4	1.5	3	1.5	3	1.2	2	1.2	3
5.2	0.9	2	1.5	3	1.5	4	1.2	3	1.2	4
5.5	1.8	8	1.5	4	1.5	4	1.2	4	1.5	5
5.8	1.8	8	1.5	3	1.5	4	1.2	6	1.5	5
6.1	1.8	7	1.5	3	1.5	4	1.2	6	1.5	5
6.4	2.4	6	1.5	4	1.5	4	1.2	5	1.5	6
6.7	2.4	7	1.5	5	1.5	5	1.2	6	1.5	7
7.0	2.4	6	1.5	5	1.5	4	1.2	7	1.5	7
7.3	2.4	6	1.5	4	1.5	5	1.2	7	1.5	9
7.6	2.4	5	1.5	5	1.5	5	1.2	9	1.8	9
7.9	2.4	5	1.5	6	1.5	5	1.2	8	1.5	8
8.2	2.4	6	1.5	6	1.5	5	1.2	7	1.5	8
8.5	2.4	5	1.5	6	1.5	5	1.2	8	1.5	8
8.8	2.4	5	1.5	6	1.5	5	1.2	8	1.5	9
9.1	2.4	4	1.8	6	1.5	6	1.2	10	1.5	10
9.5	2.4	4	1.8	8	1.5	8	1.2	11	1.5	10
9.8	2.4	5	1.5	8	1.5	7	1.2	11	1.5	10
10.1	2.4	6	1.5	7	1.5	7	1.2	11	1.5	9
10.4	2.4	5	1.5	8	1.5	8	1.2	12	1.5	10
10.7	2.4	5	1.5	7	1.5	8	1.2	13	1.5	10
11.0	2.4	6	1.5	9	1.5	8	1.2	11	1.5	12
11.3	2.4	6	1.5	9	1.5	9	1.2	11	1.5	15
11.6	2.4	6	1.5	11	1.5	12	1.2	14	1.5	14
11.9	2.4	7	1.5	9	2.1	9				
12.2	2.4	8	2.4	8	2.1	7				
12.5	2.4	8	2.4	9	2.1	8				
12.8	2.4	10	2.4	9	2.1	8				

13.1	2.4	11	2.4	6	2.1	6
13.4	2.4	11	2.4	9	2.4	9
13.7	2.4	11	2.4	9	2.4	9
14.0	2.4	10	2.4	10	2.4	10
14.3	2.4	11	2.4	9	2.7	9
14.6	2.4	11	2.4	9	2.7	11
14.9	2.4	12	2.4	9	2.7	11
15.2	2.4	13	2.4	9	2.7	12
15.5	2.4	13	2.4	13	2.7	12
15.9	2.4	12	2.4	11	2.7	14
16.2	2.4	13	2.4	12	2.7	14
16.5	2.4	12	2.4	11	2.7	14
16.8	2.4	12	2.4	11	2.7	13
17.1	2.4	12	2.4	11	2.7	12
17.4	2.4	13	2.4	10	2.7	13
17.7	2.4	12	2.4	10	2.4	14
18.0	2.4	12	2.4	11	2.4	11
18.3	2.4	13	2.4	10	2.4	12
18.6	2.4	12	2.4	11	2.4	12
18.9	2.4	12	2.4	11	2.4	12
19.2	2.4	14	2.4	12	2.4	13
19.5	2.4	14	2.4	14	2.4	12
19.8	2.4	13	2.4	13	2.4	13
20.1	2.4	14	2.4	14	2.4	12
20.4	2.4	16	2.4	14	2.4	12
20.7	2.4	16	2.4	15	2.4	13
21.0	2.4	17	2.4	15	2.4	12
21.3			2.4	15	2.4	14

11. References

Andrus, R.D. and Stokoe, K.H., II (2000). "Liquefaction resistance of soils from shear-wave velocity." J. Geotech. and Geoenvir. Engrg., ASCE, 126(11), 1015-1025.

Boulanger, R.M. and Idriss, I.M. (2004). "Evaluating the potential for liquefaction or cyclic failure of silts and clays." Report UCD/CGM-04/01, Civil Engineering Dept. University of California at Davis, Davis, California, 131 p.

Bustamante, M., and Gianeselli, L.. (1982). "Pile Bearing Capacity Predictions by Means of Static Penetrometer CPT". Procs., 2nd European Symp. on Penetration Testing, ESOPT2, Amsterdam, 1982, p. 493-500.

Eslami, A., and Fellenius, B.H. (1997). "Pile Capacity by Direct CPT and CPTu Methods Applied to 102 Case Histories." Canadian Geotechnical Journal, Vol. 34, No. 6, p. 886-904.

EQE (1995) "The January 17, 1995 Kobe Earthquake" Summary Report, www.eqe.com/publications/kobe/economic.htm

Fellenius, B.H., (1998). "Recent advances in the design of piles for axial loads, dragloads, downdrag, and settlement." ASCE and Port of NY & NJ Seminar

Fellenius, B.H., (1999). "Bearing capacity of footings and piles—a delusion?" Deep Foundation Institute Annual Meeting.

Fellenius, B.H., (2004). "Unified design of piled foundations with emphasis on settlement analysis." Geo-Institute Geo-TRANS conference, Los Angeles

Freeze, R.A. andCherry, J.A. (1979). *Goundwater*, Prentice-Hall, Inc., Englewood Cliffs, New Jersey.

Gohl, B. (2002). "Report on Gravel Drain Testing at South End of George Massey Tunnel", Prepared for Buckland & Taylor, Ltd. and British Columbia Ministry of Transportation, Pacific Geodynamics, Inc., Vancouver, BC, Canada.

Holzer, TL. (1998). "Introduction". The Loma Prieta, California, Earthquake of October 17, 1989-Liquefaction, U.S. Geological Survey Professional Paper 1551-B, U.S. Government Printing Office, B1-B8.

Kulhawy, F. H. and Mayne, P. W. (1990) *Manual on Estimating Soil Properties for Foundation Design*, Electric Power Research Institute, Palo Alto, California, Research Report EERI EL-6800.

Lew, M. and Hudson, M. B., (2004). "Liquefaction basics." Structure magazine.

Monahan, P.A., Luternauer, L., Barrie, J.V., (1995). "The geology of the CANLEX phase II sites in Delta and Richmond British Columbia." *In* Proceedings of the 48th Canadian Geotechnical Conference, Vancouver, B.C., pp. 59-68.

National Research Council (1985). Liquefaction of Soils During Earthquakes, National Academy Press, 240 p.

Onoue, A. (1988). "Diagrams Considering Well Resistance for Designing Spacing Ratio of Gravel Drains." Soils and Foundations, Japanese Soc. of Soil Mechanics and Foundation Engineering, Vol. 28, No.3, 160-168.

Pestana, J.M., Hunt, C.E. and Goughnour, R.R. (1997). "FEQDrain: A Finite Element Computer Program for the Analysis of the Earthquake Generation and Dissipation of Pore Water Pressure in Layered Sand Deposits with Vertical Drains," *Report No. EERC 97-17*, Earthquake Engineering Research Ctr., Univ. of Calif., Berkeley, CA.

Rathje, E.M., Chang, W.-J, Cox, B.R., and Stoke, K.H.II (2004). "Effect of prefabricated vertical drains on pore pressure generation in liquefiable sand." Procs. 11th Intl. Conf. on Soil Dynamics and Earthquake Engineering, Stallion Press, Vol. 2, 529-536.

Robertson, P.K., Campanella, R.G., Gillespie, D., and Grieg, J. (1986). "Use of piezometer cone data". Procs., In-Situ '86, ASCE Specialty Conference, Blacksburg, VA, p. 1263-80.

Robertson, P.K., Wride, C.E., List, B.R., Atukorala, U., Biggar, K.W., Byrne, P.M., Campanella, R.G., Cathro, D.C., Chan, D.H., Czajewski, K., Finn, W.D.L., Gu, W.H., Hammamji, Y., Hofmann, B.A., Howi, J.A., Hughes, J. Imrie, A.S., Kinrad, J.M., Küpper, A., Law, T., Lord, E.R.F., Monahan, P.A., Morgenstern, N.R., Phillips, R., Piché, R., Plewes, H.D., Scott, D., Sego, D.C., Sobkowicz, J., Stewart, R.A., Watts, B.D., Woeller, D.J., Youd, T.L., Zavodni, Z., (2000). "The Canadian Liquefaction Experiment: an overview." Canadian Geotechnical Journal, **37**: 499-504.

Rollins, K. M. and Anderson, J.K.S., 2004. "Performance of vertical geocomposite drains based on full-scale testing at Massey Tunnel, Vanvouver, B.C.", Final Report, NCHRP-IDEA Project 94, Transportation Research Board, Washington, D.C., 107 p

Rollins, K.M., Goughnour, R.R., Anderson J.K.S. and McCain, A. (2004). "Liquefaction hazard mitigation using vertical composite drains," Procs. 13th World Conf. on earthquake Engineering, EERI, Vancouver

Rollins, K.M., Lane, J.D., Dibb, E., Ashford, S.A., Mullins, A.G. (2005). "Pore Pressure Measurement in Blast-Induced Liquefaction Experiments," Transportation Research Record 1936, "Soil Mechanics 2005", Transportation Research Board, Washington DC, p. 210-220.

Seed, H.B., and Booker, J.R. (1977). "Stabilization of Potentially Liquefiable Sand Deposits Using Gravel Drains," J. Geotech Engrg. Div., ASCE, 103(GT7), 757-768.

Seed, H.B., Martin, P.P., and Lysmer, J. (1976). "Pore-Water Pressure Changes During Soil Liquefaction", *J. Geotech. Engrg. Div.,* ASCE, 102(GT4), pp. 323-346.

Terzaghi, K. and Peck, R.B. (1948). *Soil Mechanics in Engineering Practice*, John Wiley and Sons, New York.

Tokimatsu, K. and Seed, H.B. (1988). "Evaluation of settlements in sand due to earthquake shaking." J. Geotech. Engrg., ASCE, 113(8), 861-878.

Tucker, L. M., and Briaud, J. L. (1986). *User's Manual for PILECPT.* Texas A&M Univ., Civil Engineering Department, 1986, 25 p.

U.S. Bureau of Reclamation (1974). Earth Manual, 2nd Edition, U.S. Dept. of the Interior, US Government Printing Office, Washington, D.C., p. 573-593

Youd, T.L., Idriss, I.M., Andrus, R.D., Arango, I., Castro, G., Christian, J.T., Dobry, R., Finn, W.D.L., Harder, L.F., Hynes, M.E., Ishihara, K., Koester, J.P., Liao, S.S.C., Marcuson, W.F., Martin, G.R., Mitchell, J.K., Moriwaki, Y., Power, M.S., Robertson, P.K., Seed, R.B., and Stokoe, K.H. (2001). "Liquefaction Resistance of Soils: Summary Report from the 1996 NCEER and 1998 NCEER/NSF Workshops on Evaluation of Liquefaction Resistance of Soils, *J. Geotech. and Geoenvir.. Engrg.*, ASCE, 127(10), 817-833.